ASTROGEOLOGIC STUDIES

ANNUAL PROGRESS REPORT

July 1, 1964 to

July 1, 1965

PART B: CRATER INVESTIGATIONS

October 1965

This preliminary report is distributed

without editorial and technical review

for conformity with official standards

and nomenclature. It should not be

quoted without permission.

This report concerns work done on behalf of the

National Aeronautics and Space Administration.

DEPARTMENT OF THE INTERIOR

UNITED STATES GEOLOGICAL SURVEY

CONTENTS

PART B--CRATER AND SOLID STATE INVESTIGATIONS

i

CONTENTS--Continued

CONTENTS--Continued

CONTENTS--Continued

INTRODUCTION

This Annual Report is the sixth of a series describing the results of research conducted by the U.S. Geological Survey on behalf of the National Aeronautics and Space Administration. This report, which covers the period July 1, 1964 to July 1,1965, is in three volumes corresponding to three main areas of research: Part A, Lunar and Planetary Investigations: Part B, Crater Investigations; and Part C, Cosmic Chemistry and Petrology; and a map supplement. An additional volume presents in abstract form summaries of the papers in Parts A, B, and C.

The major long-range objectives of the astrogeologic studies program are to determine and map the stratigraphy and structure of the Moon's crust, to work out from these the sequence of events that led to the present condition of the Moon's surface, and to determine the processes by which these events took place. Work being carried out that leads toward these objectives includes a program of lunar geologic mapping; studies on the discrimination of geologic materials on the lunar surface by their photometric, polarimetric, and infrared properties; field studies of structures of impact, explosive, and volcanic origin; laboratory studies on the behavior of rocks and minerals subjected to shock; and study of the chemical, petrographic and physical properties of materials of possible lunar origin and the development of special techniques for their analysis.

Part B, Crater Investigations, contains the results of field and laboratory studies of crater phenomenology, including volcanic, explosives, and impact events. Investigations of naturally formed terrestrial craters from three localities are: (1) the Henbury meteorite craters in Australia, (2) the Sierra Madera structure in west Texas, and (3) the Flynn Creek structure in east Tennessee. Another report discusses the distribution of mercury in shocked and unshocked rocks at the Odessa meteorite craters near Odessa, Texas, and another report discusses the possible origin of pseudotachylite from Archean granite of the Vredefort dome in Africa.

Two experimental impact studies are reported: (1) a study of impact craters formed in water-saturated sediments by impacting missiles, and (2) a study of the fragmented material produced by two colliding spheres

of basalt. Another report discusses the geology of a part of a large body of granite in central Colorado that is being considered as a site for conducting high-explosive cratering experiments in hard, polymineralic rocks.

One report discusses the geology of the Moses Rock diatreme in San Juan County, Utah, and its similarity to rilles on the lunar surface.

GEOLOGY OF THE SIERRA MADERA STRUCTURE, TEXAS:

PROGRESS REPORT

by H. G. Wilshire

Introduction

This paper is a report of progress on the detailed mapping program, begun by Shoemaker and Eggleton (1964), of the Sierra Madera crypto-explosion structure in west Texas. Two months during early 1965 were spent mapping in detail a small area of the Sierra Madera structure and making a reconnaissance in the nearby Glass Mountains (fig. 1) for rocks equivalent in age to those exposed at Sierra Madera.

Regional setting

Sierra Madera is near the northeast end of the Glass Mountains (fig. 1) and at the southwest edge of the Edwards Plateau (Sellards, 1932, p. 28), which is made up of subhorizontal Cretaceous rocks. In the Glass Mountains monocline 5000 to 7000 feet of Permian rocks are exposed; these represent formations from the Neal Ranch (Ross, 1963) at the base to Tessey at the top (table 1). The Permian rocks are un-conformably overlain by Cretaceous rocks of the Comanchian Series and dip 5° to 10° to the northwest; normal faults of post-Comanchian age are widely spaced and strike approximately in the direction of dip of the Permian rocks.
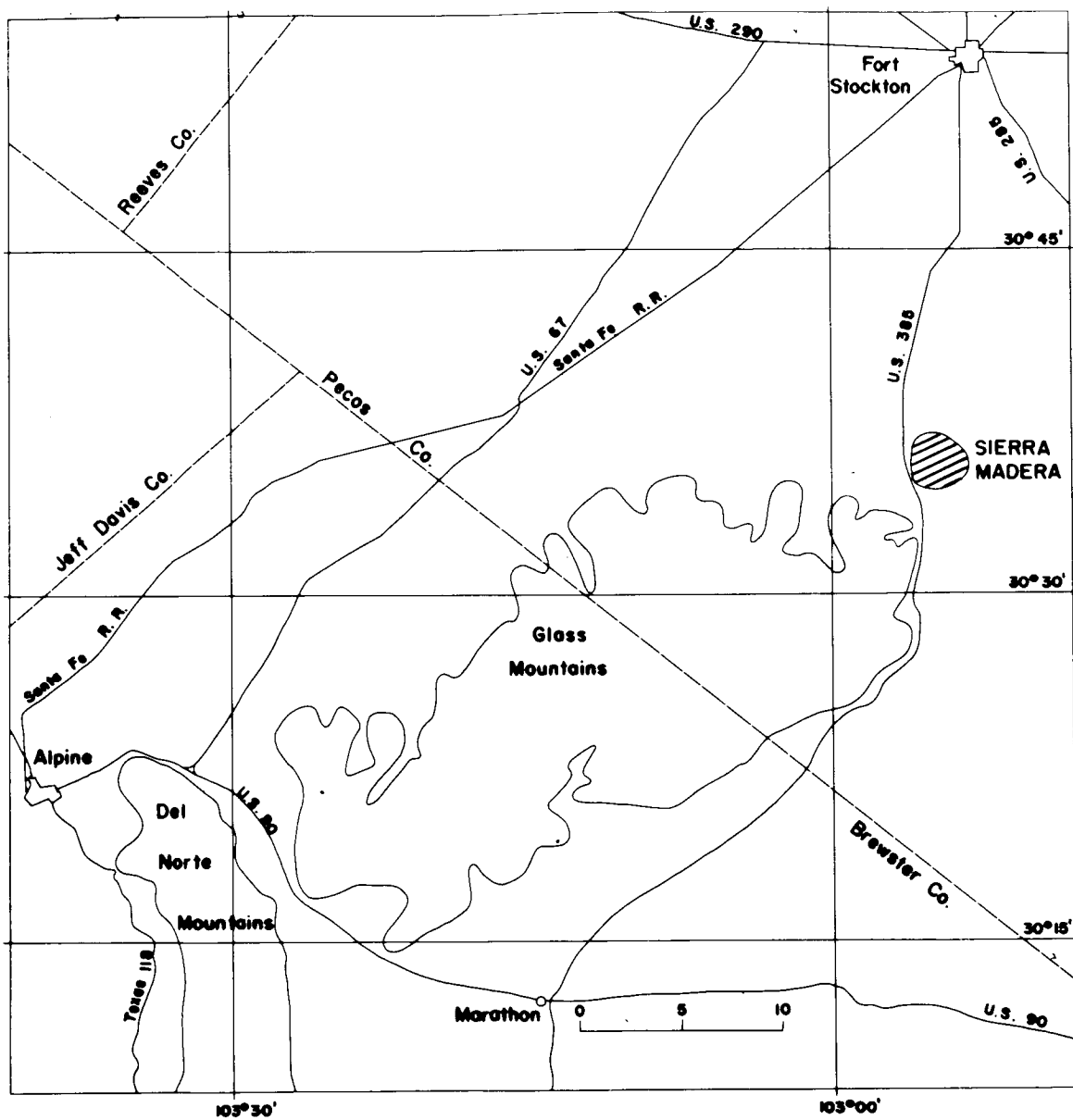
Fig. 1.--Index map showing location of Sierra Madera.

Table 1. Stratigraphic correlations in the Glass Mountains--
Permian and Cretaceous sections illustrating changing concepts of the stratigraphy

Formation and Members

System	Series	Group	King, 1930	King, 1937	Lewis, 1941 / King, 1942	Ross, 1963	Cooper & Grant, 1964
Cretaceous	Comanchian	Fredericks-burg	Edwards Ls / Comanche Peak / Walnut				
		Trinity	Basement Ss / Glen Rose				
Tri-assic			Bissett Cgl				
Permian	Ochoan		Capitan Ls / Tessey Mbr	Tessey Ls / Capitan Ls / Gilliam Mbr / Vidrio Mbr	Tessey Ls / Capitan Ls / Gilliam Ls		
	Guadalupian		Gilliam Mbr / Vidrio Mbr		Word Fm / Vidrio Mbr		Word Fm / Road Canyon Mbr / Cathedral Mtn Fm / Skinner Ranch Fm / Sullivan Peak Mbr / Poplar Tank Mbr / Decie Ranch Mbr / Hess Fm
			Word Fm	Word Fm			
	Leonardian		Leonard Fm / Hess Fm	Leonard Fm / Hess Mbr	Leonard Fm / Hess Mbr	Leonard Fm / Hess Mbr / Lennox Hills Fm	
	Wolf-campian		Wolfcamp Fm	Wolfcamp Fm	Wolfcamp Fm	Neal Ranch Fm	

The intensity of deformation at Sierra Madera is unique in an area of otherwise little deformed rocks. Structure contours drawn on the base of the Cretaceous Fredericksburg Group (King, 1935a, p. 240) indicate that Sierra Madera is situated on a broad anticlinal nose extending east-northeast from the Glass Mountains; however, data from drill holes at and near Sierra Madera (Eggleton and Shoemaker, 1961) suggest that the local strong deformation at Sierra Madera has a shallow root. Three domical structures in the Glass Mountains were described by King (1930, p. 120); two are intruded by igneous plugs, and none is very strongly deformed. A fourth domical structure, about 2 miles in diameter, was mapped by King (1930) in the Del Norte Mountains (fig. 1). This structure also involves Permian and Cretaceous rocks at the surface, but drilling indicates that, in contrast to Sierra Madera, the structure is deep-rooted and involves strata at least as old as the Ordovician; also, the deformation at the present level of exposure is very much simpler than that at Sierra Madera.

Stratigraphy

Permian rocks of the northeastern Glass Mountains, including formations from the upper Leonard to the Tessey (table 2), are dominantly shallow-water marine dolomite and limestone with some interbedded sandstone and conglomerate that were deposited on the southern shelf of the Delaware basin (fig. 2). The rocks grade into deep-water, fine-grained clastic rocks in the basin. The thickness and lithology of

4
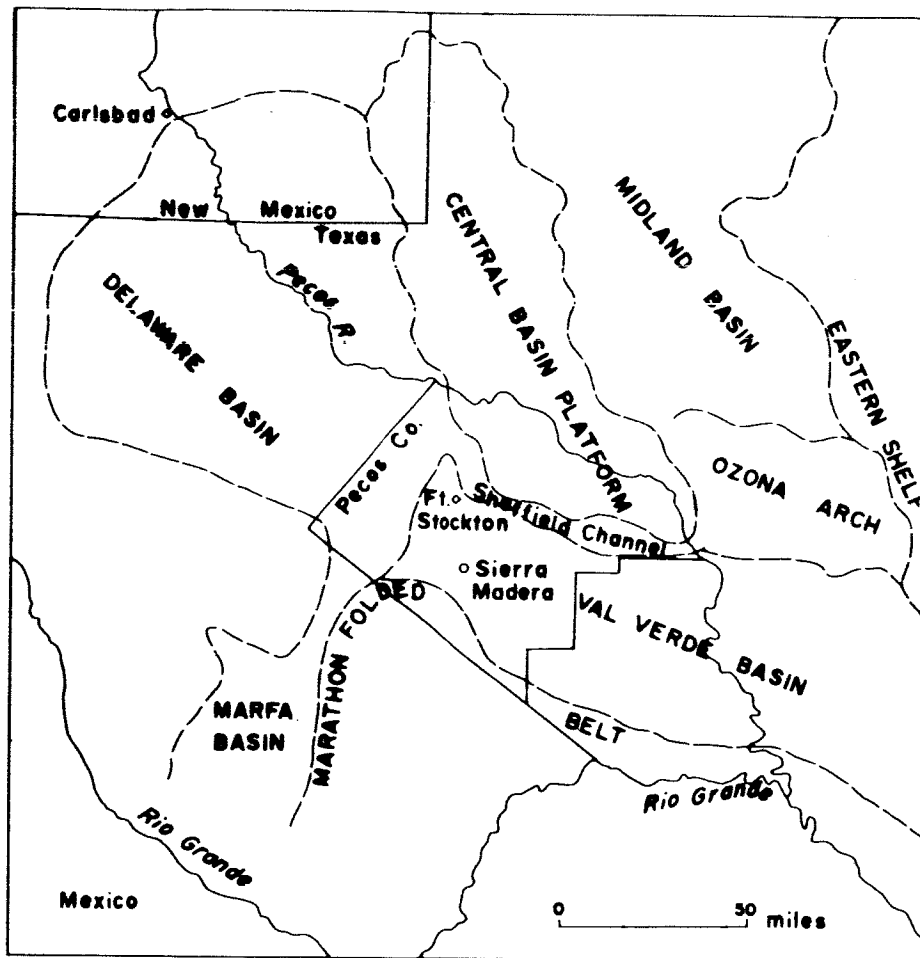
Fig. 2.--Major geologic features of the southern Permian basin.

Early Permian rocks (Wolfcampian) found in the Phillips No. 1 Elsinore well at Sierra Madera (fig. 3; Young, 1952) indicate that the Delaware and Val Verde basins were continuous (fig. 2) in Wolfcampian time (Vertrees and others, 1959). The change, in Leonardian time, to a shelf environment at Sierra Madera and in the northeastern Glass Mountains was due partly to the filling of the Val Verde Basin and partly to northward thrusting in the Marathon folded belt (Ross, 1962). The uppermost Permian carbonate rocks (Tessey Limestone) of the northeastern Glass Mountains grade toward the Delaware Basin into a saline section correlative with the Rustler, Salado, and Tansill formations (King, 1942, p. 658).

Major lateral changes in lithology may occur over short distances in the shelf sediments. Such changes led King (1930) to separate the Permian formations of the Glass Mountains into an eastern and western facies. Further changes in a northeasterly direction were found by comparing the lithologies of Permian formations described by King (1930) with the lithologies in the Glass Mountains exposures nearest Sierra Madera.

The general nature of the facies changes in the northeastern Glass Mountains is shown in table 2. A few additional observations are noteworthy. Although King (1930, p. 124) states that the conglomerate member of the Leonard Formation is the most reliable marker horizon in the central part of Sierra Madera, a thin conglomerate in the Word Formation was found to be lithologically similar to that in the Leonard

Formation. The northeasternmost exposures of the Word Formation are distinguishable from the Hess Member of the Leonard Formation and the Vidrio Member of the Word Formation by the abundance of fossils and by the more calcareous nature of the Word Formation. The Tessey Limestone contains abundant breccias throughout the section, not only in the upper part as suggested by King (1930, p. 77). Massive and brecciated, apparently unfossiliferous, limestones and intraformational limestone conglomerates are common and locally dominant over dolomite in the northeastern exposures of the Tessey; these limestones are lithologically indistinguishable from some unfossiliferous limestones of the Cretaceous Edwards Limestone. Beds of fine-grained calcareous sandstone and dolomite breccia with a sandstone matrix, included in the Tessey Limestone by King (1930), are lithologically similar to beds in the underlying Gilliam Limestone. The Bissett Conglomerate, which occurs between the Permian Tessey Limestone and the Cretaceous Basement Sandstone in the north-central Glass Mountains, was considered by King (1935b) to be Triassic, and lithologically similar conglomerate and claystone at Sierra Madera were provisionally labelled Triassic by Shoemaker and Eggleton (1964); but Adams (1935), among others, considered the Bissett to be Cretaceous. In the northeastern Glass Mountains a thin conglomerate that is identical with parts of the Bissett Conglomerate was found between the Basement Sandstone and the Gilliam Limestone; there is no apparent angular discordance between the Basement Sandstone and the conglomerate and it appears likely that the

conglomerate is Cretaceous. At Sierra Madera, a similar conglomerate was found at the top of the Basement Sandstone, another near the base, and others within the Edwards Limestone; this casts considerable doubt on the Triassic age designation of conglomerates at the bottom of the Basement Sandstone. The tentative Triassic label (fig. 4) is retained, however, pending palynologic study of the claystones.

The lithologies of formations so far distinguished at Sierra Madera are compared with those of the same formations in the Glass Mountains in table 2. The oldest formation mapped to date is the Word(?) which is in fault contact with the Gilliam Limestone. Identification of the Word is tentative and is based on a lithologic correlation with the Glass Mountain rocks; however, the fossiliferous limestones at Sierra Madera are interbedded(?) with dolomite breccias unlike any lithologic units found in the Glass Mountains exposures of the Word. The Vidrio Member of the Word Formation has not yet been recognized at Sierra Madera. The Gilliam Limestone at Sierra Madera closely resembles that in the Glass Mountains except for a greater abundance of sandstone and a much commoner brecciation and calcite cementation of thin dolomite beds at Sierra Madera. The Tessey Limestone at Sierra Madera is the same in essential features as that in the Glass Mountains, although basal sandstones are included for convenience in the Gilliam at Sierra Madera. Subdivision of the Tessey into an upper breccia unit and a lower massive to thinly laminated unit as proposed by Shoemaker and Eggleton (1964) was found to be untenable in the area adjacent to that

mapped by them; dolomite breccias were found throughout the section and are subordinate in quantity to massive and thinly laminated units. Limestones in the Tessey at Sierra Madera are distinguishable from un-fossiliferous limestones of the Edwards Limestone only where the latter occur with exposed Basement Sandstone. The Basement Sandstone and Edwards Limestone have the same lithology as in the Glass Mountains, except possibly for a greater abundance of breccias and conglomerates at Sierra Madera.

The most important difference between the Permian section of the Glass Mountains and Sierra Madera is the abundance of dolomite breccia in the Gilliam Limestone and the Word Formation(?) at Sierra Madera. That these breccias, as well as those in the Tessey Limestone, are sedimentary breccias (possibly formed by current action shortly after lithification) is indicated by lateral transition of thinly laminated units into mildly brecciated rocks in which the individual pieces have been only slightly displaced and then into completely mixed breccia in which the individual laminated pieces are randomly oriented. It is noteworthy that the fine-grained calcite cement is macroscopically similar to the cement of the central breccia mass as distinguished by Eggleton and Shoemaker (1961). Several interpretations of this feature are possible, but the observations made to date suggest that at least as early as Word(?) time deposition was in shallower water at Sierra Madera than in the nearest Glass Mountains.

Table 2.--Lithologic comparison of Permian, Triassic(?), and Cretaceous rocks

Rock	Eastern Glass Mountains (King, 1930)	Northeasternmost Glass Mountains (author)	Sierra Madera (author)
Edwards Limestone	Light gray, dense to finely crystalline; thin-bedded; abundant brown, gray chert nodules. Interbedded with buff marly beds. Fossils abundant.	Light to dark gray, light brown, dense to medium-grained; thin-bedded; platy parting subparallel to bedding; fossils concentrated in certain horizons, missing from many beds; chert nodules locally in layers; limestone weathers white to light gray, generally smooth or slightly pitted surface, interbedded yellowish, fine- to medium-grained marls; weather reddish brown, varicolored. Interbedded light brown breccia of angular to subrounded limestone pebbles and small cobbles in medium-grained limestone matrix.	Light gray, light brown, dense to medium-grained limestone; poorly bedded to thin-bedded; local concentrations of fossils, local bands of chert nodules, and thin sheets (1-3 in.) of richly fossiliferous chert; weathers light gray to white, smooth to slightly pitted surface. Interbedded with lenticular limestone breccias with calcite cement; conglomerates composed of limestone pebbles and cobbles with subordinate sandstone, chert, and quartz pebbles in sandy limestone matrix.
Basement Sandstone	Brown, bluish to pinkish, coarse-grained sandstone; cross-bedded; friable; dominantly quartz, scattered well-rounded chert and quartz pebbles, rare subrounded limestone pebbles. Interbedded, thin, impure brown to red limestones.	Red-brown to pinkish, very fine- to coarse-grained quartz sandstone with minor chert and dark minerals; weakly to strongly cemented with calcite; locally cemented with silica; locally cross-bedded, generally poorly bedded; weathers rust red. Inter-	Very light gray, pale orange, varicolored, fine-to coarse-grained quartz sandstone with minor chert and dark minerals; weakly to strongly cemented with calcite, locally cemented(?) with silica to form very hard quartzite; cross-bedded to poorly bedded;

Table 2.--Continued. Lithologic comparison of Permian, Triassic(?), and Cretaceous rocks

Rock	Eastern Glass Mountains (King, 1930)	Northeasternmost Glass Mountains (author)	Sierra Madera (author)
Basement Sandstone		.bedded with conglomerate of well-rounded chert and quartz granules, pebbles, and cobbles and subrounded limestone and dolomite pebbles.	local slump structures. Interbedded with lenticular limestone granule conglomerate with rare chert and quartz pebbles; local lenses of argillaceous sandstone and claystone; thin conglomerate of limestone pebbles with rare chert and quartz pebbles in medium-grained sandstone or siltstone matrix near base.
Bissett Conglomerate	Well-rounded large pebbles of limestone, dolomite in sandy, calcareous matrix; interbedded with red shales in lower part; rare chert, quartz, and quartzite pebbles in upper part. Interbedded yellow, dense limestone and brown, fine-grained sandstone in upper part.	Conglomerate composed of subrounded to well-rounded pebbles, cobbles, and boulders of limestone, dolomite, and sandstone in calcite matrix; locally sandy matrix; locally contains chert and quartz pebbles and cobbles. Some interbedded buff, very fine- to fine-grained quartz sandstone lenses to 10 feet thick.	Bissett(?) conglomerate. Pebbles and cobbles of limestone, dolomite, sandstone, chert, and quartz in coarse, calcareous sandstone matrix. Interbedded with mottled yellowish gray, moderately silty claystone.

11

Table 2.--Continued. Lithologic comparison of Permian, Triassic(?), and Cretaceous rocks

Rock	Eastern Glass Mountains (King, 1930)	Northeasternmost Glass Mountains (author)	Sierra Madera (author)
Tessey Limestone	Gray to dark gray dolomite and dolomitic limestone; poorly bedded, locally laminated; locally oolitic; rarely fossiliferous; local dolomite breccia with sandstone matrix interbedded with sandstone, gypsum. Upper part has many angular limestone and dolomite cobbles in dolomitic matrix.	Light to medium brown, dense to fine-grained dolomite; massive to crudely bedded; locally laminated; no fossils, chert rare; dolomites often brecciated and show transitions from unbrecciated, laminated dolomite to thoroughly mixed breccia in single beds; breccias of angular dolomite fragments from microscopic to cobble size or larger in calcite matrix; weathers dirty gray, jagged surface. Interbedded with light gray or light brown, dense to medium-grained, unfossiliferous limestone, limestone breccia, and limestone conglomerate; weathers with smooth or slightly pitted surface. Local dolomite breccia with fine-grained sandstone matrix and buff, fine-grained sandstone near base.	Light to dark brown, dense to medium-grained dolomite; massive, locally crudely bedded, locally laminated; thin-bedded at base; breccias of angular dolomite fragments from sand size to large boulders in calcite matrix; locally oolitic. Interbedded with light gray, dense to medium-grained, unfossiliferous limestone and limestone breccias; limestone locally laminated.

12

Table 2.--Continued. Lithologic comparison of Permian, Triassic(?), and Cretaceous rocks

Rock	Eastern Glass Mountains (King, 1930)	Northeasternmost Glass Mountains (author)	Sierra Madera (author)
Gilliam Limestone	Light gray to light brown, dense dolomite; thin-bedded. Interbedded with brown, fine-grained sandstone; local gypsum beds to 3 ft thick. Upper sandstones have much interbedded red shale, some blue shale and a few thin gypsum beds. Great abundance of fusulinids.	Light to medium brown or light gray, dense to microcrystalline dolomite; very thin-bedded; interbedded with yellowish, very fine-grained calcareous sandstone and siltstone; no fossils, no chert; both sandstones and dolomites are lenticular; dolomites are rarely brecciated and show lateral transitions from breccia to massive dolomite in single beds. Dolomites have pronounced bedding plane parting; sandstones locally have slump folds. Dolomite weathers light gray, generally with smooth surface; sandstones weather yellowish orange.	Light to medium brown, dense to microcrystalline, unfossiliferous dolomite; thin-bedded; commonly brecciated and cemented by fine-grained calcite; lateral transitions from brecciated to unbrecciated dolomite in single beds. Interbedded with buff to brown, very fine- to fine-grained quartz sandstones with calcareous cement.
Word Formation	Gray dolomite; massive; contains large masses of calcite; interbedded thin beds of dolomite. Dense, platy, bituminous limestone at base. Upper limestone unit contains abundant fossils and chert.	Light gray or light brown, dense to medium-grained limestone; thin-bedded, locally thinly laminated; chert fossils abundant, fossils rare. Interbedded with light brown, dense to very fine-grained calcareous dolomite, some thin	Word Formation(?). Light gray, light brown, dense to fine-grained, locally fossiliferous limestone. Interbedded(?) with light to dark brown, microcrystalline dolomite and dolomite breccia with fine-grained calcite cement.

Rock	Eastern Glass Mountains	Northeasternmost Glass	Sierra Madera (author)
Word Formation, Vidrio Member		buff marly beds; thin (to 2 ft) conglomerate of chert and quartz granules and small pebbles in fine-grained calcareous quartz sandstone matrix. Limestones weather dirty gray, smooth to slightly pitted.	Light to dark brown, dense to medium-grained, unfossiliferous dolomite; massive to thick-bedded, rarely laminated; irregular and disc-shaped cavities common and often filled with coarse calcite; chert nodules rare. Uncommon lenticular buff marly beds a few inches thick. Dolomite weathers gray-brown, hackly surface. Marly beds weather yellowish.
Leonard Formation, conglomerate member	Limestone with abundant quartz pebbles in lower part. Grades up into fossiliferous limestone interbedded with marl and siliceous shale. In east consists of dolomites distinguishable from Hess and Word only in content of sand and pebbles.		Light yellowish-white to pinkish conglomerate and sandstone; conglomerates of chert, quartz, dolomite, and limestone granules and pebbles in fine-grained quartz sandstone matrix; locally matrix is sandy dolomitic limestone; sandstones are buff, fine-grained, quartzose with calcareous matrix. Interbedded with thin (1-2 ft) dolomitic limestone and calcareous dolomite.

Table 2.--Continued. Lithologic comparison of Permian, Triassic(?), and Cretaceous rocks

Rock	Eastern Glass Mountains (King, 1930)	Northeasternmost Glass Mountains (author)	Sierra Madera (author)
Leonard Formation, Hess Member	Dark dolomitic limestone; thin-bedded; abundant fusulinids. Thin limestone with limestone pebbles in upper part. Thin basal conglomerate. Marls, sandstone, and shale in lower part to east.	(upper 300 feet only) Light to dark brown, light gray, dense to microcrystalline calcareous dolomite and dolomite; thin-bedded with prominent bedding plane parting; locally thinly laminated; fossils rare and poorly preserved; chert rare; locally sandy; locally veined by coarse calcite; weathers dirty gray, sometimes with hackly but generally with smooth surface. Interbedded thin (to 3 ft) conglomerates of quartz, chert, and dolomite granules and pebbles in dolomitic matrix.	

Because of the severe deformation at Sierra Madera, reliable
thicknesses of formations are difficult to obtain. The Tessey Limestone
was estimated to be about 400 feet thick (Shoemaker and Eggleton, 1964)
in contrast to its thickness of 1000 feet in the northeastern Glass
Mountains. The Basement Sandstone has an irregular thickness, with a
maximum of about 50 feet, but is missing in places, probably by non-
deposition. This indicates the presence of local relief at Sierra
Madera during deposition of the Basement Sandstone. Estimates of thick-
nesses of the Gilliam Limestone and older formations must await further
mapping.

Structure

The Sierra Madera structure is nearly circular (fig. 3) and, as
presently recognized, has a diameter of about 9 miles. The principal
subdivisions of the structure, most of which are clearly revealed by
the topography (fig. 3), include a central breccia core about 1-1/2
miles in diameter (fig. 3, zone 1), an inner belt of severely deformed
Permian and Cretaceous rocks about 1 mile wide (fig. 3, zone 2), an
alluviated depression about 2-1/2 miles wide on the west side and 1/2
mile wide on the east side (fig. 3, zone 3), and an outer rim about
1/2 to 1-1/2 miles wide of generally mildly deformed Cretaceous rocks
(fig. 3, zone 4). Zones 3 and 4 have not been included before in the
Sierra Madera structure, but the topography of zone 4 is concentric
to the core and the inner belt of highly deformed rocks and so probably
formed during the same event or events that formed the central part of
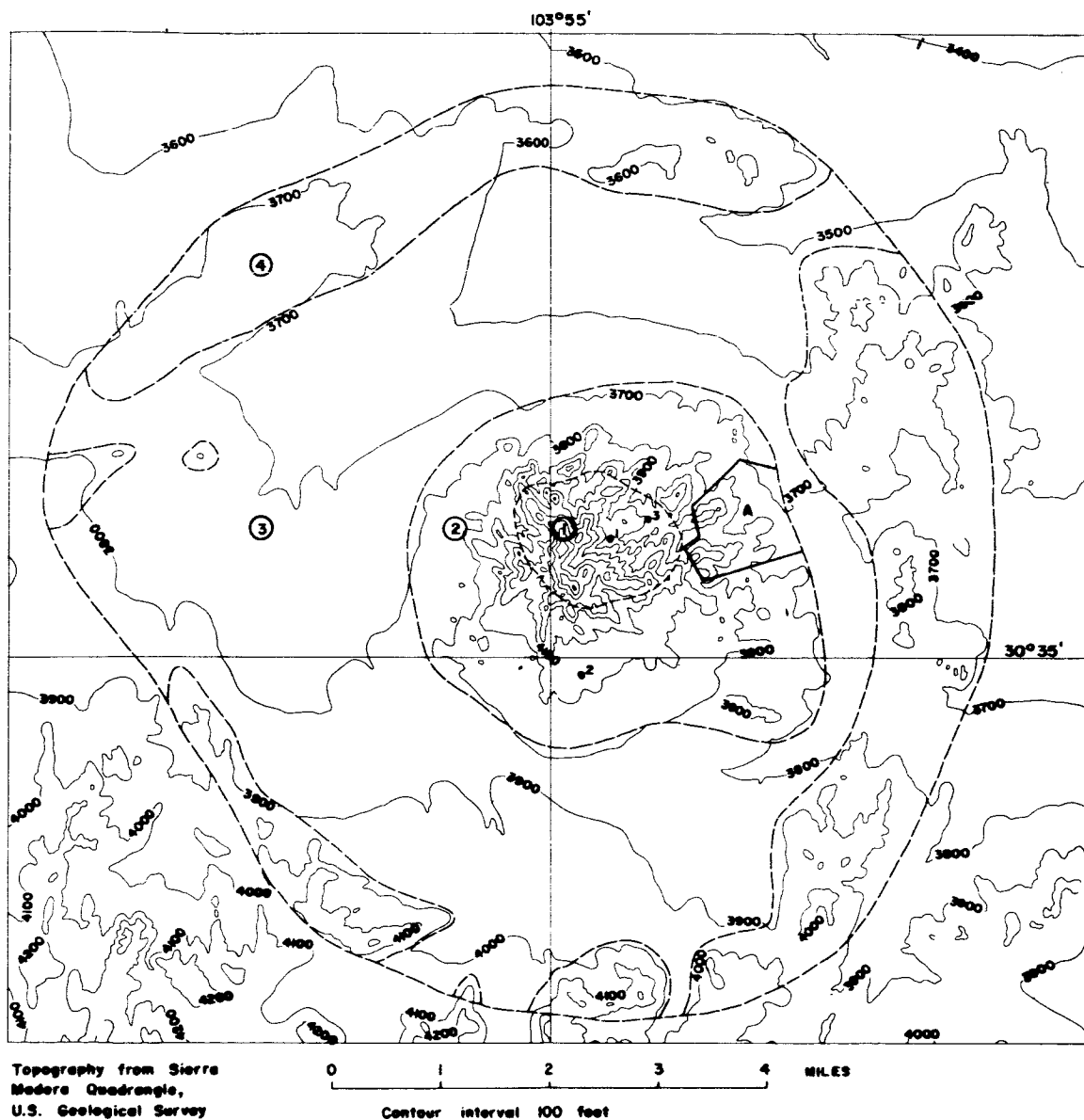
Fig. 3.--Topographic map of Sierra Madera showing principal structural subdivisions. Circled numbers: 1, breccia core; 2, severely deformed Permian and Cretaceous; 3, alluvium-filled depressions; 4, mildly deformed Cretaceous. Area labeled A is that shown in figure 4. Drill holes shown by dots: 1, Phillips Elsinore 1; 2, Hunt Elsinore 48; 3, Thompson Elsinore 1.

Geology by E.M. Shoemaker
and R.E. Eggleton, 1961-1962;
H.G. Wilshire, 1965.

102°53'

0   500   1000   2000   FEET
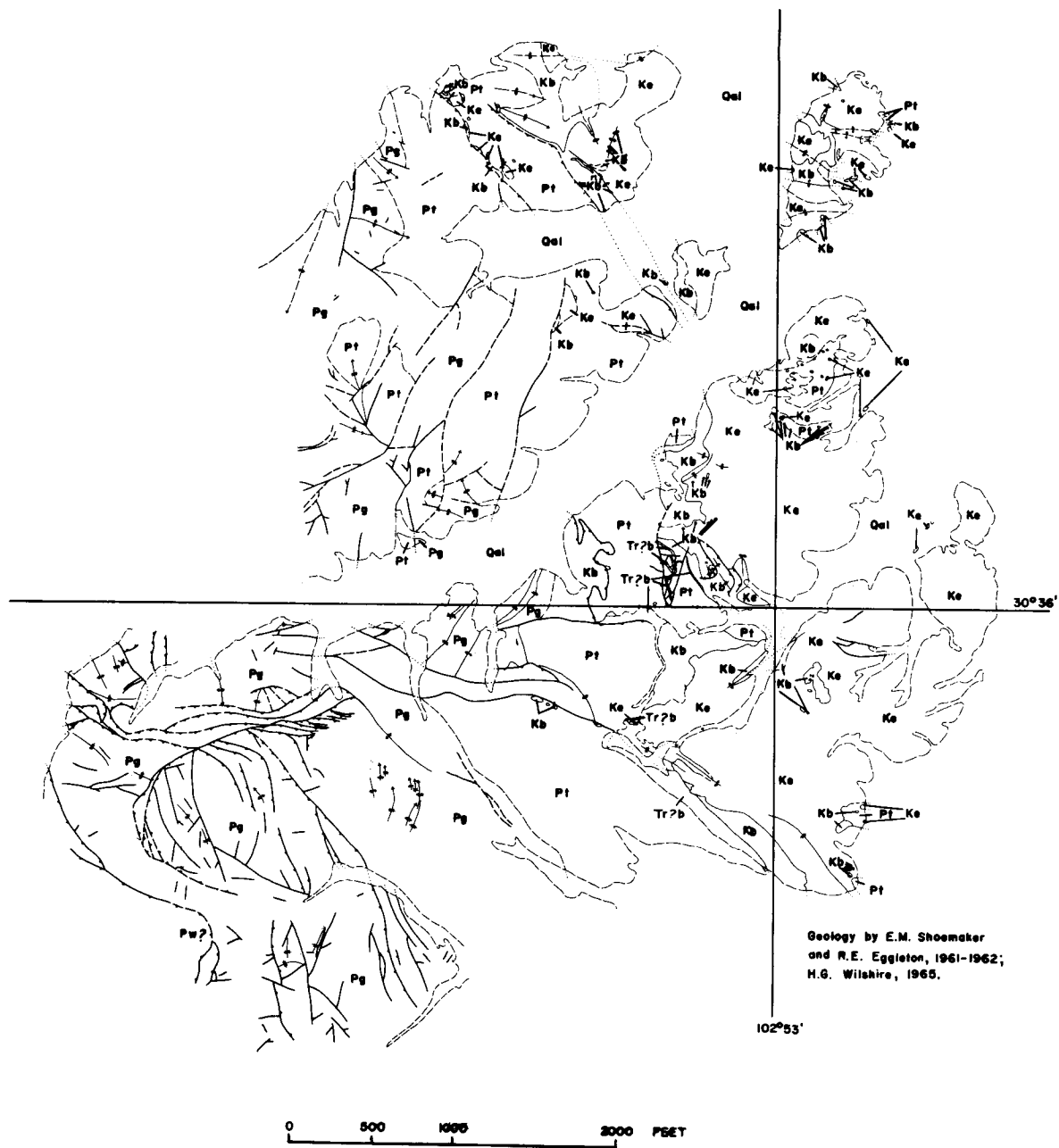
Fig. 4.--Generalized geologic map of part of Sierra Madera.

EXPLANATION

Qal

Alluvium

Ke

Edwards Limestone

Kb

Basement Sandstone

Tr?b

Bissett Conglomerate (?)

Pt

Tessey Limestone

Pg

Gilliam Limestone

Pw

Word Formation (?)

Quaternary

Cretaceous

Triassic?

Permian

Contact
   Dashed where approximately located; dotted where concealed by alluvium.

$\dfrac{U}{D}$

Fault
   Dashed where approximately located; dotted where concealed by alluvium.
U, upthrown side; D, downthrown side.

▲ ▲ ▲ ▲ ▲ .....
Thrust fault
   Teeth on upper plate; dashed where approximately located; dotted where concealed by alluvium.

Anticline
   Direction of plunge showing

Syncline
   Direction of plunge showing.

the structure; there are, furthermore, local areas within zone 4 of intense deformation unlike that found in Cretaceous rocks elsewhere in the region. The discontinuous nature of zone 4 (fig. 3) is due to postdeformation erosion, and the outer limit of zone 2 is based on the limits of exposure; modifications of these boundaries are to be expected as detailed mapping progresses.

Mapping to date has been confined to zone 2 and is shown in generalized form in figure 4. Field mapping is being done on aerial photographs at an approximate scale of 1:5000.

On the ridge north of that mapped by Shoemaker and Eggleton (1964), the structural elements are essentially the same, but major steeply dipping normal(?) and reverse faults trend nearly at right angles to the transverse faults mapped by Shoemaker and Eggleton. The valley separating the two ridges is probably structurally controlled, but the nature of the structure has not yet been determined. All of the formations mapped on the north ridge are tightly folded and severely faulted by normal(?) and reverse faults with slight transverse movement. Thrust faults resulted in movement of the Tessey Limestone away from the center of the structure and over the Cretaceous formations. Rocks above and below the thrust faults are folded and faulted, but no transition of thrust faults into folds was observed on the north ridge, nor is there any clear indication here that the amount of displacement on thrust faults diminishes away from the center of the structure as noted

by Shoemaker and Eggleton on the south ridge. There is no doubt, however, that the general severity of deformation increases toward the center of the structure.

The irregular outcrop pattern of the Basement Sandstone and Edwards Limestone at the northeast edge of the mapped area (fig. 4) is interpreted entirely as folds whose axes trend toward the center of the structure, but bedding attitudes are generally lacking and the relief of that area is too low for observation of the three-dimensional relations. However, the attitude of the contact between the Basement Sandstone and Edwards Formation was measured in several places and dips of as much as 80° were recorded.

Variation in the bedding attitudes of the Tessey Limestone indicate severe internal deformation, but there are too few mappable subdivisions to locate the structures precisely. This formation is generally massive or thick-bedded, and it is unlikely that many of its contacts with the tightly folded Gilliam Limestone are unfaulted. However, the lack of transverse movement on the northeast-trending faults separating the Gilliam and Tessey (fig. 4) suggests that relative movements along contacts not indicated as fault contacts is slight.

Internal structures in the Gilliam Limestone are more easily located because the formation is composed of dolomite and sandstone in thin, mappable beds. Except in places farthest from the center of the structure, the Gilliam dolomites and sandstones are tightly folded and are cut by numerous faults of every description. The major faults

in the southwest part of the mapped area (fig. 4) are low-angle thrust faults, some of which probably pass laterally into steeply dipping reverse faults, and reverse faults whose traces are roughly concentric with the core of the structure. Many of the small faults that trend roughly toward the center of the structure are tear faults on the upper plate of the thrust faults, and most of the other faults have formed along minor fold axes of apparently random orientation; few fold axes remain unfaulted.

Although zone 1, the central breccia core, has not yet been mapped, new data from the Phillips No. 1 Elsinore well (fig. 3) have an important bearing on earlier interpretations. Correlations by Addison Young (see Eggleton and Shoemaker, 1961) of a middle Leonard anhydrite zone between the Phillips well and other nearby wells (fig. 3) indicates a structural relief of only about 500 feet at a depth of about 3000 feet. Breccia was found in the Phillips well cuttings to a depth of 1600 feet and possibly to 2800 feet (Eggleton and Shoemaker, 1961) and was identified, along with unbrecciated dolomite to a depth of 4100 feet, as the **Formation Leonard** (Young, as cited by Eggleton and Shoemaker, 1961, p. 153). The thickness of 4100 feet assigned to the Leonard is nearly twice that in the Glass Mountains and is about 1500 feet thicker than that found in the nearby Hunt No. 48 Elsinore well (fig. 3). The abnormal thickness of the Leonard Formation in the Phillips well was considered by Young (1952) to be due to steep dips, and by Eggleton and Shoemaker to be due to brecciation, both inter-

22

pretations being somewhat compromised by the low structural relief

on the anhydrite member of the Leonard Formation.

Re-examination of fusulinids from the upper 3000 feet of the

Phillips well by C. A. Ross (written communication, 1965) revealed,

however, that the rocks in the top 1300 feet belong to the Word

Formation.[1] The Leonard Formation is, therefore, less than 150 feet

thicker in this well than in the Hunt well, and the total known thick-

ness of the Word Formation is comparable to its thickness in the Glass

Mountains. These data suggest that the subsurface structure from the

Leonard to older formations, is simple despite the high degree of

brecciation in the top 1600 feet of the section, and, combined with

the low structural relief on the anhydrite bed and downward decrease

in amount of brecciation, lend further support to the theory that

Sierra Madera is an impact structure.

------

[1]Identification of surface exposures as Leonard at the Phillips
well site was probably based on King's (1930) map which is now consid-
ered to be in error. Three reconnaissance traverses to the center of
the structure failed to reveal the conglomerate member of the Leonard
Formation which was the basis of King's identification of Leonard in
the core of the structure. A specific outcrop of this member cited by
King (1930, p. 67) was found to be a conglomerate interbedded with
fusulinid limestones of probable Word age. Other fossiliferous lime-
stones lithologically similar to limestones of the Word Formation in
the Glass Mountains were found near the center of the breccia core and
about 300 feet higher than the Phillips well site.

References

Adams, J. E., 1935, Upper Permian stratigraphy of west Texas Permian

 Basin: Am. Assoc. Petroleum Geologists Bull., v. 19, no. 7,

 p. 1010-1022.

Eggleton, R. E., and Shoemaker, E. M., 1961, Breccia at Sierra Madera,

 Texas: U.S. Geol. Survey Prof. Paper 424-D, p. 151-153.

King, P. B., 1930, The geology of the Glass Mountains, Texas--Pt. 1,

 Descriptive geology: Univ. Texas Bull. 3038, 167 p.

_____ 1935a, Outline of structural development of trans-Pecos Texas:

 Am. Assoc. Petroleum Geologists Bull., v. 19, no. 2, p. 221-261.

_____ 1935b, Age of Bissett conglomerate: Am. Assoc. Petroleum

 Geologists Bull., v. 19, no. 10, p. 1544-1546.

_____ 1942, Permian of west Texas and southeastern New Mexico: Am.

 Assoc. Petroleum Geologists Bull., v. 26, no. 4, p. 535-763.

Ross, C. A., 1962, Permian tectonic history in Glass Mountains, Texas:

 Am. Assoc. Petroleum Geologists Bull., v. 46, no. 9, p. 1728-1746.

_____ 1963, Standard Wolfcampian Series (Permian), Glass Mountains,

 Texas: Geol. Soc. America Mem. 88, 205 pp.

Sellards, E. H., 1932, The pre-Paleozoic and Paleozoic systems in

 Texas, in The geology of Texas, v. 1: Univ. Texas Bull. 3232,

 p. 15-231.

References--Continued

Shoemaker, E. M., and Eggleton, R. E., 1964, Re-examination of the stratigraphy and structure of Sierra Madera, Texas, in Astrogeologic Studies Ann. Prog. Rept., Aug., 1962-July, 1963, pt. B: U.S. Geol. Survey open-file report, p. 98-106.

Vertrees, C., Atchison, C. H., and Evans, G. L., 1959, Paleozoic geology of the Delaware and Val Verde Basins, in Geology of the Val Verde Basin and field trip guidebook: West Texas Geol. Soc., p. 64-73.

Young, A., 1952, Geologic section in Phillips Petroleum Company's Elsinore Cattle Company No. 1, in Marathon Basin, Brewster and Pecos Counties, Trans-Pecos Texas field trip guidebook: West Texas Geol. Soc., p. 72-73.

STRUCTURAL GEOLOGY OF THE LARGER HENBURY CRATERS[1]

by Daniel J. Milton

Introduction

The meteorite craters at Henbury, Northern Territory, Australia, were mapped geologically during the winter of 1963 as part of a program of investigations of meteorite impact features being conducted by the U.S. Geological Survey on behalf of the National Aeronautics and Space Administration. The Henbury craters have been known since the reconnaissance investigation by A. R. Alderman (1932). Although studies of the meteorites and of impact metamorphosed material (Spencer, 1933; Chao, 1964; Taylor and Kolbe, 1964) and a magnetic survey (Rayner, 1939) have been made, no detailed geologic examination had previously been carried out.

Twelve craters (Alderman's "ill-defined and doubtful" crater No. 9 is probably not a crater) occur within a quarter mile square at 24°34'S, 133°08'E, about 7 miles west-southwest of the Henbury homestead. During the first month of the field season, F. C. Michel and the writer made plane-table geologic maps of two of the smaller craters, No. 3 (Milton and Michel, 1965) and No. 10, and made a

---

[1] The sections and units referred to in this paper are those on the map of the Henbury crater field in the Map Supplement to this report.

plane-table topographic map at a scale of 1 inch to 30 feet of the main

group of large craters: the Main Crater (No. 7), the Water Crater

(No. 6) to the southeast and No. 8 of Alderman (1932) to the southwest.

The writer then spent the remaining two months mapping the geology

on this base (see map in Map Supplement).

The regional geography is well covered by R. A. Perry and others

(1962); the description of the Chandlers land system of their classi-

fication fits the vicinity of the craters well. Rainfall is about

8 inches, mostly in summer storms. Mulga grows along water courses,

but the plains around the craters and the crater walls have only a

sparse growth of needle bush and other shrubs. The floor of the Main

Crater is sparsely covered by saltbush. The wall of the Water Crater

has been breached and the upper part of a preimpact drainage system

has been captured so that water stands in the crater floor after rains.

Consequently, the largest trees in the vicinity grow in this crater,

among which whitewood is dominant. Cattle browse over the area, par-

ticularly when the Water Crater is the only nearby source of water.

Rabbits have discovered that the section of pediment gravel exposed

in the upper walls of the craters is the best place in the vicinity

for burrowing. Erosion of the craters probably has accelerated since

the native fauna was augmented by cattle and rabbits.

Geologic setting

The bedrock at the Henbury craters belongs to the Pertatataka
Formation of Late Proterozoic age (Ranford, Cook, and Wells, in press).
The craters are on the south flank of a broad anticline. Resistant
sandstones predominate in the upper part of the Pertatataka Formation
and a series of ridges (the Bacon Range) lie at the south edge of the
crater field (fig. 2B). At the main group of craters, however, bedrock
consists of weak shales and siltstones with only a few thin beds of
indurated sandstone. As a consequence, the vicinity of these craters
lie in a "gibber plain," a gently sloping pediment in which bedrock is
concealed by alluvial cover. Exposed bedding near the crater field
shows consistent attitudes with strikes close to east-west and dips to
the south of about 35°. Although a major thrust fault is exposed near
the crest of the Bacon Range, no faults and only a few small folds
were noted in reconnaissance nearer the crater field. Preimpact de-
formation may have been greater, however, in the incompetent beds near
the large craters and might be responsible for some of the unexplained
stratigraphic and structural anomalies. Nevertheless, with minor local
exceptions, the structures mapped may be assumed to have formed at the
time of impact from a simple homoclinal sequence.

Only a single nearby outcrop is on strike with the larger craters.
The stratigraphic column is therefore based entirely on interpretation
of the exposures in the crater walls, and some uncertainties remain

because of original lenticularity of units, precrater deformation, or incomplete decipherment of impact deformation. The units in the sequence from E through H closely resemble corresponding units in the sequence from A through D, but there are sufficient differences to rule out repetition of section. Instead, a cyclic pattern of deposition seems to be indicated. About 450 feet of section is exposed in the larger craters, in which twelve major units and several minor beds have been mapped. As exposed in the crater walls, the shales and siltstones, which make up the bulk of the section, crumble into chips or fragments a few inches in size, and can easily be excavated with a shovel. The sandier siltstones and sandstones are more indurated and break into larger plates. Only in the south wall of the Water Crater are there sandstone beds sufficiently indurated to break into blocks several feet across.

The bedrock is covered by a varying thickness of pediment gravel consisting of cobbles and smaller subrounded fragments of sandstone and "gray billy" (strongly silicified rock) from the ridges to the south, and rounded pebbles of more distant provenance, in a red silty matrix. The thickness of the pediment gravel depends on the underlying material--it is thin or even absent over the more resistant sandstone beds and may be 10 or 15 feet thick over shale. Shale units are commonly weathered as much as 10 or 15 feet below the pediment gravel and may grade upward into a reddish clayey soil.

29

Structures in the crater walls

The Henbury craters are not large--the larger end of the apparent-
ly double Main Crater (fig. 1) is less than 500 feet in diameter. Com-
plexities of structure, however, are well exhibited by displacements
of the dipping beds and of the essentially horizontal unconformity at
the base of the pediment gravel. Dissection of the craters has reached
a nearly ideal point--the spurs between the gullies have retreated
only slightly from the original crater walls, while the gullies them-
selves present an opportunity to examine cross sections of the walls.
Much of the walls are covered by alluvium, but exposures are well
distributed to allow examination of structures up dip, down dip, and
on strike with the centers of impact.

Separation of the structures in the crater walls from those on
the crater rims is somewhat arbitrary but convenient for the purpose
of discussion. The greater amount of erosion in Meteor Crater, Arizona
(Shoemaker, 1963), and of fill at the Odessa craters, Texas (Evans,
1961), have restricted study of the walls to the upper portions near
the crater lip. Structures in previously mapped meteorite craters are
thus not closely comparable to those of the Henbury craters.

The structures in the walls are largely described in terms of
folds. These are not continuous folds like those formed by slow in-
tragranular movement in ordinary geologic environments but rather
mosaics formed by the reorientation of fracture-bounded blocks that

Fig. 1.--Main crater from northwest rim. Ejecta from units B, C, and D in foreground, pediment gravel in middle ground.
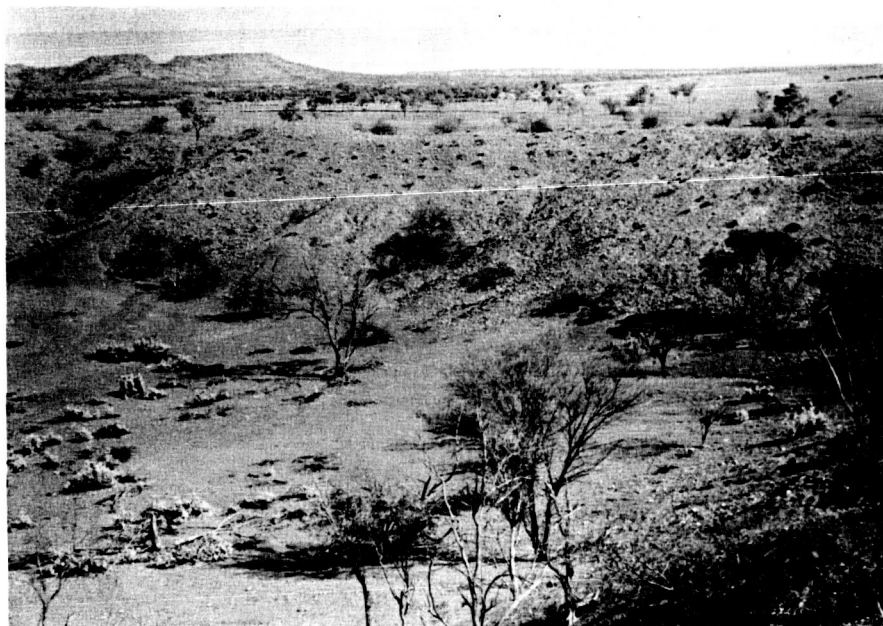
31

Fig. 2A.--North wall of Main Crater. Units A and B in anticline crop out in pebble-free areas along base of wall.

Fig. 2B.--South wall of Main Crater. Line of section E-E' follows gully in center. Water Crater in left middle ground and Bacon Range on skyline.

are themselves little deformed. The fractures are usually so closely spaced--commonly on the order of an inch or inches--that the appearance of continuous smooth folds is produced.

Section A-A' is taken nearly parallel to the regional strike, so that it should be comparable to a section through the wall of a crater in flat-lying strata. The major structures are a synclinal fold that brings up unit B at the base of the wall and a broad anticline in the midslope. In detail the lower wall exhibits an imbricate structure, with thin plates thrust outward[2] short distances. The plate between the two thrust surfaces shown on the section has nearly horizontal bedding with a steeply upturned outer edge. This plate overrides the next segment of the wall above, which again has flat-lying beds that steepen outward at the synclinal bend shown on the map. The transition to the next segment of gentle dips is in this case not a discontinuity but a small sharp anticline which is too small to show on the section.

Section B-B' is typical of the wall of the Main Crater. The dominant feature is an anticline with a nearly horizontal axis running along the base of the wall just above the present crater floor (fig. 2A). The anticline is asymmetric--the dip of the craterward limb is little different from the original dip of the beds, whereas the short outer

------

[2]The reference point for "inward" and "outward" is the center of the crater, so that beds may dip outward into the crater wall, and so on.

limb is, on the whole, close to vertical, with the beds rotated more than 120°, although it contains some tight subsidiary folds. Along much of the anticline the inner limb is thrust over the crest. There are culminations and depressions along the axis of the anticline and broad open cross folds on the gently dipping limb which plunge radially inward. Higher on the crater wall are some very tight but small-amplitude horizontal folds and some open radially plunging folds.

The topographic expression of the anticline is in part erosional --units A and B are slightly more resistant than unit C--but in part it may be an original feature of the postimpact topography. If so, it would suggest a complex pattern of deformation. Either a simpler wall was produced by the first compression and rarefaction waves and was then deformed, or the acceleration did not decrease monotonically outward from the point of burst. In connection with the latter possibility it may be noted that in certain experimental hypervelocity impact craters a doughnut-shaped ring of material remains around the lower part of the crater walls (H. J. Moore, oral communication). It is perhaps also significant that certain lunar craters, for example Ritter (see Ranger VIII, camera A photographs), have low ridges around the base of the walls.

A different type of folded structure predominates on the opposite wall of the Main Crater, where the original dip of the beds is outward from the crater (fig. 2B). At the base of the wall tight folding about more or less vertical axial planes indicates radial compression.

Above (see section E-E'), the overall dip steepens to form a synclinal structure, but superimposed on this are a series of small folds with axial planes dipping shallowly into the crater (fig. 3). A minor thrust fault parallel to the axial planes (fig. 3A) indicates that the folds are not simple compressional folds but rather shear folds produced by principal stresses acting parallel to the axial planes and varying in intensity at right angles to them. It might be noted that, as erosion proceeds into the wall, the type of fold apparent at any level on the surface will alternate from synclinal to anticlinal.

The same effect can be seen in section D-D', where within an apparently little deformed wall is a zone in which the rock is displaced outward in an open fold with a smaller but much sharper fold of the same sense in the upper part. The base of the main fold is in part a thrust surface on which the folded rocks moved outward over unfolded rocks. The whole structure indicates a localized punchlike stress into the wall.

The middle portion of section D-D' illustrates the deformation in a wall between two craters. As might be expected, the rock is thrown into a series of folds. The bedrock at the crest is at least 20 feet higher than its preimpact elevation. The structure at depth is unknown; a series of décollements along small thrusts seems likely.

A more complex wall structure is exhibited in section C-C'. The ridge in the vicinity of this section is the remnant of a wall between coalescing craters produced by the impact of objects in the centers of

Fig. 3A.--Gully wall along line of section E-E'.
Unit E with unit F at extreme right. Small thrust
fault offsets prominent sandstone bed from below pick
point to one foot uphill from handle.

Fig. 3B.--Closeup of
folds at left in figure 3A.

Fig. 4A.--Lowermost fault shown on section C-C'. Flat faces to left are bedding in upper craterward plate. Knife blade is in plane of bedding in overturned lower plate, with tops to left.

Fig. 4B.--Head of gully south of line of section C-C' near rim crest. Gently dipping unit E has moved outward (to left) overriding steeply dipping overturned beds below. Pediment gravel crops out just below picture.

Fig. 5A (above).--Wall of gully opposite line of section C-C'. "Thrust" surface separating unit E above and D below follows steplike course from lower right to upper left corner. Flexures to both right and left in top of lower block can not be interpreted as due to drag; they may have formed by the sudden fall of the upper plate onto the lower block.

Fig. 5B (left).--Detail along "thrust" surface across gully from line of section C-C'. Bedding in block to left of knife is nearly at right angles to bedding either above or below "thrust" surface.

38

the two ends of the oval Main Crater. Although some of the complexity is probably due to the two interacting stress fields, for the most part these cannot be resolved and the structure may be considered as resulting simply from stresses acting in the plane of the section. A plate of rock only slightly deformed and retaining nearly its original attitude over-lies a zone of much more deformed rock below and outward from it. To this extent the section resembles section B-B', but in fact the sense of deformation is exactly opposite. The fold in section B-B' formed by a couple in which the upper part moved outward over the lower. In section C-C' the lower block is displaced outward relative to the upper plate (fig. 4A). In the exposed portion of the lower block the dip has been rotated from the original south dip to an overturned north dip. The completion of the folds in the lower concealed portion is hypothetical. The structural relations of this block are analogous to those of the upper portion of the fold in section D-D', much magnified and with a break at the top as well as at the bottom. The attitudes in the lower block are maintained farther outward in the gully east of the line of section and probably represent the same sense of displacement (fig. 5A). Indicators of bedding tops are lacking in these beds, however, and the possibility of isoclinal folding cannot be eliminated.

The actual surface of the underthrust is not smooth but irregularly stepped (fig. 5A), so that actual motion along it would be impossible. Figure 5B shows a small block along the fault surface with its bedding oriented nearly at right angles to that both below and above. It could have reached its present orientation only while out of contact with the adjacent blocks. Impact must have produced a momentary dilatation,

during which structural blocks in the wall deformed and rotated more or less independently of each other, and then the whole mass settled into its present interlocked pattern. Such a mechanism of deformation is supported by the absence in all of the craters of slickensides or gouge related to the impact and the scarcity (except in ejecta) of fine-grained breccia.

Structures in the crater rims

The structural style on the rim crests and rim flanks is as varied as that in the walls. The distinction between debris and disturbed bedrock is much less clear-cut than was found at Meteor Crater by Shoemaker (1963) and these have not been explicitly distinguished on the map. Attitudes were, however, recorded wherever consistent orientations could be found so that areas of bedrock units on the rims without attitude symbols may be assumed to consist of small fragments with little or no common orientation (this is not necessarily true of areas on the walls, where colluvium hinders the measurement of attitudes). In these patches, however, the fragments are entirely or predominantly from a single bedrock unit. The mixed ejecta unit consists mostly of intimately mixed fragments of several bedrock units and in most places of pediment gravel, but in some areas, particularly on the southeast rim crest of the Main Crater, discrete monolithologic patches or bands can be distinguished, although they are too small and discontinuous to be mapped.

The structural style of coherent ejecta on the rim is related to the style in the walls below. In section E-E' the dips in the upper part of the wall progressively steepen through the vertical into an overturned

attitude (fig. 3A). This synclinal structure is continued on the rim, where a flap consisting of three bedrock units in inverted sequence lies on pediment gravel (fig. 6A). Where it is thinnest, only about a foot of pediment gravel is exposed between the bedrock in place in the wall and the bottom of the flap. The consistent attitudes in the flap might suggest that it is merely the overturned limb of a fold, but the greatly reduced thickness of the beds and the pinchout of unit F between units G and E down the wall of the Water Crater show that this is not so. To explain the thinning it must be assumed that the flap consists of thin slices that formed by strong shearing parallel to the bedding and active simultaneously with the outward rotation. Much of the minor structure in the flap, such as the two plunging inverted synclines, is probably a reflection of the topography on which the flap fell. The extension of the flap far down on the wall of the Water Crater raises problems concerning the relative ages (which must be measured in fractions of a second) of the Main and Water Craters. If the impacts of bolides in the Main and in the Water Craters were simultaneous, the propagation of the shock wave along the greater radius of the Main Crater may have introduced sufficient delay to allow the flap to settle into the Water Crater. It is also possible that the gully at the northwest corner of the Water Crater developed by erosional modification from another small crater or even a preimpact depression. Exposures on the rim to the west suggest intermingling and interpenetration of ejecta from the Main and Water Craters, but the pattern is not clear.

The greatest thickness of throwout on the rim flank lies on a ridge extending northeast from the Main Crater to beyond the map area. The axis

41

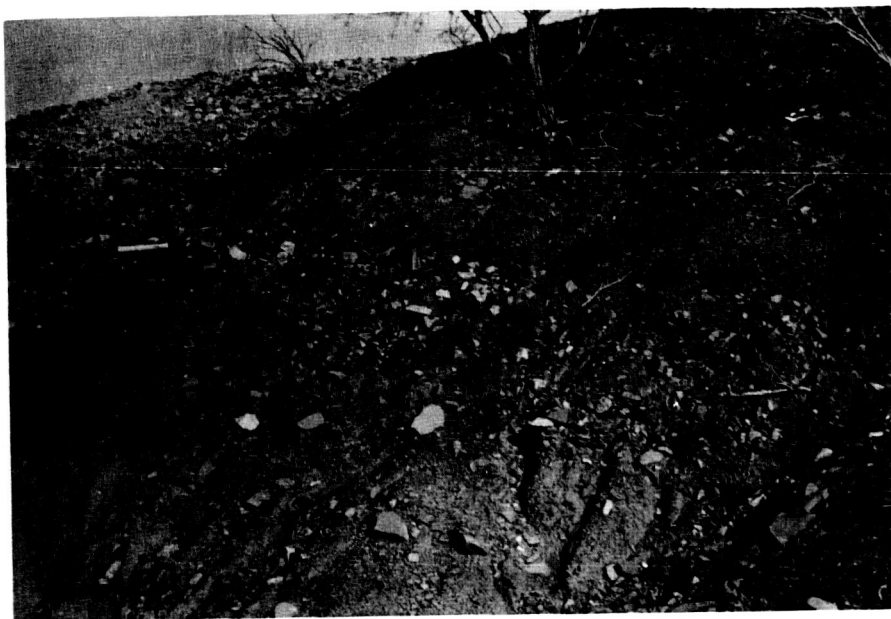Fig. 6A.--Upper wall of Main Crater slightly west of line of section E-E'. Pediment gravel crops out in band running to right from hammer with units F and G in place below and units G, F, and E in overturned flap above.
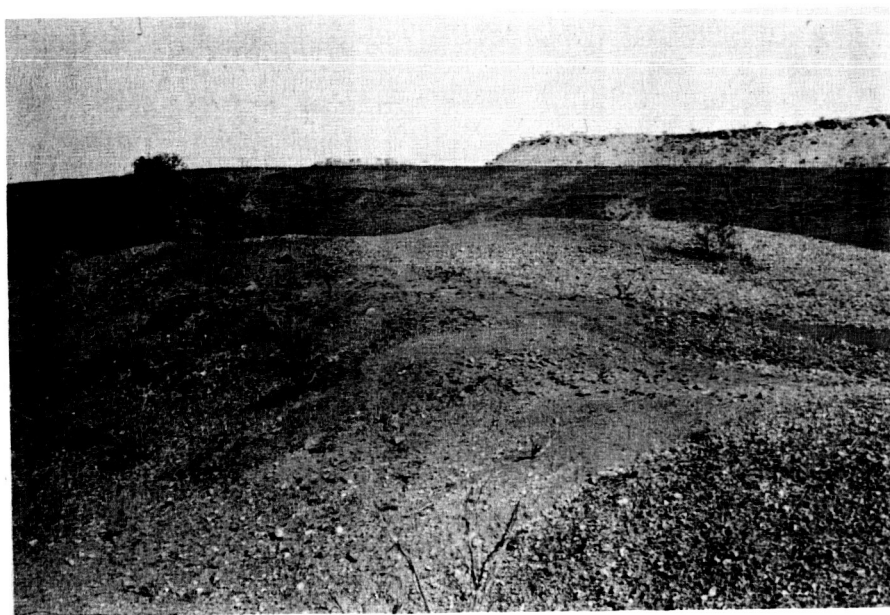

Fig. 6B.--Southwest rim of Main Crater showing thin ejecta over pediment gravel. Smooth areas are unit E with more resistant subunits in blocky areas. Tops of trees growing in the Water Crater at left.

of this ridge lies along the normal to a line joining the centers of circles inscribed in the large and small ends of the oval Main Crater. Vortman (1965) shows topographic maps of similar ridges associated with intersecting craters formed by the simultaneous detonation of separate buried explosive charges.

The structure in the rim near the line of section C-C' again matches the structure in the wall. The general structure is a pile of thrust slices overlying the pediment gravel. For the most part, bedding in these slices is flat-lying or simply folded. The basal parts are more disturbed, but commonly thrust slices with internally consistent attitudes overlie pediment gravel with only a few inches of breccia at their base. Along the line of section, pediment gravel crops out between the bedrock in the wall and on the rim, but in a segment about 40 feet wide to the southeast there is complete continuity between the plate of rock maintaining approximately its preimpact attitude, described with the wall structures, and the thrust slices. The same moderate dips continue outward but the strikes swing into parallelism with the ridge. The beds at the base of this plate are rolled under like a caterpillar tread, so that there is an anticlinal fold with an overturned lower limb (fig. 4B). The axial surface of the fold is sharply defined with some displacement along much of it. Downward, the overturned limb becomes increasingly broken by a series of thrust faults, until a breccia several feet thick overlies the pediment gravel. A similar structure appears in the next gully to the southeast, but on the craterward side of the pediment gravel in the wall. The northwest-trending steeply dipping block of units E_1 and E_2 seems to correspond to the steeply dipping or overturned limb in unit E to the north. The plate of unit F,

43

forming the broad face of the ridge, has ridden above this with the opposite sense of deformation--the outer end has been folded up into a synclinal rather than down into an anticlinal bend.

The contrast with Meteor Crater, where the upturned bedrock only very locally grades into the debris unit, is striking. The increasing sparsity outward of attitude symbols on the map reflects a steadily increasing degree of brecciation. The contact of the ejecta from specific units with mixed ejecta is somewhat arbitrary. The stratigraphic relation of the mixed and unmixed ejecta is uncertain--it could be a lateral transition or an overlap with either unit on top.

A complex structure is shown by the thin patch of ejecta on the southwest rim of the Main Crater (fig. 6B), where the inverted syncline is shown on the map. The beds at the crater lip immediately above pediment gravel are right side up, but within a few feet outward they are folded through nearly 180° to form an overturned flap. Top sense is determinable in these beds, so the structure is well defined. It grossly resembles the structure to the east in the vicinity of section E-E', except that, instead of an overturned syncline with the normal limb lying in the wall and the overturned limb in a detached flap on the rim, both limbs lie on the rim. Apparently simultaneously with or immediately after folding of the rim flap, the entire overturned flap, together with the upper part of the unfolded bedrock, was thrust outward onto the pediment gravel.

Impact metamorphism

All of the mapped ejecta corresponds to the throwout debris mapped at Meteor Crater by Shoemaker (1963). This ejecta (and that exposed in the

crater walls) exhibits no gross indication of impact metamorphism. An exception is the patch of unit E_4 lying just beyond the pediment gravel outcrop east of the northeast ridge. This patch contains fragments of sandstone that are more cohesive than the unmetamorphosed material, but are less dense and have open fractures normal to the bedding. In gross aspect, the fragments resemble the shocked Coconino Sandstone from Meteor Crater, except that broken surfaces have a glassy, granular appearance rather than a chalky one. These fragments are apparently some of the material described by Chao (1964) in which quartz grains were transformed to glass by shock below the melting point, so that the original sand grains are preserved as glass.

The Henbury impactites described by Spencer (1933) and Taylor and Kolbe (1964) lie scattered on the surface of the ejecta blanket north of the Main Crater. They are probably remnants of a blanket corresponding to the fallout layer of Shoemaker (1963), which has nowhere survived erosion as a distinct unit. The impactites probably formed from shaly material in units C or D. Material that has been partially melted but with the original bedding still visible is concentrated on the northeast ridge outside the rim crest. Such material is commonly folded on itself or is even wrapped into the form of lava bombs, indicating that the material was actually molten, unlike the shock-vitrified fragments of unit E_4.

Comparison with other craters

Shoemaker and Eggleton (1961) have suggested that meteorite craters fall into two structural types: the Barringer (Meteor Crater) type in

which the bedding at the crater wall is turned increasingly upward and outward closer to the crater and to the ground surface, culminating in an overturned synclinal flap at the rim; and the Odessa type, in which the bedding is deformed into an anticline with its axial surface just outside the crater wall. Largely by analogy with craters produced by buried nuclear devices, the Barringer type was attributed to greater penetration of the meteorite and the Odessa type to lesser. The Rieskessel in south Germany was suggested as a variant of the Odessa type, characterized by imbricate thrust slices (the Schollen and Schuppen of Bentz, 1927) on the rim, and attributed to the greater relative importance of gravity in the mechanics of large craters (the Rieskessel is 24 km in diameter).

The characteristics of all three structural types can be found in the Henbury craters. The distribution of the features can in part be fitted into a pattern. In the Main Crater, anticlinal folding seems to dominate in the lower part of the walls and synclinal folding above (this is indeed indicated in a generalized crater structure drawn by Shoemaker and Eggleton). The predominance of imbricate thrust slices, much like those of the Rieskessel, on the northeast ridge may be due in part to the near parallelism of the original bedding to the direction of thrust. The underfolding in the lower part of the same section suggests an extreme case of the anticlinal buckling observed at Odessa, perhaps combined with underthrusting of the type observed at Meteor Crater. There is a certain symmetry in this section. In the lower part, beds were overturned by a couple with the greater outward displacement below (fig. 4A), and in the upper part by a couple with the greater outward displacement above (fig. 4B). The small structure in the wall of the Main Crater shown in section D-D', on the

46

other hand, indicates that the outward displacement in at least a small area of the middle part of the wall exceeded that above or below. The variation of structural type from place to place in the crater walls and rims must be partly related to local conditions that cannot be reconstructed after the event.

Summary

Considerable variety is found in the structures in the walls and rims of the larger craters at Henbury. Beds originally dipping into the crater were deformed into concentric folds overturned outward with generally steeply dipping axial planes. Some thrust faulting accompanied the folding and in places an imbricate series of thrust sheets was shoved over the precrater surface on the rim. Beds on the opposite wall of the main crater, which originally dipped away from the crater, were deformed into a series of folds with shallowly dipping axial planes. An overturned flap lies on this side of the crater rim; part of the flap is thrust outward as well as overturned. There is, in general, structural continuity between the crater walls and rims. Outside the rim crests the ejected materials become increasingly broken, but there is rarely a clear line between coherently deformed rock and throwout debris.

Acknowledgments

References

Alderman, A. R., 1932, The meteorite craters at Henbury, central Australia, with addendum by L. J. Spencer: Mineralog. Mag., v. 23, p. 19-32; also *in* Smithsonian Inst. Ann. Rept. 1932, p. 223-234.

Bentz, Alfred, 1927, Geologische Beobachtungen am westlichen Riesrand [Geological study of the western rim of the Ries]: Deutsche Geol. Gesell. Zeitschr., v. 79, p. 405-438.

Chao, E. C. T., 1964, Selective mineral transformation as evidence of meteorite impact, *in* Astrogeologic Studies Ann. Prog. Rept. July 1, 1963-July 1, 1964, pt. B: U.S. Geol. Survey open-file report, p. 39-57.

Evans, G. L., 1961, Investigations at the Odessa meteor craters, *in* Proceedings of the Geophysical Laboratory/Lawrence Radiation Laboratory Cratering Symposium: California Univ., Livermore, Lawrence Radiation Lab. Rept. UCRL-6438, pt. 1, paper D, 11 p. (Report prepared for U.S. Atomic Energy Commission.)

Milton, D. J., and Michel, F. C., 1965, Structure of a ray crater at Henbury, Northern Territory, Australia: U.S. Geol. Survey Prof. Paper 525-C, p. C5-C11.

Perry, R. A., Ed., 1962, General report on lands of the Alice Springs area, Northern Territory, 1956-57: Australia Commonwealth Sci. Indus. Org. Land Research Ser. no. 6, 280 p.

Ranford, L. C., Cook, P. J., and Wells, A. T., in press, The geology of the central part of the Amadeus Basin: Australia Bur. Mineral Resources Rept. no. 88.

References--Continued

Rayner, J. M., 1939, Examination of the Henbury meteorite craters by the methods of applied geophysics: Australian and New Zealand Assoc. Adv. Sci., v. 24, p. 72-78.

Shoemaker, E. M., 1963, Impact mechanics at Meteor Crater, Arizona, in Middlehurst, Barbara, and Kuiper, G. P., eds., The Moon, meteorites and comets--The solar system, vol. IV: Chicago, Univ. of Chicago Press, p. 301-336.

Shoemaker, E. M., and Eggleton, R. E., 1961, Terrestrial features of impact origin, in Proceedings of the Geophysical Laboratory/Lawrence Radiation Laboratory Cratering Symposium, Washington, D. C., March 28-29, 1961: California Univ., Livermore, Lawrence Radiation Lab. Rept. UCRL-6438, pt. 1, paper A, 27 p. (Report prepared for U.S. Atomic Energy Commission.)

Spencer, L. J., 1933, Meteorite craters as topographical features on the earth's surface: Geog. Jour., v. 81, no. 3, p. 227-248; 1935, Smithsonian Inst. Rept. 1933, p. 307-325.

Taylor, S. R., and Kolbe, P., 1964, Henbury impact glass--parent material and behavior of volatile elements during melting: Nature, v. 203, no. 4843, p. 390-391.

Vortman, L. J., 1965, Craters from four equal charges in a horizontal square array: Sandia Corp. Rept. SC-RR-65-6, 107 p. (Report prepared for U.S. Atomic Energy Commission.)

RECENT GEOLOGIC AND LABORATORY INVESTIGATIONS

OF THE FLYNN CREEK STRUCTURE, TENNESSEE

by David J. Roddy

Introduction

The Flynn Creek structure in north-central Tennessee (fig. 1) has been under study as part of a larger program of crater investigations by the Branch of Astrogeology. Although this intensely deformed, circular structure has been interpreted both as a meteorite impact structure (Boon and Albritton, 1937, 1938, 1942; Dietz, 1946, 1963; Baldwin, 1949, 1963; Wilson, 1953, 1962; Shoemaker and Eggleton, 1961) and a "cryptoexplosion" structure (Bassler, 1932; Bucher, 1936, 1963; Wilson and Born, 1936), systematic investigations had not been previously carried out.

This report summarizes the results of recent field mapping and selected chemical, mineralogic, and petrographic studies. Earlier reports dealt with precrater stratigraphy, structure of part of the east and west rims, breccia, structure of the central hill, and postcrater stratigraphy (Roddy, 1963, 1964a), level of precrater ground surface, amount of postcrater erosion, body of forcefully ejected breccia, precrater lithostatic pressures, and structure of part of the southeast rim (Roddy, 1964b).

Geologic setting

Flat-lying Middle and Upper Ordovician limestones and dolomites surround the Flynn Creek structure but are folded and faulted into a circular rim which encloses a partly buried crater about 3.5 km in diameter.
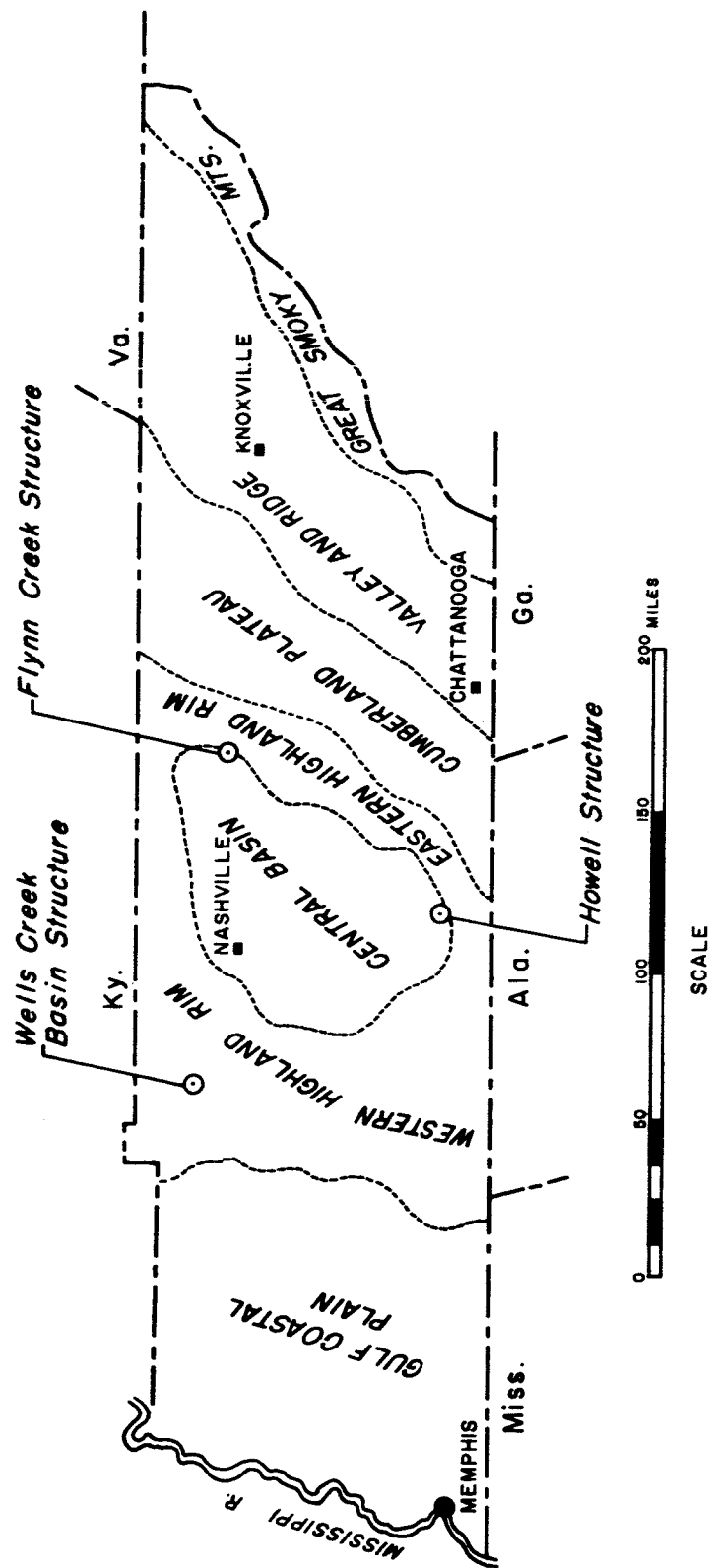
Fig. 1.--Index map showing location of the Flynn Creek structure, Tennessee. Dotted lines are boundaries of the physiographic provinces.

51

The crater floor is underlain by breccia of Middle and Upper Ordovician limestone and dolomite fragments ranging in size from a fraction of a millimeter to nearly 100 meters. In the central part of the crater, a partly buried hill consisting of intensely deformed Middle Ordovician limestones and dolomites of the Stones River and Knox Groups rises nearly 100 meters above the surrounding crater floor. Brecciated rocks of the Knox Group containing shatter cones have been raised at least 300 meters above their normal level.

In the southern part of the deformed crater rim two major fault zones are present (Roddy, 1964b). Within this part of the faulted rim, preservation of strata of probable Richmond age indicates postcrater, pre-Chattanooga erosion of less than 50 meters. Breccia in part of this faulted section is interpreted as having been forcefully ejected during the structural deformation which occurred in the interval between Richmond and early Late Devonian time (between about 420 and 350 million years ago).

A thin marine deposit of early Late Devonian age, consisting of bedded breccia and cross-bedded dolomite overlies the breccia of the crater floor. Chattanooga shale of early Late Devonian age averages 10 meters in thickness throughout the region, locally thickens within the crater to nearly 60 meters, and unconformably overlies all older rocks. Chert and shale of the Maury and Fort Payne Formations of early Mississippian age disconformably overlie the Chattanooga Shale. Dissection during Recent time by Flynn Creek and its tributaries has produced one of the best exposed cryptoexplosion structures in the United States.

Field and laboratory studies

Mapping at a scale of 1 inch to 500 feet of the deformed rim and of the brecciated section, encompassing an area of about 21 square miles, is approximately 75 percent completed. Approximately 50 percent of an additional area of about 17 square miles surrounding the Flynn Creek structure has been mapped at a scale of 1 inch to 1000 feet. The geologic contacts have been mapped with an elevation control accurate to ± 1 foot per 100 feet of elevation on both maps.

Conant and Swanson (1961, p. 13) have described the early Late Devonian erosion surface in Tennessee as ". . .a peneplain that is notable for its extent and degree of perfection." The contacts of this surface are exposed in the valley walls throughout the mapped area and many hundreds of field measurements show that relief in the area rarely exceeded 20 meters and more commonly averaged a few meters, with slopes less than 4°.

Any debris that might have been present on the crater rim was completely removed before the deposition of the Chattanooga Shale. Throughout the mapped area the contact is very sharp between the rocks which formed the early Late Devonian erosional surface and the basal unit of the Chattanooga Shale. However, the crater was not in existence long enough to have been filled during erosion of the rims and probably was about 100 meters deep before deposition of the Chattanooga Shale.

The unusual basal facies of the Chattanooga Shale within the crater consists of cross-bedded carbonates and bedded breccia. These units thicken to at least 15 meters in the crater and rapidly thin out on the upper flanks of the crater walls. Evidence for a Late Devonian crater has caused speculation that these beds are lake deposits consisting of fresh-water limestones

and breccia fragments cemented by fresh-water limestones (Wilson and Born, 1936; Conrad and others, 1957). However, Conant and Swanson (1961) and Huddle (1963) have described early Late Devonian conodonts in these rocks, which indicate a marine depositional environment. Mineralogical and trace-element studies indicate that the limestones occur only as fragments derived from Ordovician limestones in the crater breccia and crater walls. Other breccia fragments consist of dolomites and dolomitic limestones derived from the surrounding contemporaneous erosion surface. X-ray analysis indicates that the cementing material of this bedded breccia is well-ordered dolomite with less than 10 percent calcite. Ordering diffraction lines of the dolomite superstructure agree well with those given by Gold-smith and Heard (1961) for a well-ordered dolomite lattice. The cross-bedded, thinly laminated unit overlying the bedded breccia consists almost entirely of dolomite with less than 3 percent calcite. Dolomite in this unit also exhibits a well-ordered lattice structure. The mineralogy of this dolomite strongly suggests as a source area the rocks underlying the early Late Devonian surface that surround the crater.

Some time after the crater was formed, relief in the Flynn Creek area consisted of very low hills on the order of a few meters high with a few as high as 20 meters. Deposition of the bedded breccia and cross-bedded dolomite probably occurred in a coastal plain environment in the shallow waters of the slowly advancing Chattanooga sea. Organic content in the crater was probably high, but restricted circulation in the crater bottom may have caused reducing conditions with dolomitizing brines similar to those suggested by Deffeyes and others (1964) and Berner (1965).

The breccia outcrops and much of the deformed rim of the Flynn Creek

structure have been carefully examined, but no unusual mineral assemblages of any type have been observed in the field or in hand specimens. Anomalous trace-element concentrations and mineral assemblages, high pressure polymorphs and crystalline deformation have also been searched for by laboratory methods.

Analyses were made on total rock samples collected from ten horizons outside of the deformed crater, three fragments in the breccia, and eight breccia matrix samples. To test natural variations, trace-element percentages were also determined on rocks from outside the deformed crater for the same horizon but with the samples separated by several thousand meters. The trace-element percentages for these samples from the same horizon were very nearly identical, indicating only natural low percentage variations for these rocks.

The rocks from the breccia for analyses suggest they are all from a level equivalent to the upper quarter of the deformed strata in the rim. The trace-element percentages of these breccia fragments have values consistent with the same upper quarter of the deformed rim strata and show no trace element anomalies.

The trace-element levels in the breccia matrix differ from the levels in the fragments only in that they have equal or lower percentages for nearly all the elements. Perhaps the most important aspect is that there were no trace-element enhancements of meteorite or volcanic constituents in either the breccia fragments or the breccia matrix.

Extensive examination of the Flynn Creek rocks in outcrop and in thin section has shown no traces of mineralization. Particular attention was directed to possible very low temperature carbonate thermal metamorphism

EXPLANATION

QUATERNARY

Alluvium

MISSISSIPPIAN

Fort Payne Formation

DEVONIAN

Chattanooga Shale

Bedded Dolomite and
Bedded Breccia

UPPER ORDOVICIAN – UPPER DEVONIAN

Breccia of Cannon, Catheys,
and Leipers Fragments

Faulted, Folded, and Brecciated
Pre–Cannon Rocks

MIDDLE and UPPER ORDOVICIAN

Cannon, Catheys, and
Leipers Formations

Major High Angle Fault
Dashed Where Approximately Located
Dotted Where Concealed

Dip and Strike   A—A' B—B'   Cross Sections
                      C—C' D—D'

Approximately Horizontal, Dip Less Than 3°

BASE MAP BY
J. ALDERMAN
1963–1964

GEOLOGY BY
D.J. RODDY
1962–1964

10,000 FEET

5000

SCALE

0

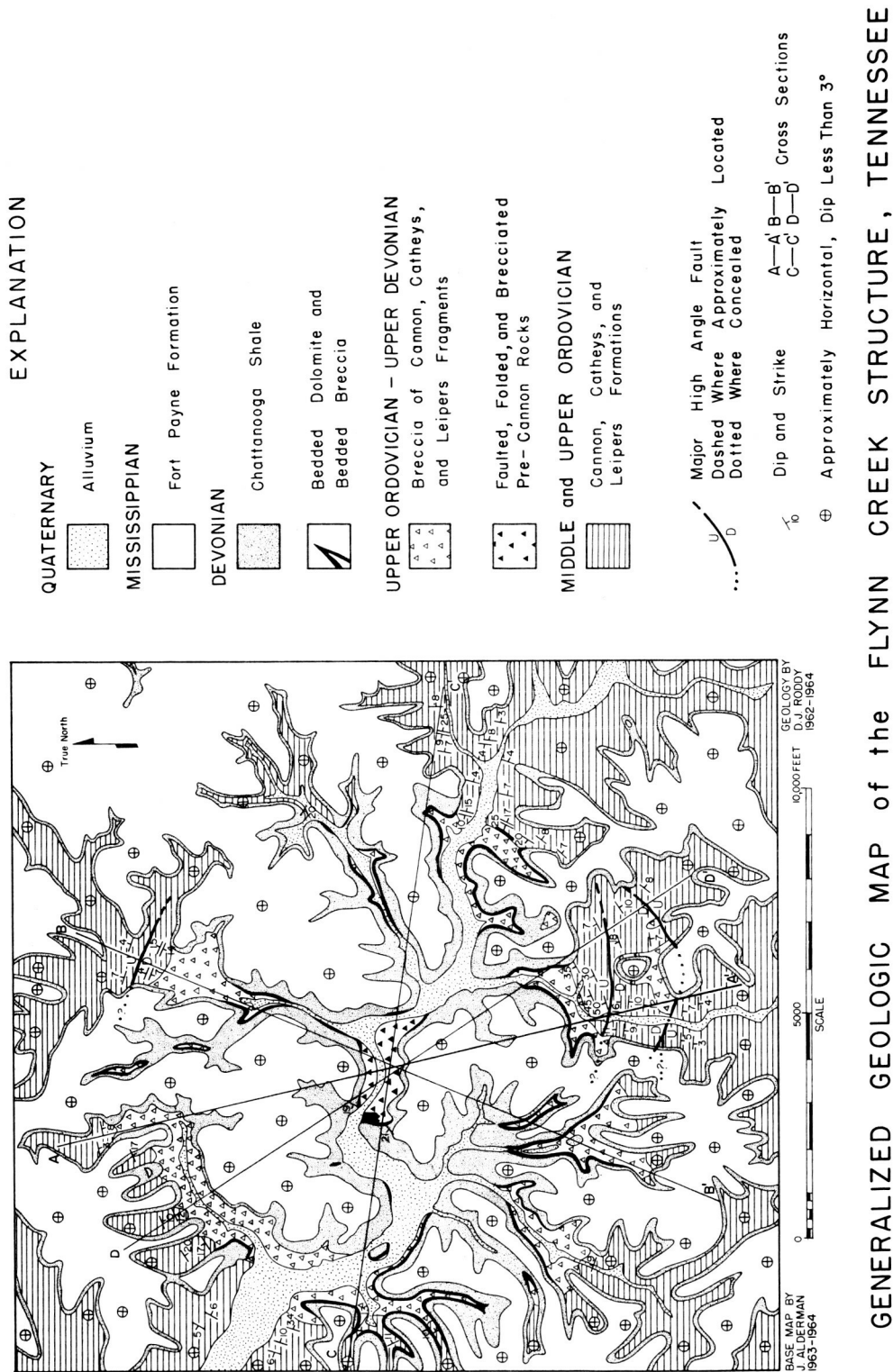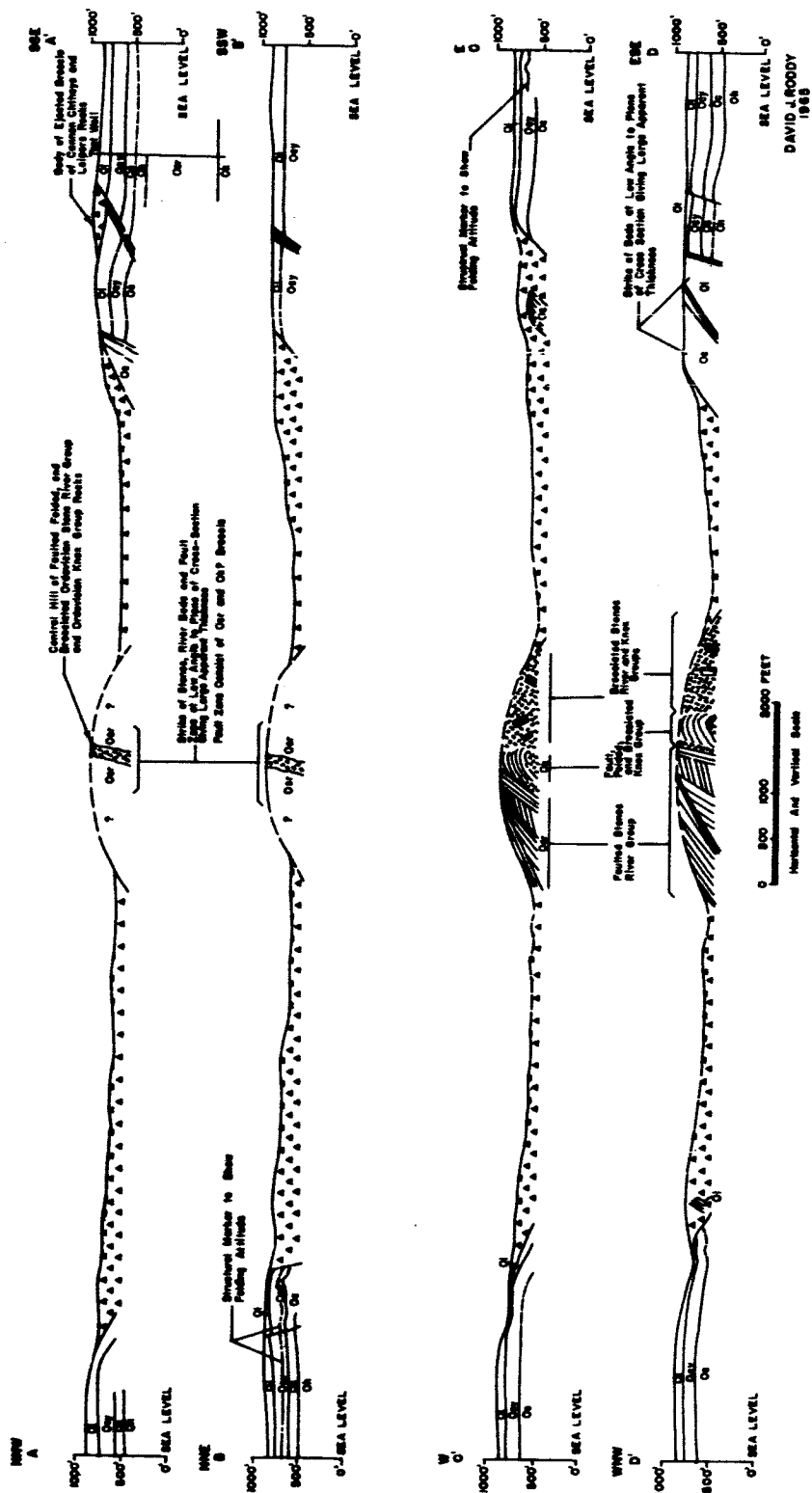GENERALIZED GEOLOGIC MAP of the FLYNN CREEK STRUCTURE, TENNESSEE

Fig. 2.

Fig. 3.—Generalized geologic cross sections of the Flynn Creek structure. Sections show structure shortly before deposition of Chattanooga Shale in early Late Devonian time.

such as the production of talc alterations in clay carbonate zones, but no thermal alterations of any type have been noted in the deformed rim rocks, breccia fragments, or breccia matrix.

Rocks from the Flynn Creek structure have been examined for high-pressure silica polymorphs (Roddy, 1964b) and aragonite, the high pressure form of calcite, but none were found.

Petrofabric studies of the deformed rim rocks at the Flynn Creek structure have shown that the number of twin lamellae definitely increase toward the crater. Microfracturing parallel to the carbonate cleavage directions also increases slightly toward the crater. The increase in both the twin lamellae and the microfracturing is commonly restricted to a narrow band a few meters to a few tens of meters wide around the crater rim and adjacent to the breccia contact. Most of the large blocks located in the breccia adjacent to the deformed rim also exhibit a large number of twin lamellae and microfractures.

Structure

Noteworthy structural elements, shown in four cross sections in figure 3, are a slightly to moderately raised rim; slight to intense rim folds; major and minor normal, reverse, and thrust faults in the rim; a major body of continuous breccia within the crater; a localized body of probable forcefully ejected breccia; and a central uplift of faulted, folded, and brecciated rocks. The location of these cross sections is shown on the geologic map in figure 2.

Parts of the raised rim have nearly 50 meters of uplift, while in other parts of the rim there is only a few meters of uplift. Where broad

58

down-folding occurs in the rim, a broad gentle uplift is also present. Normal fault blocks in parts of the north and south rim exhibit considerable folding.

In the southeast rim, downthrow on one fault block is nearly 100 meters, but it appears that this is part of a very large rotated block rather than a simple normal fault (Roddy, 1964b). High-angle thrusts and reverse faults are present in the southeast and east part of the rim.

An unusual type of fold suggesting strong horizontal compression is shown in cross section B-B' in the northeast rim and in C-C' in the east rim (fig. 3). Both folds have vertical axial planes, approximately concentric with the rim, and with horizontal shortening on the order of 35 percent. Beds below these folds are not exposed, but beds above rapidly flatten, suggesting considerable bedding plane slippage in the tightly folded strata. The beds forming these folds were less than 100 meters below the ground surface when the Flynn Creek deformation occurred (Roddy, 1964b).

References

Baldwin, R. B., 1949, The face of the Moon: Chicago, Univ. of Chicago Press, 239 p.

_____ 1963, The measure of the Moon: Chicago, Univ. of Chicago Press, 488 p.

Bassler, R. S., 1932, The stratigraphy of the central basin of Tennessee: Tennessee Div. Geology Bull. 39, 268 p.

Berner, R. A., 1965, Dolomitization of the mid-Pacific atolls: Science, v. 147, no. 3663, p. 1297-1299.

Boon, J. D., and Albritton, C. C., 1937, Meteorite scars in ancient rocks:
    Field and Lab., v. 5, no. 2, p. 53-64.

_____ 1938, Established and supposed examples of meteoritic craters and
    structures: Field and Lab., v. 6, no. 2, p. 44-56.

_____ 1942, Deformation of rock strata by explosions: Science, v. 96,
    no. 2496, p. 402-403.

Bucher, W. H., 1936, Cryptovolcanic structures in the United States:
    Internat. Geol. Cong., 16th, United States 1933, Rept., v. 2, p. 1055-
    1084.

_____ 1963, Cryptoexplosion structures caused from without or from within
    the Earth? ("Astroblemes" or "Geoblemes?"): Am. Jour. Sci., v. 261,
    no. 7, p. 597-649.

Conant, L. C., and Swanson, V. E., 1961, Chattanooga shale and related
    rocks of central Tennessee and nearby areas: U.S. Geol. Survey Prof.
    Paper 357, 91 p.

Conrad, S. G., Elmore, R. T.,Jr., and Maher, S. W., 1957, Stratigraphy of
    the Chattanooga black shales in the Flynn Creek structure, Jackson
    County, Tennessee: Tennessee Acad. Sci. Jour., v. 32, no. 1, p. 9-18.

Deffeyes, K. S., Lucia, F. J., and Weyl, P. K., 1964, Dolomitization--
    Observations on the Island of Bonaire, Netherlands Antilles: Science,
    v. 143, no. 3607, p. 678-679.

Dietz, R. S., 1946, Geological structures possibly related to lunar craters:
    Pop. Astronomy, v. 54, p. 465-467.

_____ 1963, Cryptoexplosion structures, a discussion: Am. Jour. Sci.,
    v. 261, no. 7, p. 650-664.

References--Continued

Goldsmith, J. R., and Heard, H. C., 1961, Subsolidus phase relations in the system $CaCO_3$-$MgCO_3$: Jour. Geology, v. 69, no. 1, p. 45-74.

Huddle, J. W., 1963, Conodonts from the Flynn Creek cryptoexplosion structure, Tennessee: Art. 74 in U.S. Geol. Survey Prof. Paper 475-C, p. C55-C57.

Roddy, D. J., 1963, Flynn Creek structure, Tennessee, in Astrogeologic Studies Ann. Prog. Rept., Aug. 25, 1961 - Aug. 24, 1962, pt. B: U.S. Geol. Survey open-file report, p. 118-126.

_____ 1964a, Geologic section across the Flynn Creek structure, in Astrogeologic Studies Ann. Prog. Rept., Aug. 25, 1962 - July 1, 1963, pt. B: U.S. Geol. Survey open-file report, p. 53-76.

_____ 1964b, Recent investigations of the Flynn Creek structure, with a section on geophysical studies, in Astrogeologic Studies Ann. Prog. Rept., July 1, 1963 - July 1, 1964, pt. B: U.S. Geol. Survey open-file report, p. 163-180.

Shoemaker, E. M., and Eggleton, R. E., 1961, Terrestrial features of impact origin, in Proceedings of the Geophysical Laboratory/Lawrence Radiation Laboratory Cratering Symposium: California Univ., Livermore, Lawrence Radiation Lab. Rept. UCRL-6438, pt. 1, paper A, 27 p. (Report prepared for U.S. Atomic Energy Commission.)

Wilson, C. W., Jr., 1953, Wilcox deposits in explosion craters, Stewart County, Tennessee, and their relations to origin and age of Wells Creek Basin structure: Geol. Soc. America Bull., v. 64, p. 753-768.

References--Continued

Wilson, C. W., Jr., 1962, Stratigraphy and geologic history of Middle Ordovician rocks of central Tennessee: Geol. Soc. America Bull., v. 73, p. 481-504.

Wilson, C. W., Jr., and Born, K. E., 1936, The Flynn Creek disturbance, Jackson County, Tennessee: Jour. Geology, v. 44, p. 815-835.

GEOLOGY OF THE MOSES ROCK INTRUSION,

SAN JUAN COUNTY, UTAH

by Thomas R. McGetchin

Introduction

The Moses Rock intrusion is one of four known intrusive pipes or dikes of kimberlite (micaceous serpentine breccia) on the Colorado Plateau. All are within the Navajo Indian Reservation, in southeast Utah and northeast Arizona. Three are just south of the San Juan River along Comb Ridge, a pronounced topographic feature formed as a result of differential weathering of rocks in the Comb monocline. This fold forms the eastern border of the Monument upwarp, a major structural feature of this part of the Colorado Plateau, and the intrusions are localized within 2 or 3 miles of the axis of this fold.

The intrusion at Moses Rock has not been described in detail previously, but was mentioned by Shoemaker (1962). The pipe at Mule Ear has been mapped by Shoemaker and Moore (in preparation); and the pipes at Garnet Ridge, approximately 13 miles south of Moses Rock, were described by Malde (1954), and Malde and Thaden (1963). A serpentine intrusion at Buell Park, near Fort Defiance in northeast Arizona, occurs on the Defiance monocline (Allen and Balk, 1954).

Location and local geology

The intrusion at Moses Rock is a large dike rather than a pipe, about 7 airline miles east-southeast of Mexican Hat, Utah. It has intrusive contacts with the red beds of the Permian Cutler Formation. At the east end of Monument Valley, the Cutler rocks dip gently eastward into the Comb monocline, where they locally attain dips of 40°. The local structure is complicated by open folding forming the Raplee anticline and Mexican Hat syncline, west of the intrusion.

Two types of intrusive rocks are locally present: serpentine breccia dikes and numerous necks and dikes of minette, a potassium-rich lamprophyre (see Williams, 1936). Dikes of both types trend

63

generally north-south; the necks commonly occur along dikes. No cross-cutting relationships have been observed locally, although at Buell Park, minettes cut the kimberlites. The question of the age and genetic relationship of the two rock types is open.

The main intrusion was formed by coalescence of two en echelon dikes that strike north-south and dip steeply westward. Its total length is unknown because the southern end is buried beneath recent sand dunes, but it is well exposed for more than four miles of its length. The north end reaches the San Juan River canyon. Its width reaches approximately 1000 feet locally, but for most of its length it is much less.

Intrusive material

The dike is filled by lithologically distinct, but in part gradational, breccia units. These may be described as mixtures of three end members: (1) kimberlite--serpentine breccia bearing olivine, pyroxene, garnet, calcite and small angular rock and mineral fragments; (2) inclusions of basement rocks--metamorphic and igneous rock fragments not exposed locally; and (3) inclusions of sedimentary rocks--limestone and clastic sedimentary rocks derived from Paleozoic and Mesozoic strata now exposed at the surface or known from drilling records. Units may be mapped within the intrusion on the basis of relative abundance of these materials and the size of inclusions, which varies considerably from place to place.

Dense kimberlite occurs as smaller dikelike bodies within the main intrusion at four known localities. Generally, the kimberlite contains finely comminuted grains and blocks of sedimentary rocks that make up as much as 90 percent of the dike locally.

Inclusions

The largest blocks in the intrusion were derived from the Paleozoic and Mesozoic sedimentary rocks lining the vent and are as much as several hundred feet long. Grain and fragment size varies continuously from these large blocks through silt-size grains. It is possible to identify blocks

64

derived from specific stratigraphic horizons, and thus to determine displacement accurately. In general, very large blocks are displaced downward relative to their original stratigraphic position, whereas smaller blocks are displaced upward. Larger blocks are generally angular and smaller blocks, more spherical. Size-frequency distributions of smaller blocks contained in bulk samples taken at five localities have the form of Gaudin-Meloy size distributions, which are characteristic of comminution produced by ball mills (Meloy, 1963). Metamorphism and alteration of included blocks derived from red beds and limestones are minor or absent.

The size of the basement inclusions varies greatly from place to place, and unlike the sedimentary inclusions, their size-frequency distribution does not have the form of a simple grinding relationship. Preliminary results suggest that populations, in terms of presence and absence of specific rock types, are not identical from locality to locality. Basement inclusions are essentially unmetamorphosed rhyolite, granite, syenite, diorite and gabbro; unfoliated but altered greenstone porphyries (metabasalts or meta-andesite porphyries); foliated, low-grade calc-silicate rocks; foliated sillimanite-bearing, pelitic schists; garnet-bearing gabbroic rocks; granite gneiss; and pyroxenite and garnet-pyroxene rock (eclogite). Clearly, these rocks were transported upward during the eruption which produced the dike, and thus were derived from the section through which the intrusive material passed. These rocks, then, represent a badly scrambled vertical section of unknown, but certainly great, thickness.

Contacts

Contacts dip from 90° to about 70°. A well-developed fracture system is present everywhere at the contact and is parallel to the contact. The density of fractures diminishes with distance from the contact, disappearing within 200 to 300 feet. Deformation of wall rocks is very slight or absent. Beds are locally uparched slightly. Metamorphism and alteration at the contact are restricted to very thin bleached zones in

red sandstone, siltstone and limey sandstone units. Bleaching is restricted to joints very near the contacts and generally disappears within about 50 feet from the contact.

Satellite intrusions and structures

A number of small intrusions bearing serpentine breccia and inclusions of basement rocks occur within several miles of the main dike at Moses Rock, and are significant since they are almost certainly genetically related. These include several dikes, 2 to 3 feet wide at most, carrying spherical inclusions up to several inches in diameter.

About a mile southeast of the southern end of the main dike is a small elliptical plug, 800 by 500 feet in plan, with vertical or steeply dipping contacts. The intrusive material is nearly all comminuted clastic sedimentary rock and moderately large blocks, all displaced downward stratigraphically. A search revealed a very few basement inclusions near the center of the plug, all less than an inch in diameter. A well-developed fracture system forms a collar surrounding the vent in the wall rocks. These fractures are commonly stained near the contact, decrease in number away from the contact, and are essentially missing within 100 feet from the contact.

Just south of this small pipe is a large collapse depression, about 4000 feet in diameter. Its southern extremity is covered with dunes, but a hemispherical area is well exposed. At the contacts, undeformed wall rocks are folded abruptly downward along a well-defined hinge line; a set of local joints in the wall rocks parallels this hinge. Units are not brecciated or severely deformed within the structural depression except in an area measuring about 1700 by 400 feet and slightly off-center toward the northeast. Here the beds are disrupted into individual blocks which have been rotated to various orientations; however, the coherence of the lithologic units is maintained, so that blocks derived from specific units can be traced along the projected strike of the unbrecciated beds and through the breccia plug. Basement rocks have been found in alluvium covering part of the breccia plug, but they are rare and are always small.

66

Bleaching of rocks along joints is common. Faulting is present but displacements are small.

Summary and conclusions

This project deals with the geology of a kimberlite (serpentine breccia) dike, 4 miles long, in southeast Utah and with the petrology of the large number of inclusions contained within it. The interesting and significant feature of these inclusions of basement rock is that they represent samples derived from a vertical section of unknown but certainly great thickness. The variety and abundance of these rocks and the presence of a suite of very dense rocks, including pyroxenite and eclogite, suggests that this column may extend into the mantle itself. Thus, in effect, the intrusion may have provided a natural "mohole."

The intrusion is probably of mid- or early-Tertiary age; thus the present surface is probably more than 1000 feet lower than the surface at that time. A best guess of the original surface expression of the intrusion would be very similar to certain lunar rilles that contain crater chains, for example, the Hyginus rille, the Stadius chain, and the prominent rille in the eastern part of the floor of the crater Alphonsus, as shown in the Ranger IX photographs. Although, of course, nothing can be said regarding composition of the lunar material, the similarity of form suggests a similar type of violent, probably highly gaseous, eruptive volcanism.

References

Allen, J. E., and Balk, Robert, 1954, Mineral resources of Fort Defiance and Tohatchi quadrangles, Arizona and New Mexico: New Mexico Bur. Mines and Mineral Res. Bull. 36, 192 p.

Malde, H. E., 1954, Serpentine pipes at Garnet Ridge: Science, v. 119, p. 618.

Malde, H. E., and Thaden, R. E., 1963, Serpentine at Garnet Ridge: U. S. Geol. Survey Bull. 1103, p. 54-61.

Meloy, T. P., 1963, Cumulative and weight retained tables for Gaudin-
    Meloy size distribution: Am. Inst. Min. Metall. Petroleum Eng.
    Trans., v. 226, p. 357-361.

Shoemaker, E. M., 1961, The interpretation of lunar craters, in Kopal,
    Zdenek, ed., The physics and astronomy of the Moon: New York,
    Academic Press, p. 283-359.

Williams, Howel, 1936, Pliocene volcanoes of the Navajo-Hopi country:
    Geol. Soc. America Bull., v. 47, p. 111-172.

PSEUDOTACHYLITE FROM ARCHEAN GRANITE

OF THE VREDEFORT DOME

by H. G. Wilshire

Introduction

The Vredefort dome, located in the Transvaal and Orange Free State, South Africa, is a nearly circular structure about 75 km in diameter. Rocks exposed in the structure consist mainly of granite and a thick sequence of shale, sandstone, conglomerate, and volcanic rocks, all of Precambrian age. Granite, the oldest abundant rock type, forms the core of the structure and has been raised ". . .as a solid cylindrical plug through a vertical distance of at least 40,000 feet" (Nel, 1927, p. 107). The Precambrian sedimentary and volcanic rocks are deformed concentrically about the granite and are overturned through several thousand feet of the section. The sedimentary and volcanic rocks are metamorphosed for a distance of as much as 10 km from the granite core, but not concentrically about it (Nel, 1927, p. 84). Approximately the southeastern one-third of the structure is covered by undeformed sandstone and shale of middle Permian age (Ecca Series, Karroo System), which provides the only information as yet available on the minimum age of the structure.

Pseudotachylite, a very fine-grained rock, occurs in irregularly distributed patches in all rock types of pre-Karroo age in the Vredefort dome (Hall and Molengraff, 1925). The origin of the pseudotachylite, in some way related to the origin of the dome structure, has been the subject of many theories. These include shock of unspecified origin or gas fluxing resulting from deep-seated explosions (Shand, 1916), crushing and partial

fusion during doming of the structure (Hall and Molengraff, 1925), crushing and metamorphic recrystallization (Willemse, 1938), fluidization (Reynolds, 1954; Whitten, 1959; Bisschoff, 1962; Poldervaart, 1962), and crushing and fusion caused by meteorite impact (Daly, 1947; Dietz, 1960). Most of these theories have in common the assumptions of high temperature and pressure and crushing without significant shearing.

The purpose of this paper is to describe some microscopic features of pseudotachylite from Archean granite in the core of the Vredefort dome that bear on the above interpretations. The samples studied were collected by Warren Hamilton, U.S. Geological Survey, from a quarry on Otavi farm about 6 km northeast of Parys.

Mode of occurrence

Occurrences of pseudotachylite in the Vredefort dome are shown by Hall and Molengraff (1925, map following plate 39) and by Nel (1927). The pseudotachylite is not concentrated along mapped faults, but is best developed in the more intensely deformed part of the structure. Bisschoff (1962, p. 210) states that there is no relation between the occurrence of pseudotachylite and major faults, but (p. 222) does consider that local faulting in the occurrence northeast of Parys is possible.

In the quarry exposures northeast of Parys, and about 4 km into the granite core of the dome, pseudotachylite occurs as a complex net-vein system in a breccia of foliated Archean granite (fig. 1). The top of the zone of pseudotachylite is marked by a thin pseudotachylite stringer with a low dip (Bisschoff, 1962, fig. 1), but the bottom is not exposed. Veins of pseudotachylite form the matrix of randomly oriented, angular to

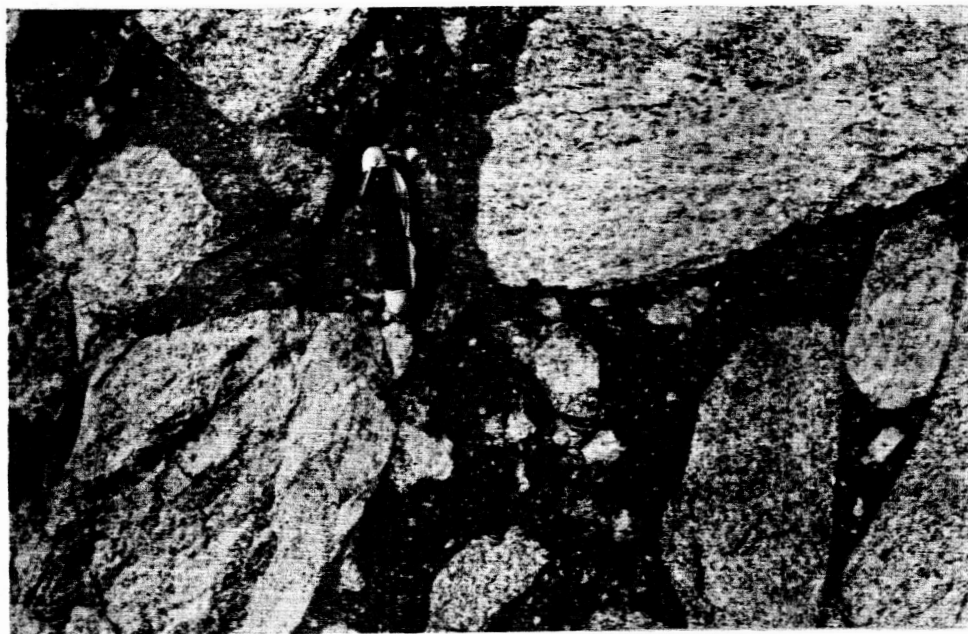Fig. 1A.--Pseudotachylite net veins in granite northeast of Parys.

Fig. 1B.--Randomly oriented, subrounded, foliated granite blocks in pseudotachylite; same location as figure 1A. (Photographs by Warren Hamilton.)

subrounded blocks of granite, and fill cracks separating large, slightly rotated blocks of granite, some of which may not have been completely detached from the wall rock.

Microscopic characters of inclusions
and pseudotachylite from Otavi farm

Inclusions

Almost all of the rock fragments enclosed in the pseudotachylite are of the adjacent granite, but two fragments of quartz diorite of unknown origin were found in thin sections.

Granitic inclusions have a hypidiomorphic granular fabric and a weak foliation. Principal minerals are perthite, oligoclase, and quartz with accessory biotite, and minor sphene, ilmenite, rutile(?), apatite, zircon(?), and secondary muscovite, chlorite, and clinozoisite. Perthite occurs as large, irregular grains with rod-shaped exsolved albite. Oligoclase is anhedral or subhedral and is unzoned. Myrmekite occurs at some boundaries between oligoclase and perthite grains. Both feldspars are slightly sericitized, and plagioclase is slightly chloritized. Large interstitial quartz grains are invariably cut by strain bands and are crossed by thin, irregular veins of unstrained polygonal and granular quartz mosaics. Interstitial pockets of quartz mosaics (fig. 2A) occur throughout the inclusions. The boundaries of polygonal quartz grains are probably irrational faces and closely resemble recrystallized olivine and plagioclase in ultrabasic xenoliths in basalts (see Talbot and others, 1963). Greenish brown biotite occurs as large books, generally cut by strain bands, and as small, undeformed books. Sphene and ilmenite are commonly intergrown

72

with biotite; sphene has incomplete rims of small anatase(?) rods, and in places rims the ilmenite.

Along the boundaries of the granitic inclusions, the feldspars and, to a lesser extent, quartz are mylonitized (fig. 2B). The perthitic structure of alkali feldspar is retained up to the thin marginal mylonite, and plagioclase shows no sign of change other than granulation. In places, the light-colored mylonite is interlayered with pseudotachylite containing minute prisms of rutile(?) or anatase, plates of hematite(?)[1], minor particles of an Fe-S(?) phase, and rods or plates of pale green mica. Generally the mafic mineral content of pseudotachylite in the layered rock is less than that in the main pseudotachylite vein. Quartz is locally irregularly fractured, the cracks being occupied by minute opaque grains; unstrained polygonal grains of quartz remain unchanged up to the granulated margin of the inclusion. Biotite near margins of the inclusions is partly replaced by hematite(?) and rutile(?) and becomes less colored. At the inclusion boundary, the biotite is broken down into randomly oriented, minute flakes of brown to pale green mica with abundant opaque grains and rutile(?). Thin veinlets of such new mica and opaque minerals extend from the biotite into adjacent minerals (fig. 2B). There are no concentrations of opaque minerals or mica in pseudotachylite adjacent to decomposed biotite at the inclusion boundary. Very thin veins of pseudotachylite extend into the inclusions along grain boundaries and irregular cracks and commonly terminate in small patches of chlorite and carbonate. Ilmenite, sphene, and apatite

---

[1] Opaque minerals were identified in polished section by B. F. Leonard, U.S. Geological Survey (written communication, 1965). Leonard considers all of the identifications of opaque minerals in the pseudotachylite to be tentative because of the extremely fine grain size.
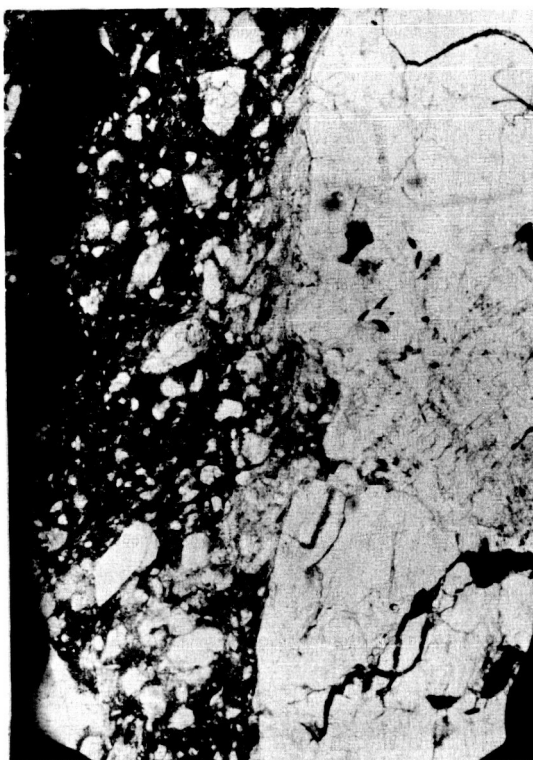
74

Fig. 2.--Top left, Polygonal and granular quartz mosaic in granite inclusion. Crossed nicols.

Bottom left, Granite inclusion (bottom, white) in pseudotachylite (dark, spotted) containing abundant angular and subrounded fragments of granite. Light-colored mylonite band at center edge of large inclusion. Note thin, irregular black bands of fine-grained mica and opaque minerals in granite at left and right sides of photograph. Plane-polarized light.

Top right, Same as preceding, crossed nicols. Mylonite band appears dark.

Bottom right, Well-rounded fragment of quartz mosaic isolated in pseudotachylite. Left side of fragment bounded by mylonite. Crossed nicols.

are unchanged at the inclusion margins.

One granitic inclusion has an unmylonitized boundary, and minute plates of mica in the pseudotachylite protrude into feldspars of the inclusion. There are no indications of partial melting of any constituents of the granite.

Fragments of quartz diorite have a hypidiomorphic granular fabric and consist of quartz, plagioclase, blue-green amphibole, and greenish brown biotite, sphene, and apatite. Plagioclase locally has a patchy undulatory extinction, and quartz exhibits strain banding or occurs as small, interstitial pods of interlocked polygonal and irregular grains like those in granitic inclusions. The amphibole occurs as undeformed subhedral or euhedral prisms and as irregular grains interstitial to the felsic minerals. Biotite is interstitial and is generally strongly deformed by strain bands.

Except for local mylonitization of quartz and plagioclase, the mafic and felsic constituents of the quartz diorite fragments are not granulated at the edges of the inclusions. Plagioclase at the margins has strong undulatory extinction and strain bands and is penetrated by minute plates of mica as in the granitic inclusion. Biotite and amphibole are decomposed at and near the inclusion margins, biotite as in the granitic inclusions, and amphibole to minute opaque minerals and other unidentified minerals. Sphene at the boundaries of these inclusions is also replaced by opaque minerals.

Very small rock fragments isolated in the pseudotachylite are composed dominantly of the irregular, strained quartz and mosaics of polygonal quartz (fig. 2D) found in the granite and quartz diorite inclusions. Plagioclase, often severely distorted, and perthite are present in places

⊢_____⊣ .02"

Fig. 3A.--Well-rounded fragment of plagioclase (white) and perthite (small dark gray patch in upper right part of inclusion) in pseudotachylite (black). Fragment is entirely surrounded by mylonite (dark gray, spotted). Crossed nicols.

⊢_____⊣ .01"

Fig. 3B.--Mylonite envelope around granular quartz mosaic (white, high relief) stretched in plane of foliation in pseudotachulite (dark). Plane-polarized light.

in the quartzose aggregates, and occur uncommonly as isolated fragments. Identifiable biotite is extremely rare in the small rock fragments, and no amphibole was observed. Many of the smaller fragments are well rounded, and elongate ones have a common orientation; most are partly bounded by thin mylonite rinds and some are completely enclosed in mylonite (fig. 3A). In places the mylonite rind has been stretched out parallel to the foliation in pseudotachylite (fig. 3B). Many of the small fragments are cut by thin mylonite bands, some of which are localized along grain boundaries, some confined to specific mineral types, and some cut randomly across all minerals present. Pseudotachylite locally penetrates the rock fragments along mylonite bands, and minute opaque minerals and flakes of green mica like those in the pseudotachylite are found along grain boundaries and cleavages.

Bisschoff (1962, p. 211 and plate 2, fig. 2) considers the mosaics of quartz to have recrystallized during formation of the pseudotachylite. About half of those mosaics, however, are identical in all respects with the small interstitial pods in the granitic and dioritic inclusions (compare figs. 2A and 2D). Although it is likely that the polygonal quartz mosaics were formed by recrystallization, the recrystallization predates the pseudotachylite, and such fragments were derived without change from the country rock. The remainder of these fragments are somewhat finer grained than any seen in the inclusions and may have been derived from other parts of the granite not represented in the samples studied.

Pseudotachylite

Pseudotachylite consists of minute pale green mica flakes[2] in a grano-
blastic to optically unresolved matrix of quartz and feldspar. Minute
crystals of rutile(?) and hematite(?) make up considerably less than 10
percent of the rock (B. F. Leonard, written communication, 1965), and
small amounts of chlorite and carbonate are present. Rock and mineral
fragments grade down in size to submicroscopic. The coarser mylonites have
a granoblastic fabric produced by welding or cementation of the rock flour,
so the original shapes of comminuted grains could not be determined. There
are no indications of partial fusion or resorption of any mineral grains.

All the common minor accessories--ilmenite, sphene, apatite, and zir-
con--found in the granite and quartz diorite inclusions are also present
in pseudotachylite. Recognizable biotite of a size comparable to that
in the inclusions, however, is rare and no amphibole survived formation
of the pseudotachylite. As noted before, sphene at the edges of quartz
diorite inclusions is partly replaced by opaque minerals; no relicts of
sphene were found in pseudotachylite near the quartz diorite.

Near the boundaries of inclusions, much of the pseudotachylite is
darker than elsewhere because mica and opaque minerals are more abundant.
Locally the dark pseudotachylite is interlayered with thin bands of
mylonite and bands intermediate between pure mylonite and the darker pseudo-
tachylite; dark layers contain considerably more large rock and mineral

---

[2]X-ray powder photographs of pseudotachylite revealed only mica, prob-
ably a 1M or 3T polymorph, quartz, and alkali(?) feldspar. The opaque min-
erals, though apparently abundant, are not present in sufficient quantity
to be detected in whole-rock powders. No amphibole, which was reported by
several authors on the basis of optical study, was found. The strongest
peak of coesite (3.09A) was not found and the strongest peak of stishovite
(4.36A) is masked by a feldspar peak.

fragments than lighter layers. Dark pseudotachylite grades into normal
pseudotachylite abruptly, and in places there are bulbous protrusions of
dark into light pseudotachylite, but the microscopic fabric is continuous
between them. Small patches of euhedral feldspar laths are found locally
in the dark pseudotachylite.

Physical conditions of pseudotachylite formation

Most of the diverse theories that have been applied to the origin of
the Vredefort pseudotachylite require high pressure, high temperature,
and absence of shearing. The available information does not allow close
definition of pressure limits but limits the temperature, with minor ex-
ceptions, to less than about 650° C; and shearing may have played an
important role in comminution of the country rock.

If the pseudotachylite formed as a consequence of the formation of
the Vredefort dome, the pressure on the country rock, especially in the
collar of the dome, probably exceeded the lithostatic pressure. The maxi-
mum lithostatic pressure, corresponding to a possible predome cover of
13 km of sedimentary rock (Hall and Molengraff, 1925, p. 135), is on the
order of 3 kb. The apparent absence of high-pressure polymorphs of
silica and of an amorphous phase (short-range order phase; De Carli and
Milton, 1964) replacing quartz indicates pressures less than about 20-30
kb (Boyd and England, 1959). No data now available allow closer specifi-
cation of the pressure range of pseudotachylite formation.

With the exception of Willemse (1938), authors concerned with the
origin of the pseudotachylite have considered the temperature of forma-
tion to be high, generally above that required to fuse granite. These

80

opinions are based entirely on fabric relations that include fused plagioclase with flowage structures (Shand, 1916), embayments of crystal and rock fragments (Shand, 1916; Hall and Molengraff, 1925), and occurrence of newly crystallized feldspar, sometimes as spherulitic growths (Shand, 1916; Hall and Molengraff, 1925; Bisschoff, 1962). On the assumption that the fine granularity indicates low volatile content, Daly (1947, p. 132) suggested a minimum temperature of about 700° C. Following the argument that Reynolds (1952, 1954) used in determining the temperature of granophyre in the Slieve Gullion area, fusion of plagioclase of average composition An20 (Willemse, 1938, p. 84) indicates a temperature between about 1300° C at atmospheric pressure and about 900° C at 5 kb water pressure (Yoder and others, 1956).

Although there may be evidence favoring local attainment of temperatures above 700° C, the survival of perthite, both at the edges of granite inclusions and as isolated grain fragments in the pseudotachylite, is a clear indication that prevailing temperatures were less than about 650° C and perhaps much less. The temperature maximum on the alkali feldspar solvus is about 650° C and homogenization of perthite is attained in 24 hours at 700° C (Tuttle and Bowen, 1958, p. 42-43); the pressure dependence of the solvus is probably small because of the small volume differences of homogeneous and exsolved feldspars (Tuttle and Bowen, 1958, p. 42). Further evidence of low temperature is found in the survival of quartz without any indication, such as shattering inside the mylonite envelope, that it has gone through the high-low inversion; this indicates that the temperature was less than about 600° C.

These indications of low temperature necessitate a review of the

evidence cited by other authors in favor of high temperature. No one has yet demonstrated the existence of glass in the Vredefort pseudotachylite, but, as the age of the structure is known no closer than pre-Middle Permian, devitrification of glass over a long period cannot be ruled out. There are, however, good examples of mylonitized quartz and feldspar in which the mylonite envelope has been stretched out by flow in a manner closely similar to those of "fused" plagioclase and quartz illustrated by Shand (1916, plate 19, fig. 2) and Bisschoff (1962, plate 2, fig. 6). The same structures are considered by Hall and Molengraff (1925, p. 103; plate 23, fig. 1) to represent mylonitized granite. Unless the presence of glass can be demonstrated, this fabric is not evidence for fusion. In the thin sections examined by the writer, embayments and rounded corners of rock and mineral fragments like those illustrated by Shand (plate 18, fig. 1) and Hall and Molengraff (plate 20; plate 21, fig. 3) and ascribed by them to partial fusion, occur where mylonite veinlets cut the rock and mineral fragments and where mylonite envelopes surround the fragments; rather than indicating that the surrounding pseudotachylite was liquid, such structures suggest that it was solid and contributed to frictional granulation of rock and mineral fragments.

On the basis of the supposed fusion of plagioclase, Shand (p. 208) considers that heat caused the breakdown of biotite, thereby furnishing magnetite to the pseudotachylite. Although it is agreed that biotite is the principal source of the iron oxide, it seems more likely that iron was leached by low-temperature hydrothermal solutions. High-temperature breakdown of amphiboles and micas is common in volcanic rocks but also involves crystallization of pyroxene and plagioclase and is a low-pressure phenomenon

(Washington, 1896; Larsen and others, 1937); leaching of iron and titanium from biotite by low-temperature hydrothermal alteration, however, is common.

The formation of new crystals of feldspar and amphibole, as spherulitic growths in places, has been cited by the above-named authors as evidence of crystallization from a melt. That this is not a firm criterion of fusion was pointed out by Waters and Campbell (1935, p. 500). Philpotts (1964, p. 1025) determined that plagioclase microlites in pseudotachylite from near Parys have a structural state intermediate between that of high- and low-temperature plagioclase. His conclusion (p. 1030) that all the pseudotachylite from the Vredefort region was formerly in a molten state, however, does not take into account the very local occurrence of such newly formed minerals, but his evidence does suggest that local hot spots developed in the pseudotachylite.

The conclusion based on the evidence cited above, as well as the objections raised against criteria for fusion, is that the prevailing temperature during formation of the pseudotachylite was less than about 650° C and probably less than 600° C. A minimum temperature cannot be specified, but may have been well below 600° C.

The conclusion of Shand (1916, p. 207) that shearing in the granite was unimportant is based on the sharpness of contacts between the pseudotachylite and granite. Hall and Molengraff (1925, p. 99) reached the same conclusion because of the random orientation and intersection of crush zones and general absence of consistent schistosity. They found (p. 102), however, that sharp contacts are the exception, and that those that do exist are the result of injection of pseudotachylite from another source. In the thin sections described by the writer there is abundant evidence of

shearing in the form of discontinuous mylonite bands along inclusion boundaries and of mylonite envelopes around small inclusions. Neither the mylonite rinds nor the rounding of such fragments is to be ascribed to "sand blasting" in a fluidized system as suggested by Reynolds (1954, p. 592) and Bisschoff (1962, p. 223); being entirely an attritional process, this would not leave mylonite rinds on the fragments or allow for the flow distortions of such rinds. Both Hall and Molengraff (1925, p. 108) and Bisschoff (1962, p. 222) concede that some shearing has occurred in the pseudotachylite near Parys, but there is no apparent way to determine the magnitude of fault offsets.

The amount of shearing that might be expected depends on the manner in which the breccia containing the pseudotachylite was formed. Shand (1916, p. 216) suggested that the brecciation was caused by deep-seated explosions of unspecified origin. Bisschoff (1962, p. 223) supports this theory and ascribes the explosions to high magmatic pressure resulting from a subjacent pluton. Hall and Molengraff (1925, p. 99) consider the breccia as well as fine crushing to be due to omnilateral pressure of unspecified origin. As an alternative to distant causes of brecciation, the following hypothesis may be applicable to those occurrences of pseudotachylite in which faulting may have played a role (see Manton, 1962). Movement at an angle to axes of curves in a fault plane may result in locally dilated zones. If the rock is under high confining pressure, the dilated zones are temporarily at a lower pressure and rock bursting may produce a breccia whose size distribution is governed by pre-existing fractures and other structures in the country rock. Further fault movements through and along the breccia zone may then cause additional mylonitization of the breccia and injection of the mylonite into fractures separating breccia fragments.

Mylonite or fused rock may migrate over a pressure gradient for greater distances into the breccia pods, as suggested by Philpotts (1964, p. 1031). Support for this interpretation is drawn chiefly from the close similarity of the Vredefort pseudotachylite to pseudotachylite and mylonite associated with faults throughout the world (Waters and Campbell, 1935, Whitten, 1959; Philpotts, 1964). In this view, the pseudotachylite is thought to be composed dominantly of mylonitized country rock that has been slightly re-crystallized, as envisaged by Willemse (1938). The main mafic constituents, mica and iron oxide, of the pseudotachylite were derived from biotite of the country rock, the oxides having been leached from the biotite and the small mica flakes representing mylonitized biotite. Inhomogeneities in distribution of the mafic constituents are considered to be due to incomplete mechanical mixing of mylonite.

An alternative explanation of the pseudotachylite as tuffisite (Reynolds, 1954; Whitten, 1959; Bisschoff, 1962; Poldervaart, 1962) is considered unlikely for the following reasons. Evidence, such as a vesicular structure, for the former presence of very much gas is generally lacking. Pseudotachylite in fault zones (Beetz, 1937, p. 259) is found as far as 20 km from the hypothetical buried pluton that is Bisschoff's (1962, p. 223) source of fluidizing gas. Analyses of pseudotachylite and its parent rocks (Willemse, 1938, table 9) reveal only negligible oxidation of iron, a feature difficult to reconcile with an expectably high P_{O_2} in a fluidized system.

Summary

Pseudotachylite occurs in net-veins in the Archean granite core of

the Vredefort dome. The microscopic fabric of the pseudotachylite and its inclusions indicates that little, if any, fusion has taken place, and that shearing was probably a dominant factor in the rounding and comminution of rock fragments. The survival of perthite derived from the granite indicates that the prevailing temperature during formation of the pseudotachylite was less than about 650° C.

Rock bursting into dilated zones caused by movement along irregular fault planes is postulated as a cause of formation of breccias in which the pseudotachylite is found; further movement in and along the breccia zones caused mylonitization of the rock and injection of mylonite into fractures separating the rock fragments.

References

Beetz, P. F. W., 1937, Contributions to the geology of the Klerksdorp District from the results of the drilling activities by the Western Reefs Exploration and Development Company, Limited: Geol. Soc. South Africa Trans., v. 39, p. 223-262.

Bisschoff, A. A., 1962, The pseudotachylite of the Vredefort dome: Geol. Soc. South Africa Trans. and Proc., v. 65, pt. 1, p. 207-230.

Boyd, F. R., and England, J. L., 1959, Quartz-coesite transition: Carnegie Inst. Washington Yr. Bk. 58, p. 87-88.

Daly, R. A., 1947, The Vredefort ring-structure of South Africa: Jour. Geology, v. 55, no. 3, p. 125-145.

De Carli, P. S., and Milton, D. J., 1964, Shock-wave synthesis of stishovite, in Astrogeologic Studies Ann. Prog. Rept., July 1, 1963-July 1, 1964, pt. B: U.S. Geol. Survey open-file report, p. 1-9.

References--Continued

Dietz, R. S., 1960, Vredefort ring structure: an astrobleme (meteorite impact structure) [abs.]: Geol. Soc. America Bull., v. 71, no. 12, p. 2093.

Hall, A. L., and Molengraff, G. A. F., 1925, The Vredefort mountain land in the southern Transvaal and the northern Orange Free State: Akad. Wetensch. Amsterdam Verh., v. 24, no. 3, 183 p.

Larsen, E. S., Irving, J., Gonyer, F. A., and Larsen, E. S., 3rd, 1937, Petrologic results of a study of the minerals from the Tertiary volcanic rocks of the San Juan region, Colorado: Am. Mineralogist, v. 22, no. 8, p. 889-905.

Manton, W. I., 1962, Discussion of paper, The pseudotachylite of the Vredefort dome, by A. A. Bisschoff: Geol. Soc. South Africa Trans. and Proc., v. 65, pt. 1, p. 227-228.

Nel, L. T., 1927, The geology of the country around Vredefort: Geol. Survey South Africa, map expln., 130 p.

Philpotts, A. R., 1964, Origin of pseudotachylites: Am. Jour. Sci., v. 262, no. 8, p. 1008-1035.

Poldervaart, A., 1962, Notes on the Vredefort dome: Geol. Soc. South Africa Trans. and Proc., v. 65, pt. 1, p. 231-252.

Reynolds, D. L., 1952, Partially fused plagioclases in the rocks of Slieve Gullion: Geol. Soc. Edinburgh Trans., v. 15, p. 280-296.

_____ 1954, Fluidization as a geological process, and its bearing on the problem of intrusive granites: Am. Jour. Sci., v. 252, no. 10, p. 577-613.

References--Continued

Shand, S. J., 1916, The pseudotachylite of Parijs (Orange Free State),

    and its relation to "trap-shotten gneiss" and "flinty crush-rock":

    Geol. Soc. London Quart. Jour., v. 72, p. 198-220.

Talbot, J. L., Hobbs, B. E., Wilshire, H. G., and Sweatman, T. R., 1963,

    Xenoliths and xenocrysts from lavas of the Kerguelen Archipelago:

    Am. Mineralogist, v. 48, p. 159-179.

Tuttle, O. F., and Bowen, N. L., 1958, Origin of granite in the light of

    experimental studies in the system $NaAlSi_3O_8$-$KAlSi_3O_8$-SiO_2-H_2O: Geol.

    Soc. America Mem. 74, 153 p.

Washington, H. S., 1896, The magmatic alteration of hornblende and bio-

    tite: Jour. Geology, v. 4, no. 3, p. 257-282.

Waters, A. C., and Campbell, C. D., 1935, Mylonites from San Andreas

    fault zone: Am. Jour. Sci., v. 29, p. 473-503.

Whitten, E. T., 1959, Tuffisite and magnetite tuffisite from Tore

    Island, Ireland, and related products of gas action: Am. Jour. Sci.,

    v. 257, no. 2, p. 113-137.

Willemse, J., 1938, On the Old Granite of the Vredefort region and some

    of its associated rocks: Geol. Soc. South Africa Trans., v. 40,

    p. 43-120.

Yoder, H. S., Jr., Stewart, D. B., and Smith, J. R., 1956, Ternary feld-

    spars: Carnegie Inst. Washington Yr. Bk. 55, p. 190-194.

GEOLOGY OF THE NORTHERN PART OF THE TWIN LAKES BATHOLITH,

LAKE AND CHAFFEE COUNTIES, COLORADO

by H. G. Wilshire, J. T. O'Connor, and G. A. Swann

Introduction

Lake Creek, in the central part of the Sawatch Range, Colorado, dissects the Twin Lakes batholith, the northern part of which (fig. 1) is the principal subject of this report. This small batholith is exposed over about 50 to 60 square miles and is composed of porphyritic quartz monzonite, which intruded Precambrian metamorphic and igneous rocks and is itself intruded by rhyolite dikes and small, irregular bodies of granite. Howell (1919, p. 33) considered the Twin Lakes intrusion as possibly of Mesozoic age, but Stark and Barnes (1935, p. 474) list it as Tertiary. It is labeled as Tertiary on the geologic map of Colorado (Burbank and others, 1935). No radiogenic age determinations are as yet available, so the age of the intrusion cannot be specified with certainty.

The studies of the area by Howell and Stark and Barnes were both of a reconnaissance nature, and considerable revision of the shape and position of the northern part of the Twin Lakes batholith has been made in the present investigation. About 60 percent of the area studied is covered by moraine and colluvium, which are not shown on the map. Because suitable topographic base maps are not yet available, the results of mapping on aerial photographs were transferred to a U. S. Forest Service drainage map. (fig. 1).
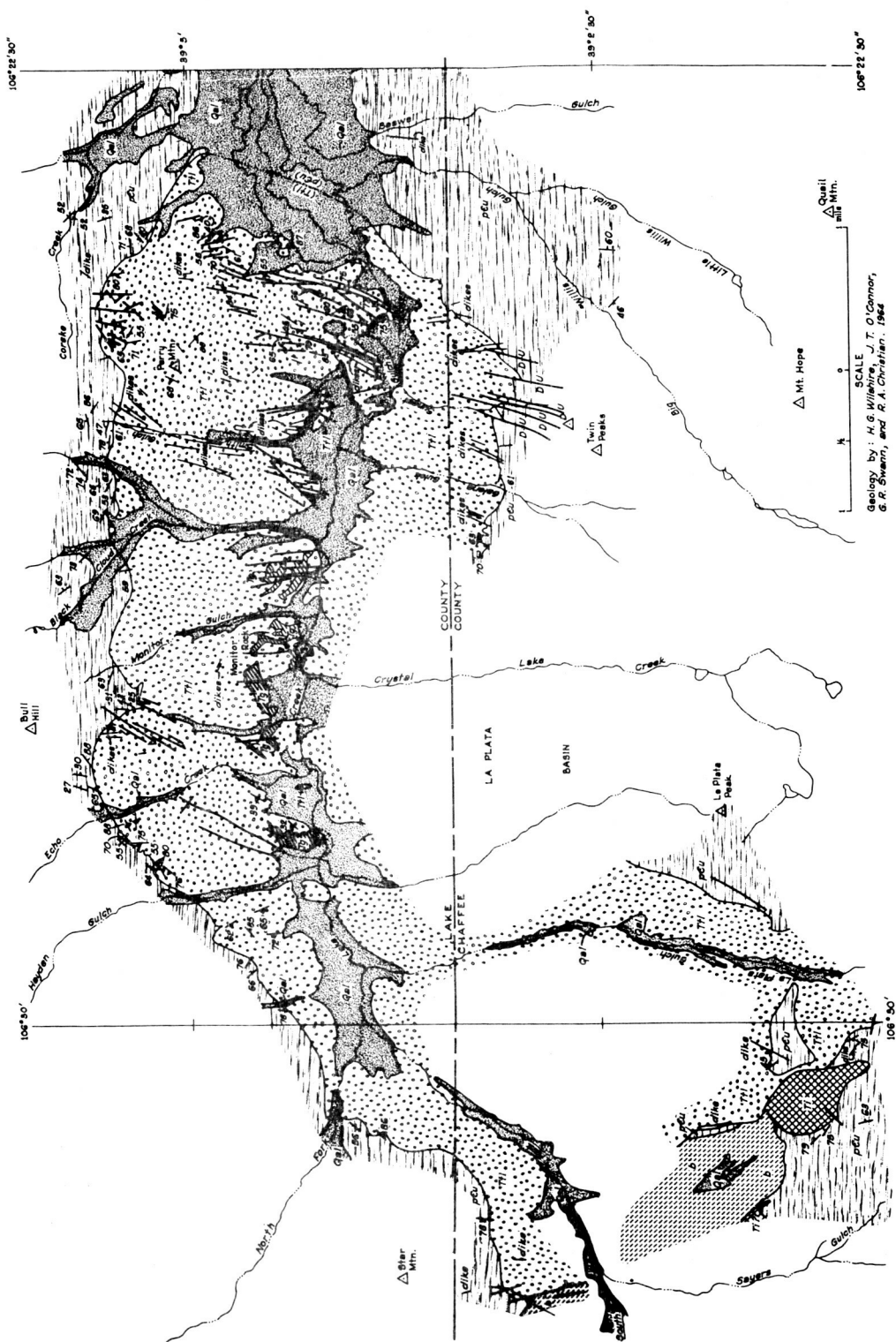
Fig. 1.—Geology of the northern part of the Twin Lakes batholith, Lake and Chaffee Counties, Colorado.

Map Explanation

Quaternary alluvium

Tertiary intrusive rocks, post-batholith; predominantly rhyolite, minor lamprophyre

Tertiary granite, post-batholith

Tertiary(?) Twin Lakes quartz monzonite

Brecciated Precambrian granodiorite

Precambrian rocks, undifferentiated

Contact
Dotted where concealed by alluvium. Tick and number indicate direction and amount of dip.

Fault
Dotted where concealed by alluvium. U, upthrown side; D,downthrown side. Tick and number indicate direction and amount of dip.

Strike and dip of flow foliation

Strike and dip of foliation in Precambrian rocks

Twin Lakes Campground

The area was mapped primarily by Wilshire and O'Connor during the summer of 1964. Swann is responsible for the petrographic work. The study was begun to establish a base for high explosive cratering investigations in granitic rocks that will be carried out in fiscal year 1966 by C. H. Roach. Although the mapping is incomplete, the area covered allows performance of cratering experiments under controlled conditions in a variety of structural settings that have application to lunar problems.

Geologic setting

The Twin Lakes batholith is within the northeastward-trending "mineral belt" series of granitic intrusions in Colorado (Tweto and Sims, 1963). A recent regional gravity survey (Case, 1964) across the Sawatch and Mosquito-Tenmile ranges suggests that the Twin Lakes intrusion and others in the area are surface expressions of a shallow and much larger granitic mass. The country rock into which the Twin Lakes quartz monzonite was intruded consists predominantly of granitic gneiss and fine- to medium-grained, weakly foliated granite with some two-mica schist, quartzite, calc-silicate rocks, and weakly foliated granodiorite. These rocks were not studied closely beyond the area adjacent to the Twin Lakes intrusion; more detailed descriptions are given by Howell (1919).

At the southwestern edge of the area mapped (fig. 1) a large zone of intensely brecciated Precambrian rock, consisting of blocks as large as 25 feet across embedded in a finely comminuted matrix, is in contact with the Twin Lakes quartz monzonite. Neither the Twin Lakes rock nor

the surrounding unbrecciated Precambrian gneiss is highly deformed, and the breccia consists of a coarse, weakly to moderately foliated, biotite-rich granodiorite. Similar Precambrian rocks are not common along the contact with the Twin Lakes intrusion, but have been observed north and northwest of the breccia zone. The breccia is perhaps the result of sub-jacent, explosive volcanic activity related to nearby rhyolite intrusions and flows, but no volcanic material was found in the breccia.

The northern part of the Twin Lakes intrusion is cut by many small (3 inches to 25 feet wide) faults with a general north to northeast trend (fig. 1). The contact with Precambrian rocks is offset by some of the faults, but the direction and amount of displacement on most of the faults, could not be determined. The fault zones are generally intensely altered and some contain a mesothermal type of mineral deposits that have been extensively prospected. Rhyolite dikes occupy many of the faults.

Contact relations of the batholith

The trend of the contacts of the Twin Lakes intrusion (fig. 1) indicates a genei ally steep dip like that shown by Stark and Barnes (1935), and different from the low dips indicated by Howell's map (1919). In detail the contact with Precambrian rocks is very irregular both in strike and dip. Even in the limited vertical exposures avail-able, the dip of the contact changes as much as 50° in a few hundred feet. The low dip of the contact south of Twin Lakes recorded by Howell (1919) and Stark and Barnes (1935) was not confirmed; the area shown by these authors as composed of Twin Lakes quartz monzonite

93

is mostly covered by moraine, and few bedrock exposures, all Precambrian, were found.

Where the contact is well exposed, the Twin Lakes quartz monzonite cuts sharply across the foliation of the Precambrian rocks. Apophyses of Twin Lakes quartz monzonite occur locally and extend several tens of feet into the Precambrian rocks. A large block of Precambrian granite is isolated in the quartz monzonite west of Echo Creek, and small angular slabs and irregular fragments of Precambrian rocks are locally enclosed in the quartz monzonite near the contact.

A small roof pendant of Precambrian gneiss occurs just east of the divide between Sayers and La Plata Gulches (fig. 1). La Plata Peak is also composed of Precambrian gneiss, and photo-interpretation of the eastward extension of these rocks by Ogden Tweto (oral communication, 1965) indicates that they form a nearly complete bridge separating the northern and southern parts of the batholith. These Precambrian rocks represent a part of the roof of the batholith.

Petrography of the Twin Lakes quartz monzonite

The Twin Lakes quartz monzonite is distinguished from neighboring intrusions by the presence of abundant orthoclase phenocrysts, some as long as 8 inches. The phenocrysts are set in a medium- to coarse-grained groundmass composed of plagioclase, quartz, orthoclase, and biotite with minor amounts of magnetite, sphene, ilmenite, apatite, rutile, allanite, and zircon. Secondary minerals include sericite, calcite, chlorite, epidote, and clinozoisite. Both quartz and plagioclase occur locally as

94

subhedral to euhedral phenocrysts ½ to 1 inch long. Orthoclase pheno-crysts are not homogeneously distributed and appear to be concentrated in a broad zone (about 2,500 feet wide) near the margins of the intru-sion. In the central part of the area mapped, orthoclase phenocrysts make up less than about 5 percent of the rock and their average length is less than an inch; this is accompanied by a change, apparently grada-tional, to a finer grained groundmass.

Because of the generally coarse-grained nature of the rock, modal compositions (table 1) were determined from stained slabs. The actual orthoclase and mafic mineral content of the entire rock body is probably slightly higher than that indicated by the average modal composition of the slabs, because large orthoclase schlieren and mafic layers were ex-cluded from samples selected for modal analysis.

Subhedral plagioclase is the most abundant mineral in the rock. Albite twins are abundant, and carlsbad and pericline twins less common in the plagioclase. Most of the plagioclase is moderately zoned (gener-ally normal zoning, but some oscillatory zoning was observed). The average composition of the plagioclase, as determined by universal stage methods, is about An25 (mol. percent). Orthoclase in the groundmass is anhedral, and the phenocrysts are subhedral to euhedral. Carlsbad twins in the phenocrysts are common. The orthoclase is perthitic, and has a somewhat variable 2V that averages about -65°. The quartz is anhedral to euhedral, and has slight undulatory extinction.

Orthoclase phenocrysts, rimmed with oligoclase (about An25), are sparsely distributed in areas surrounding the small granitic intrusions

95

Table 1. Average modal composition of Twin Lakes quartz monzonite*

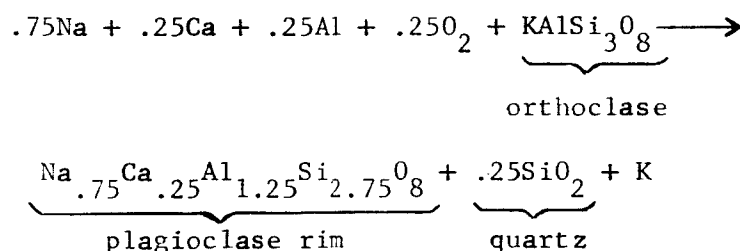| Mineral	Volume percent
Quartz	23.9
Orthoclase	27.8
Plagioclase	43.9
Mafic minerals (mostly biotite)	4.3

---

* Data obtained from stained slabs.

near Monitor Rock (fig. 1). The process that produced these rims appears to have been very selective; the rims are well developed on one out of every few thousand phenocrysts and absent on the others. This selectivity suggests that the rims are formed in some way other than by exsolution of plagioclase from orthoclase.

The majority of plagioclase grains in the rims are aligned with (010) parallel to cleavages in the orthoclase phenocrysts and protrude into the orthoclase. A few patches of orthoclase that are in optical continuity with the phenocrysts were found within some rims. A small amount of graphic quartz is present in the rims, and a lesser amount in the phenocrysts. Much of the groundmass surrounding the rims is very fine grained and appears to have been recrystallized.

Because of the localized occurrence of the rims and their textures, they are interpreted to be a replacement feature formed as solutions percolated through the Twin Lakes quartz monzonite during intrusion of the small granitic dikes and irregular masses. The graphic quartz intergrowths resulted from silica released during the replacement of orthoclase by plagioclase according to the following reaction (assuming that the orthoclase is the pure potassium end member and that silica remains constant):

$$.75Na + .25Ca + .25Al + .25O_2 + \underbrace{KAlSi_3O_8}_{\text{orthoclase}} \longrightarrow$$

$$\underbrace{Na_{.75}Ca_{.25}Al_{1.25}Si_{2.75}O_8}_{\text{plagioclase rim}} + \underbrace{.25SiO_2}_{\text{quartz}} + K$$

Flow layers

In a broad zone (about 800 to 3,000 feet wide) near the northern and
northeastern margins of the intrusion, orthoclase phenocrysts are clus-
tered in lenticular masses at least as large as 15 by 50 feet; as much as
85 percent of the clusters are made up of the phenocrysts. Near the mar-
gins and in adjacent host rock, elongate phenocrysts are commonly oriented
parallel to the contents of the pods and lenses.

In the same areas, and commonly localized near margins of pheno-
cryst concentrations, are steeply inclined layers, ¼ inch to 4 feet
thick, enriched in mafic minerals. Many mafic layers are faulted and
folded, but the fractures were healed by postdeformation crystallization.
Branching of the flow layers is very common. Truncations of layers, and
apparent truncations resulting from branching, resemble sedimentary
cross bedding. There are marked variations in grain size of mafic and
felsic constituents, both within the layers and in adjacent quartz mon-
zonite. The grain size is generally smaller in the mafic layers. The
layers are enriched in magnetite, biotite, sphene, apatite, allanite,
and locally, amphibole; all of these are minor constituents of Twin
Lakes quartz monzonite except amphibole, which is normally absent in the
quartz monzonite.

Minor intrusions within the Twin Lakes intrusion

Minor intrusions cutting the Twin Lakes quartz monzonite and the
enclosing rocks consist of rhyolite dikes, rare lamprophyric dikes, a

98

rhyolite dome, and dikes and irregular masses of fine-grained granite.

Rhyolite dikes are concentrated in the northeastern part of the batholith and commonly occupy faults. Near Smith Gulch (fig. 1), the dikes are dominantly prophyritic with prominent phenocrysts of feldspar, quartz, biotite, and amphibole in a green to pale tan or brown, aphanitic groundmass. These rocks closely resemble larger intrusions, such as Crested Butte in the Elk and West Elk mountains. Elsewhere, the rhyolite dikes are nonporphyritic or contain a few scattered phenocrysts of feldspar and quartz in a pale tan, aphanitic or microcrystalline groundmass. The dike rocks are generally severely altered, either by silicification or by conversion of primary minerals to clay minerals, carbonates, and other secondary minerals.

One lamprophyric dike was found within the Twin Lakes intrusion one-half mile west of the Twin Lakes Campground (fig. 1), and another in Precambrian gneiss adjacent to the contact with Twin Lakes quartz monzonite about one-half mile west of Galena Gulch (fig. 1). Both dikes are very dark green, fine-grained rocks composed largely of amphibole and secondary minerals.

The rhyolite dome between Sayers and La Plata Gulches (fig. 1) cuts both the Twin Lakes quartz monzonite and Precambrian rocks. It is composed dominantly of severely altered, dense, microcrystalline rhyolite with scattered phenocrysts of feldspar and quartz. The central part of the dome consists of dark vitrophyre with steeply inclined lineations defined by elongate vesicles, and contains many inclusions of coarse biotite granodiorite identical with the Precambrian breccia on the west

side of the dome. Near its northern contact the rhyolite has a pronounced platy parting that dips 20° toward the center of the dome.

The granitic intrusions near Monitor Rock (fig. 1) have an aphanitic chilled marginal zone that grades into a fine-grained granite with scattered orthoclase phenocrysts in the interior parts of the intrusions. The coarser grained parts of these intrusions are similar to the finer grained parts of the Twin Lakes quartz monzonite, and both closely resemble some intrusions such as Mt. Sopris and Snowmass Mountain in the Elk and West Elk Mountain areas.

Acknowledgments

References

Burbank, W. S., Lovering, T. S., Goddard, E. N., and Eckel, E. B., 1935, Geologic map of Colorado: U. S. Geol. Survey.

Case, J. E., 1964, Gravitational evidence for a batholithic mass of low density along a segment of the Colorado mineral belt [abs.]: Geol. Soc. America, 77th Ann. Meetings, p. 26.

Howell, J. V., 1919, Twin Lakes district of Colorado: Colorado Geol. Survey Bull. 17, 108 p.

Stark, J. T., and Barnes, F. F., 1935, Geology of the Sawatch Range, Colorado: Colorado Sci. Soc. Proc., v. 13, no. 8, p. 467-504.

Tweto, Ogden, and Sims, P. K., 1963, Precambrian ancestry of the Colorado mineral belt: Geol. Soc. America Bull., v. 74, p. 991-1014.

A MISSILE IMPACT IN WATER-SATURATED SEDIMENTS

by H. J. Moore and R. V. Lugn

Introduction

A study of craters produced by the impact of missiles is being con-
ducted jointly by the U.S. Geological Survey, the Commanding General of
White Sands Missile Range, and the Ames Research Center of the National
Aeronautics and Space Administration. This report is a detailed descrip-
tion of a crater produced by missile impact in water-saturated sediments.
The U.S. Geological Survey studied and mapped the crater and prepared this
report; the Commanding General of White Sands Missile Range allowed access
to the crater and furnished ground photography, aerial photography, and
data on the kinetic energy of the missile; Ames Research Center furnished
financial assistance for field and travel expenses.

The purposes of the study are to gather information on impact craters
for the national space program and obtain scientific data on cratering.
It is hoped that the data collected will also have engineering and mili-
tary applications.

Experimental conditions

In this test, an inert missile impacted water-saturated lake beds of
gypsum with a kinetic energy of 1.57×10^{15} ergs. This kinetic energy is
less than the nominal value of 2.27×10^{15} ergs used previously (Moore and
others, 1964, p. 59). The missile impacted at an angle of 46° from the
horizontal onto a smooth level surface underlain by lake beds. This test
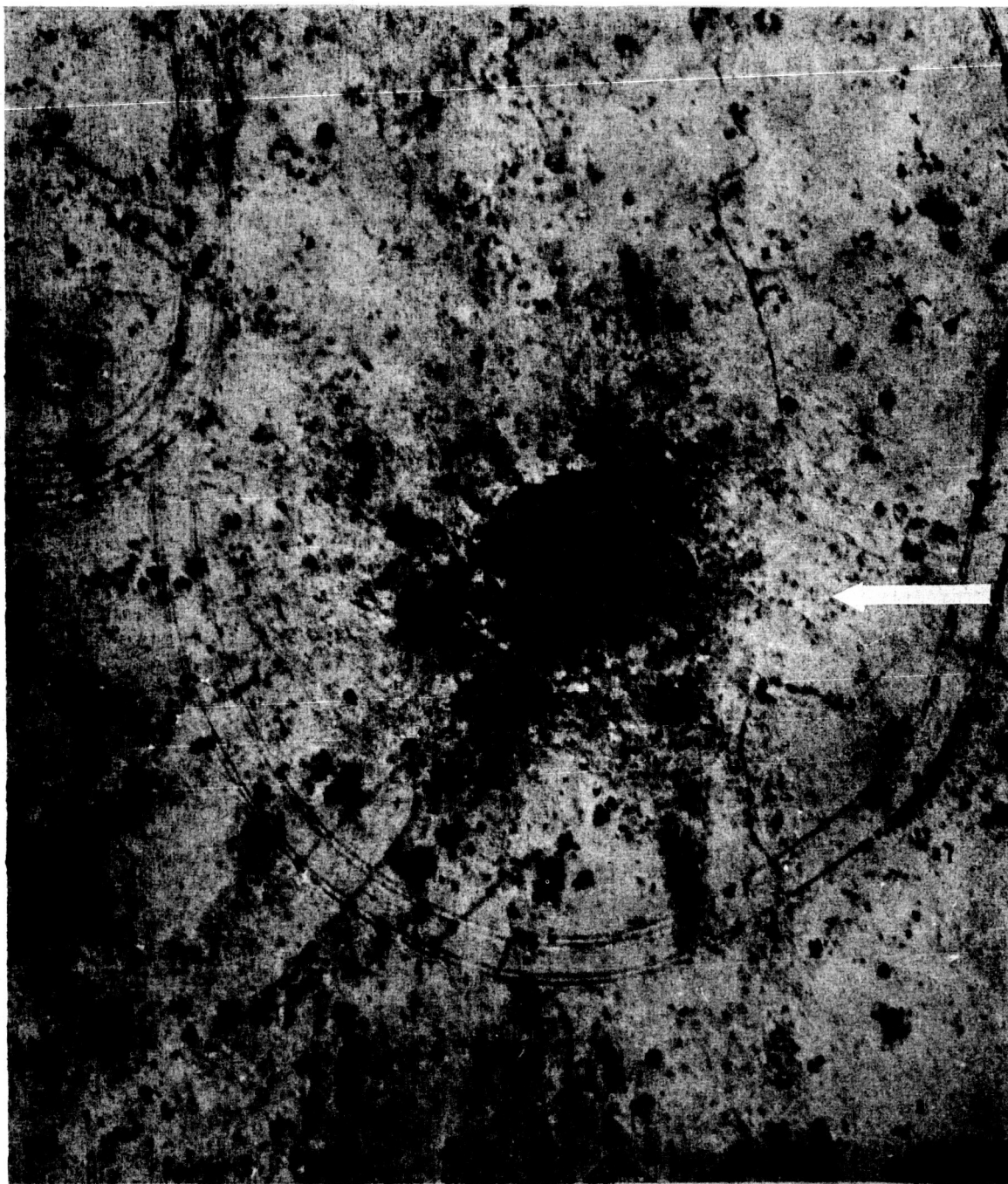is the same as crater 7 previously reported (Moore and others, 1964, p. 87-90).

Fig. 1.--Aerial photograph of crater in gypsum lake beds. Arrow indicates approximate trace of path of missile.

The target material was very pale red-brown to pale gray gypsum with some clay and about 20 percent water. Densities of the material ranged from 1.2 to 1.6 g/cm^3. Trenching revealed that the target material was layered. The upper layers consisted of very pale red-brown, moist, tough gypsum about 1.3 feet thick overlain by 0.4 feet of very pale red-brown noncohesive gypsum sand. Beneath these layers, the material changed to pale gray tough gypsum saturated with water. The top of the gray layer was coincident with the top of the water table. After completion of mapping, the crater filled with water to the level of the water table.

A topographic map of the crater and ejecta blanket was prepared, using standard plane table techniques at scales of 1:48 and 1:240. These results have been reported (Moore and others, 1964). The distribution of the secondary craters and ejecta was mapped on enlarged aerial photographs at a scale near 1:260, and a planimetric map was prepared using photogrammetric techniques. Some of the contacts for the thin to discontinuous ejecta have been revised in this report (compare Moore and others, 1964, p. 89).

Morphology of crater and ejecta

An almost circular rim (diameters 30.9 and 29.9 feet) was produced, but slopes of crater walls, the ejecta, and secondary impact distributions show marked bilateral symmetry (figs. 1 and 2). The slopes of the crater walls in the plane of the missile trajectory are not equal. The slope of the wall facing the missile trajectory is gentler than the opposing slope (see Moore and others, 1964, p. 87). In contrast, the crater walls at right angles to the plane of the missile trajectory are nearly equal and
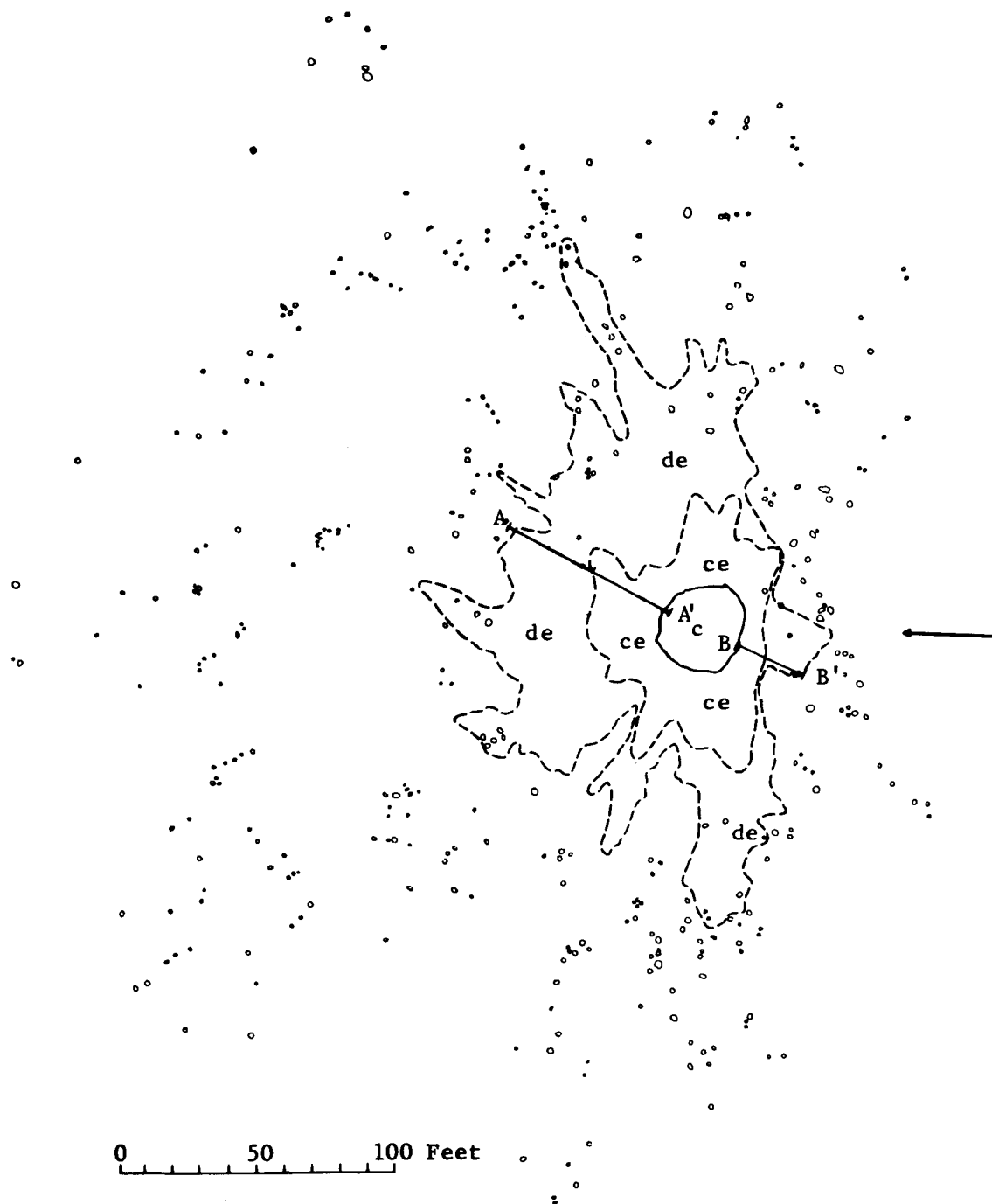
Fig. 2.--Map of ejecta and secondary impact craters around crater in gypsum lake bed.

Explanation of Figure 2.

| c | Crater, enclosing line represents crater rim crest. |

| ce | Continuous ejecta composed of blocks and fragments ranging from 1.0 foot to less than 0.03 inches. Thickness varies from 2.5 feet to about 1.0 inch. |

| de | Discontinuous patches of ejecta up to 1.0 inch thick and isolated fragments. |

Secondary impacts, ranging from implanted blocks to craters.

Trace of projectile trajectory.

slope downward to a point 7 feet below the original ground surface.

Ejecta thrown from the crater in the same direction of the missile trajectory and at right angles to it are thicker and thrown farther than ejecta thrown in opposite directions (figs. 1 and 2). Radial ridges of thick ejecta extend more than 40 feet from the crater center in the direction of the missile flight and at right angles to this direction, but only 20 feet in the direction from which the missile came.

The distribution of thin to discontinuous ejecta and secondary impact craters has bilateral symmetry (fig. 2). Lobes of thin to discontinuous ejecta up to 100 feet or more extend subradially from the crater center except in the direction from which the missile came, where a lobe extends only 45 feet from the center of the crater. Secondary impacts are found as much as 240 feet from the crater in the forward direction but only 50 feet in backward direction (fig. 2).

There was minor slumping of the crater walls. Slumped blocks are shown on one of the crater walls in figure 1.

Ejecta blanket

The ejecta blanket is a splendid example of the inversion of the original stratigraphy (fig. 3). Differences in color of the upper and lower gypsum zones permitted clear separation of these units in the ejecta. A photograph of inverted stratigraphy at the crater wall has appeared previously (Moore and others, 1964, p. 90, fig. 7d). Ejected debris from the lower, pale gray zone overlies ejected debris from the upper, pale red-brown zones to the extremities of the thick ejecta section measured (fig. 3) and further. Such inverted stratigraphy is also typical of ejecta from

A'

A"

5 — 5

Feet

0 — 0

A | 0.01'of gray zone ejecta. 0.05'of gray zone ejecta. | A'

5 — 5

Feet

0 — 0

B | 0.01' of gray zone ejecta. | B'

5 — 5

0 — 0

10   0   10   20 Feet

Explanation

Gypsum, loose non-cohesive, surface layer.

Gypsum, lake beds, pale red brown zone.

Gypsum, lake beds, pale gray zone.

Ejecta composed of debris from red brown zone and surface layer.

Ejecta composed of debris from gray zone.

Trace of beds

Original ground surface.

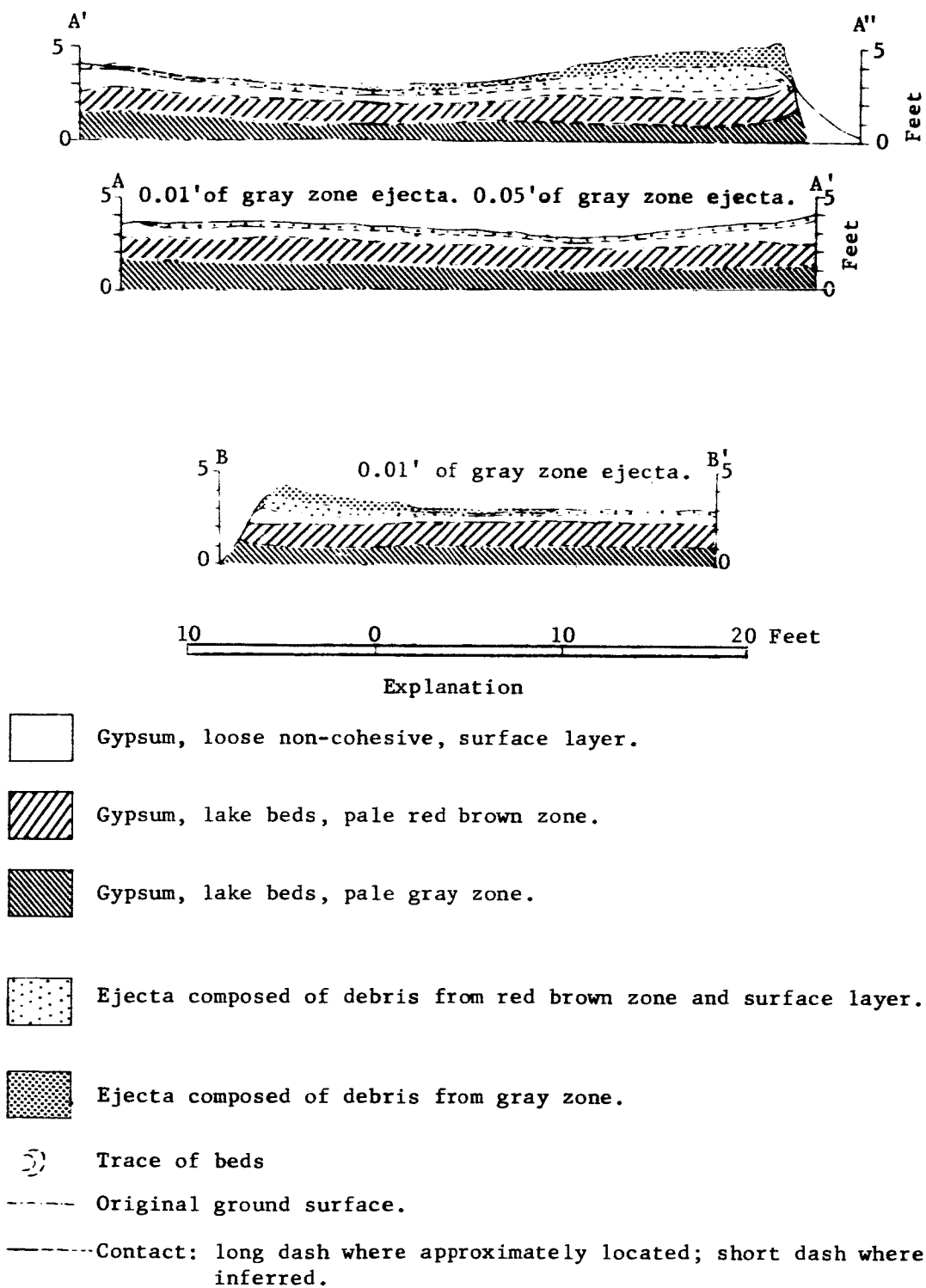Contact: long dash where approximately located; short dash where inferred.

Fig. 3.--Cross section of ejecta blanket.

some craters produced by explosives and meteorite impacts (Shoemaker, 1960, p. 422-424).

The debris in the ejecta range from blocks about 1 foot across to very fine-grained material. The various sizes of fragments in the debris are mixed but, in general, the sizes of the larger fragments decrease away from the crater and the ratio of large to fine debris decreases. Similar mixing and variations in size of ejected debris occur at Meteor Crater, Arizona.

The transition between ejecta and "bed rock" is well displayed just below the crater rim on the left side of the crater (figs. 2 and 3). Here laminae, which were originally horizontal, are tilted upward and, at the crater edge, are overturned in an arcuate fold, the upper limb of which grades into the ejecta. Overturning similar to this has been observed at Meteor Crater, Arizona, and the nuclear explosive crater, Teapot ESS (Shoemaker, 1960, p. 422-424).

Secondary impact craters

A complete series of secondary impact phenomena produced by ejected debris was found around the crater. Near the crater, ejected blocks were implanted by impact on the surface. These implanted blocks either more than filled the crater or were about the same size as the crater they made (fig. 4). Some craters were larger than the blocks or fragments that made them (fig. 5) and either small pieces of fragments remained on the crater floor or the fragment was smeared out over the crater floor. In other secondary craters, the secondary projectile was completely or almost completely ejected from the crater (fig. 6).

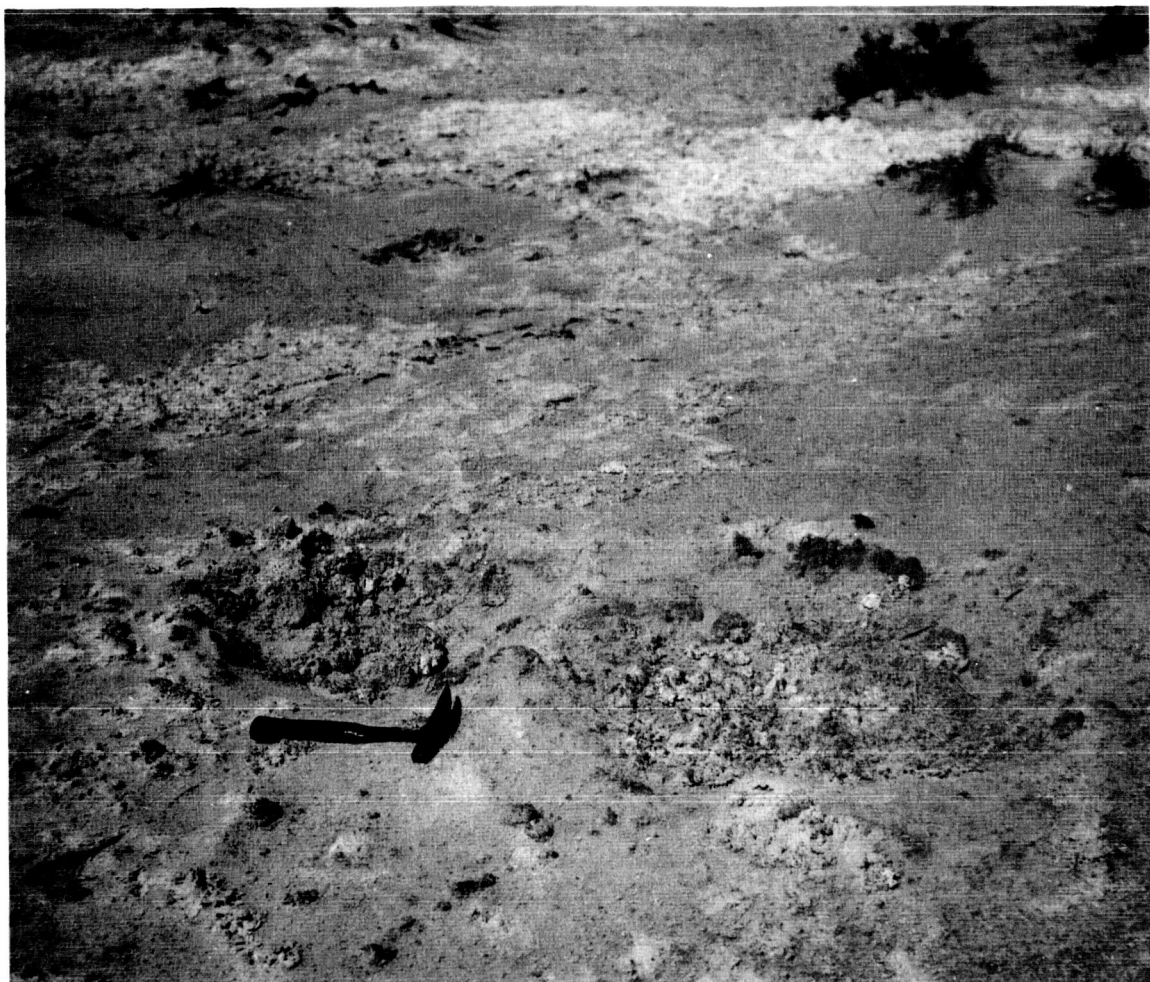Fig. 4.--Secondary impact crater filled by parts of projectile.

Fig. 5.--Secondary impact craters. Projectile fragments partly fill
one crater and are smeared out on floor of other crater.

Fig. 6.--Secondary impact crater. Projectile fragments almost completely ejected from crater.

This series is observed for impact of metal projectiles on metals. Low-velocity projectiles are found in the craters they produced either intact or somewhat deformed and fragmented (Charters, 1960, p. 129-130). As the projectile velocity increases, the metal projectile is smeared over the walls and floor of the crater (Charters, 1960, p. 129-130; Summers, 1959, p. 3). Smearing of the projectile over the crater walls is also typical for temporary craters produced by falling water drops (Charters, 1960, p. 131). Further increase in velocity of the projectile results in complete ejection of the projectile.

The velocities of the fragments that produced the secondary impact craters were low. Ballistics calculations indicate a minimum velocity for the fragments thrown 240 feet from the crater of about 27 meters (88 feet) per second. High-speed photographs show that the ejecta plumes rise about 300 feet in the air, so an impact velocity of 43 meters (140 feet) per second is indicated. The presence of secondary impact craters produced by projectiles with such low velocities can be partly attributed to the fact that the upper 0.4 feet of the target material was noncohesive and easily cratered. It is also interesting to note that crater and projectile behavior similar to that found in metals can be produced by weak projectiles impacting weak materials with velocities one to two orders of magnitude lower than those for metal-on-metal impacts.

The distribution of secondary impact craters resembles that of lunar craters such as Copernicus (Shoemaker, 1962, p. 304-305, 325-344) and Aristarchus. However, the bilateral symmetry of the distribution of the secondary impact craters is more marked than that around Copernicus and Aristarchus. Secondary impact craters are also found around some craters

112

produced by nuclear explosives such as Sedan (Roberts, 1964). Strings, clusters, loops, and irregular arrays can be found around these craters.

The distribution of secondary impact craters around primary impact craters and some explosive craters is a function of the properties of materials in which the crater occurs and the materials around the crater at the surface. The secondary impact craters around Sedan, a crater in alluvium produced by a 100-kiloton nuclear explosive at a scaled depth of burst near 1.0 $ft/lb^{1/3}$ [1], had large concentrations of secondary craters at and beyond 1 crater radius from the crater rim. Secondary impact craters around Burton-on-Trent, an explosive crater in marl, gypsum, and soil, with a scaled depth of burial near 0.56 $ft/lb^{1/3}$ [1], were present in abundance on the ejecta blanket up to and on the crater rim (Baldwin, 1963, plate XIX, facing p. 122). In contrast, secondary impact craters around nuclear craters in basalt, such as Danny Boy with a scaled depth of burst near 1.0 $ft/lb^{1/3}$ [1], and other chemical explosive craters in basalt, with scaled depths of burst commensurate with those mentioned above, are conspicuously rare everywhere. Although the secondary impact craters in the water-saturated gypsum sediments are found in abundance at 1 3/4 to 2 diameters from the crater rim, virtually no secondary impact craters are found around missile impact craters in dry alluvium. Thus, the properties of the materials in which the crater occurs as well as those at the surface around the crater are important controls on the distribution of secondary impact craters.

---

[1] The scaled depth of burst or burial used here is equal to the depth of burial of the charge in feet divided by the cube root of the weight-equivalent of TNT of the explosive charge.

The effective scaled depth of the crater must also be important. For example, deeply buried explosive charges will not eject debris during cratering as far as will charges with shallow burial. Similar results can be produced by impact. If the target material is weak and porous, the end result is similar to a camouflet and is accompanied by little or no ejection of debris. For denser targets, the amount of debris ejected is significantly larger.

Explanation of the large size of the crater

This crater, as reported previously (Moore and others, 1964, p. 66, 87-90, crater 7), is about six times larger than a crater produced by a missile impact with nearly the same energy and angle of impact in dry alluvium (Moore and others, 1964, p. 83-86, crater 6). Such a difference in size can be accounted for by the differences in stress required for failure of wet and dry materials at varying confining pressures.

The conditions for failure of soils can be represented by Mohr envelopes (see for example, Hubbert and Rubey, 1959, p. 123-125) and modified Griffith envelopes (Brace, 1960). The failure envelopes are diagrams (see figs. 7A and 7B) showing shear stresses required for failure in a unit of rock subjected to three principal compressive stresses: (1) a maximum (σ_1), (2) an intermediate (σ_2), and (3) a minimum (σ_3). When the difference between the maximum and minimum principal stresses are large enough, failure occurs. This condition occurs when a circle centered on the compressive stress axis and passing through the maximum and minimum principal stress becomes tangent to or crosses the envelope (fig. 8A). Failure then occurs during compression by shearing along planes with angles of $45° \pm \phi/2$
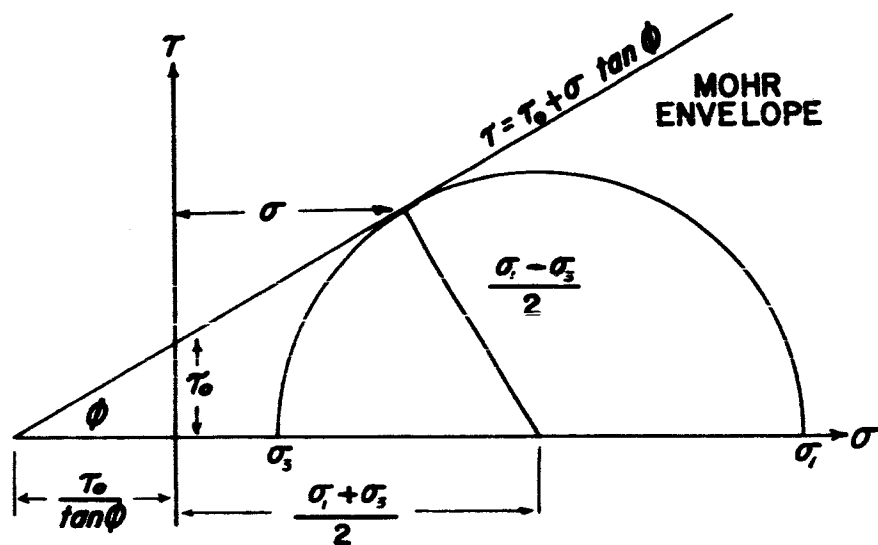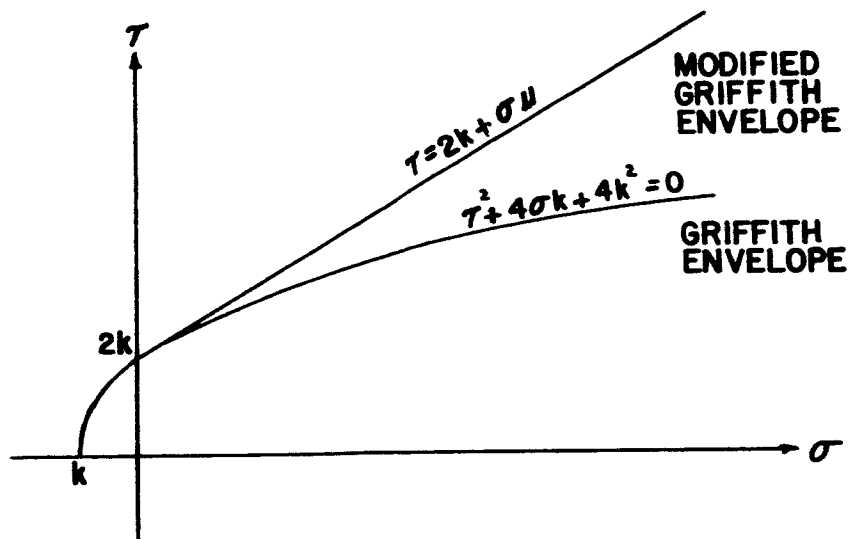
Fig. 7A.--Typical Mohr envelope for dry material.

Fig. 7B.--Modified Griffith, and Griffith, envelopes for dry material.

115

measured from the maximum principal stress. Here ϕ is the angle of internal friction. The magnitude of the shear stress for compressive failure is:

$$\tau = \tau_o + \sigma \tan \phi \qquad (1)$$

where:

> τ is the magnitude of the shear stress along the plane of failure,
>
> τ_o is the cohesion,
>
> σ is the stress normal to the plane of failure,
>
> $\tan \phi$ is the coefficient of friction;

and for the modified Griffith representation:

$$\tau = 2k + \sigma\mu \qquad (2)$$

where:

> τ is the magnitude of the shear stress along the plane of failure,
>
> $2k$ is the cohesion, which is about twice the tensile strength,
>
> σ is the stress normal to the plane of failure,
>
> μ is the coefficient of friction.

Failure in tension occurs when the difference in the maximum and minimum stresses produce a circle tangent to the Griffith envelope at the compressive stress axis.

The conditions for failure of water-saturated materials and dry materials differ significantly (Hubbert and Rubey, 1959, p. 139-142). The relationship between the stress required for failure for dry, moist, wet, and very wet materials can be expressed (Hubbert and Rubey, 1959, p. 142):
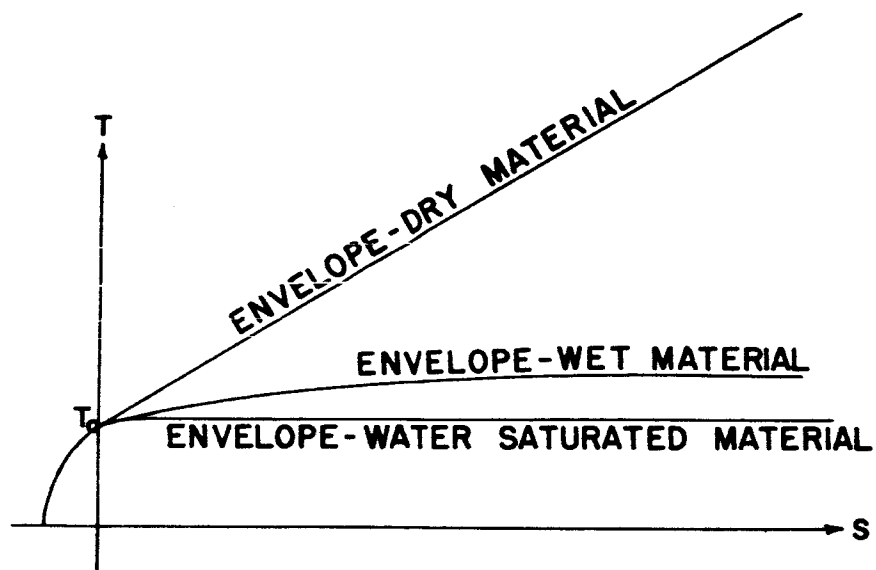
Fig. 8A.--Modified Griffith envelopes for dry, wet, and water-saturated materials.
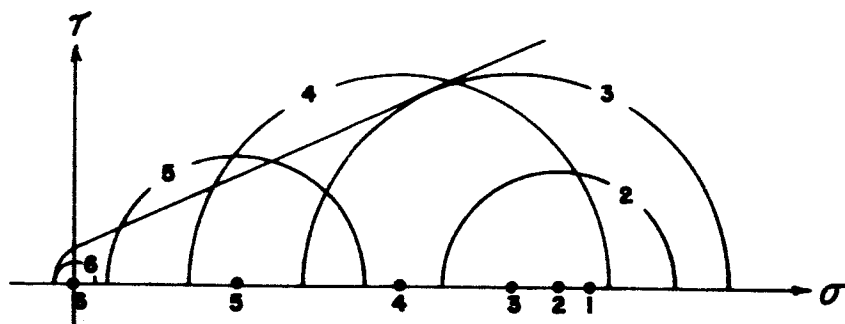

Fig. 8B.--Modified Griffith envelope for dry material illustrating sequences of stress conditions during crater formation.

$$\tau_{crit} = \tau_o + (S - p) \tan \phi$$

where

τ_{crit} is the shear stress required for failure along the

   plane of failure,

τ_o is the cohesion of the material,

S   is the total stress normal to the plane of failure,

p   is the fluid pressure,

$\tan \phi$ is the coefficient of internal friction.

The effective stress normal to the plane of failure, S - p, may vary from 0 to S depending on the conditions. Failure envelopes using total stress (S) for the abscissa for dry, wet, and water-saturated materials are shown in figure 8B. For dry materials p is zero with compression. For wet materials p may vary from some low value to S with compression of the material. For water-saturated materials, p may equal S upon initial compression.

The tensile stress required for failure of materials permeated with fluids should not differ by large amounts from that of the dry material (Jaeger, 1963). Thus, the tensile strength should be of the same order of magnitude as the cohesion according to the modified Griffith criteria for failure.

Although the failure envelopes used do not represent actual experimental determinations of failure conditions, they are typical of failure envelopes of many rocks and soils. These envelopes are, however, sufficient to illustrate the principles involved and to illustrate how confining pressures and fluids affect target failure during crater formation.

Ample evidence justifies the use of failure envelopes in interpreting

the results of cratering experiments. Significant quantities of fragments

in the ejecta and rubble in craters produced by missile impacts in dry allu-

vium have been compressed and sheared. These fragments have been compressed

from densities between 1.0 to 1.4 g/cm^3 to 2.0 $\pm$ g/cm^3. These fragments

also exhibit shear fractures with striated and grooved surfaces. Thus,

shear failure at elevated confining pressures has occurred and is important

(see Moore and others, 1964, p. 62, 85-86, crater 6). Such evidence for

shearing and compression has not been found in the crater in water-satura-

ted gypsum lake beds, but a postulate that shearing failure was important

seems reasonable by analogy with craters in dry alluvium. Such evidence

would also be substantially obscured by the presence of water. Evidence

for shearing and compression has also been observed in experiments using

chemical explosives in alluvium (Allsman, 1960), and hypervelocity impact

experiments using rock targets (Moore and others, 1962).

Failure during the late stages of crater formation in rocks and soils

is tensile. Such tensile failure is indicated by blocks of uncompressed

target material bounded by sides with ragged uneven surfaces and separa-

tions along bedding planes when the target is bedded. The upward and out-

ward ejection of materials also implies some tensile failure. There is

also evidence for tensile failure in experiments using chemical explosives

in alluvium (Allsman, 1960), and hypervelocity impact experiments using

rock targets (Moore and others, 1962).

The cratering process in dry alluvium begins with penetration of the

projectile into the target material and concomitant compression of the

target material. With continued penetration, stresses develop and produce

shear fractures resulting from the compression. During the early stages

of crater formation, target material fails by shearing during compression at high confining pressure, but as stress waves develop and propagate outward, the confining pressures decrease and stress differences required for failure decrease. Final stages of failure may be principally tensile or extension when the confining pressures drop below the ambient pressures (Moore and others, 1962; Allsman, 1960). The sequence of failure conditions during crater formation for dry materials is depicted in figure 9. For water-saturated materials, the shear stress required for failure is nearly constant with increased confining pressure.

In summary, strength considerations suggest that water-saturated materials will fail when stress differences are small and nearly equal to the cohesion of the material; these stress differences are constant and independent of confining pressure. In contrast, stress differences required for failure of dry material increase with confining pressure. Thus the average shear strength of dry material failing at varying confining pressures may exceed the cohesion of the material by significant amounts.

The magnitude of the effective deformation strength of the water-saturated gypsum during crater formation can be calculated using the Charters-Summers theory of impact crater formation (Charters and Summers, 1959) and correcting the energy for the obliquity of impact (Bryan, 1962):

$$S_{eff} = \frac{\frac{1}{2} m_p V_p^2 \cos \theta}{2 \ Vol_c}$$

where:

S_{eff} is the effective deformation strength of the target,

$\frac{1}{2} m_p V_p^2$ is the kinetic energy of the projectile,

cos θ is the correction for the angle of impact,

Vol_c is the volume of the crater.

Substitution of the appropriate values gives:

$$S_{eff} = \frac{1.57 \times 10^{15} \text{ ergs } 0.72}{2(4.60 \times 10^7 \text{ cm}^3)} = 1.23 \times 10^7 \text{ dynes/cm}^2 \approx 12 \text{ bars.}$$

Since S_{eff} is the compressive strength and the water-saturated gypsum be-

haves like a plastic material (fig. 8B), the shear strength is about 1/2

the effective deformation strength or 6 bars (≈ 90 psi). This value is

close to the cohesion of this material. The value of the cohesion com-

puted, 6 bars, is reasonable for this material and is similar to that of

a diatomaceous earth (τ_o = 4.7 bars) with similar properties.

The result above may be compared with similar calculations for a

crater in dry alluvium (crater 6, Moore and others, 1964, p. 85-87) for

which the kinetic energy and angle of impact were 1.38 x 10^{15} ergs and

46°. The volume of the crater was 7.68 x 10^6 cm^3. The calculations for

the crater in dry alluvium yield a value for the effective deformation

strength of 64.8 bars (≈ 950 psi) and, assuming an angle of internal fric-

tion of 30°, the effective shear strength is about 18.7 bars (≈ 274 psi).

This value is well above the cohesion of the alluvium which is of the order

of 0.4 bars (≈ 7 psi). On the average, the alluvium behaved like a weak

sandstone or shale. This is consistent with the presence of sheared and

compressed alluvium with densities near 2.0 g/cm^3 on the crater floor and

in the ejecta from this crater.

It is not surprising that the use of the Charters-Summers theory gives

reasonable results for these craters. The use of this theory for calcula-

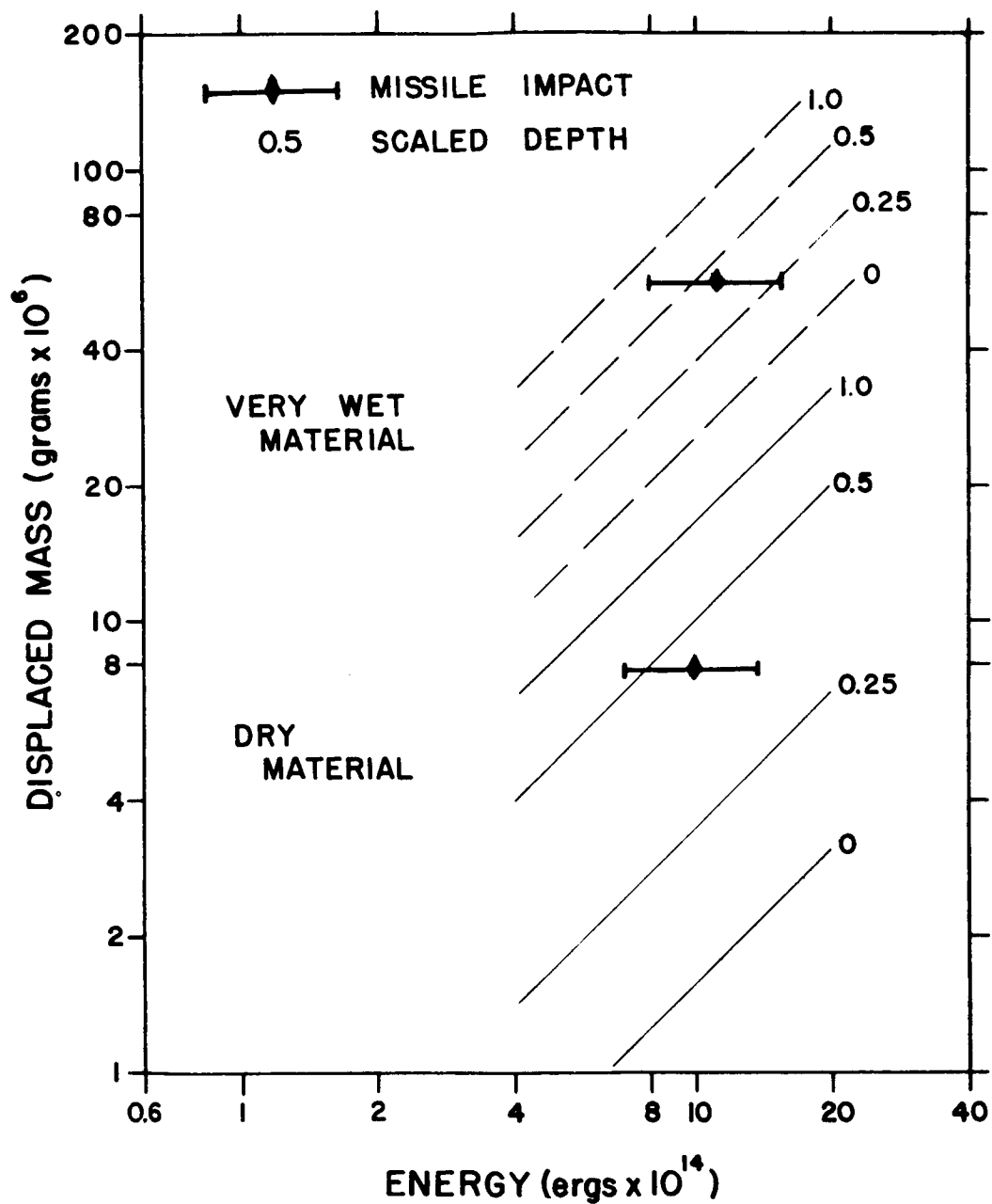ting the effective deformation strength of temporary water craters produced

Fig. 9.--Plot comparing craters produced by missile impacts and chemical explosives in dry and very wet to water-saturated materials.

by falling water drops and craters in metals and rocks yields reasonable results (Moore and others, 1963).

Comparison with craters produced by chemical explosives

Results similar to those obtained by missile impact in wet and dry materials are also obtained from cratering experiments using chemical explosives in wet and dry materials (Sager and others, 1960; Sachs and Swift, 1955). The missile-impact craters in water-saturated gypsum and dry alluvium are compared with cratering experiments using high explosives in wet clays, sands, and dry alluvium in figure 9. The cratering data for chemical explosives have been generalized in figure 9 by use of contours representing various scaled depths of burial. The figure illustrates general concordance of data for the impact and chemical explosive craters in wet and dry materials.

Students of cratering by chemical explosives should explore the role of fluid pressures on the strength of the medium since these results give some promise of at least partly answering the problem of size differences between craters in dry and wet materials.

Summary and conclusions

The impact of a missile on water-saturated materials produced a crater similar to those produced by meteorite impact and chemical-nuclear explosives. The asymmetrical ejecta and secondary impact patterns reflect the missile trajectory.

A series of secondary phenomena was observed in which secondary impacts produced implanted blocks, secondary craters containing fragments, and

secondary impact craters not containing fragments.

The anomalously large size of the crater in water-saturated gypsum may be partly attributed to fluid pressures that developed during cratering and permitted the effective target strength to be small at elevated confining pressures.

The sizes of craters produced by missile impacts in wet and dry materials are comparable to those produced by chemical explosives in wet and dry materials when the kinetic energy of the missiles is equal to the TNT energy equivalents of the explosives.

References

Allsman, P. L., 1960, Analysis of explosive action in breaking rock: Am. Inst. Mining Metall. Petroleum Engineers Trans., v. 217, p. 469-478.

Baldwin, R. B., 1963, Measure of the Moon: Chicago, Univ. Chicago Press, 488 p.

Brace, W. F., 1960, An extension of the Griffith theory of failure to rocks: Jour. Geophys. Research, v. 65, p. 3477-3480.

Bryan, G. M., 1962, Oblique impact of high velocity steel pellets on lead targets, in Symposium on hypervelocity impact, 5th, Denver 1961, Proc., v. 1, pt. 2: San Diego, U.S. Naval Research Laboratory, p. 511-534.

Charters, A. C., 1960, High-speed impact: Scientific American, v. 203, no. 4, p. 128-140.

Charters, A. C., and Summers, J. L., 1959, Some comments on the phenomena of high-speed impact, in Decennial symposium, May 26, 1959, White Oak, U.S. Naval Ordnance Laboratory, Silver Spring, Md., p. 1-21.

Hubbert, M. K., and Rubey, W. W., 1959, Role of fluid pressure in mechanics of overthrust faulting-- I. Mechanics of fluid-filled porous solids and its application to overthrust faulting: Geol. Soc. America Bull., v. 70, p. 115-166.

Jaeger, J. C., 1963, Extension failures in rocks subject to fluid pressure: Jour. Geophys. Research, v. 68, p. 6066-6067.

Moore, H. J., Kachadoorian, R., and Wilshire, H. G., 1964, A preliminary study of craters produced by missile impact, in Astrogeologic Studies Ann. Prog. Rept., July 1, 1963-July 1, 1964, pt. B: U.S. Geol. Survey open-file report, p. 58-92.

Moore, H. J., Lugn, R. V., and Gault, D. E., 1962, Experimental hypervelocity impact craters in rock, in Symposium on Hypervelocity Impact, 5th, Denver 1961, Proc., v. 1, pt. 2: San Diego, U.S. Naval Research Laboratory, p. 625-643.

Moore, H. J., MacCormack, R. W., and Gault, D. E., 1963, Fluid impact craters and hypervelocity--high velocity impact experiments in metals and rock, in Symposium on Hypervelocity Impact, 6th, Cleveland, Proc., v. 2, pt. 2: Cleveland, Firestone Tire and Rubber Co., p. 367-399.

Roberts, W. A., 1964, Secondary craters: Icarus, v. 3, p. 348-364.

Sachs, D. C., and Swift, L. M., 1955, Small explosion tests, Project Mole, final report on Project no. PU-876: Menlo Park, California, Stanford Research Inst., 2 vols.

References--Continued

Sager, R. A., Denzel, C. W., and Tiffany, W. B., 1960, Compendium of crater data; cratering from high explosive charges: U.S. Army Engineers Waterways Exptl. Station, Vicksburg, Miss., Tech Rept. no. 2-547, 32 p.

Shoemaker, E. M., 1960, Penetration mechanics of high velocity meteorites, illustrated by Meteor Crater, Arizona: Internat. Geol. Cong., 21st, Copenhagen, Rept., pt. 23, p. 418-434.

_____ 1962, Interpretation of lunar craters, in Kopal, Zdenek, ed., Physics and astronomy of the Moon: New York, Academic Press, 538 p.

Summers, J. L., 1959, Investigation of high-speed impact--regions of impact and impact at oblique angles: U.S. Natl. Aeronautics and Space Adm. Tech. Note D-94.

THE FRAGMENTATION OF SPHERES BY PROJECTILE IMPACT

by H. J. Moore and D. E. Gault[1]

Introduction

In a series of nine experiments, projectiles were fired at 2-inch spheres composed of basalt and large rectangular blocks of basalt and glass with planed surfaces. In addition, one basalt sphere was broken by compression.

The results of the experiments show: (1) more large fragments and fewer small fragments are produced by high-velocity impacts with spheres than by impacts into large rectangular blocks; (2) there is no clear correlation between the size distribution of debris from the spheres and the size distribution of meteoroids and meteorites; (3) there are similarities as well as differences between the fragmentation produced by high-velocity impacts on spheres and spheres broken by compression; and (4) breakage produced by impacts with the spheres is related to the kinetic energy of the projectile.

Experimental procedure

Basalt spheres 3/16 inch in diameter were fired at 2-inch basalt spheres suspended in lucite boxes. The small spheres were accelerated with a horizontal powder gun at Ames Research Center. Velocities of the small spheres, which were determined within ± 0.01 km/sec by spark photography of the projectiles in flight, ranged between 1.37 and 1.97 km/sec.

---

[1] Ames Research Center, Moffett Field, California.

Projectiles were mounted in four-piece nylon sabots, which guided the projectiles down the launch tube and were separated from the projectiles by aerodynamic drag. Projectile energies ranged from 1.52 to 4.95 x 10^9 ergs. Experimental procedures for the cratering experiments in large rectangular blocks with planed surfaces (semi-infinite targets) have been described elsewhere (Moore and others, 1963, p. 53). The experimental conditions and those for selected impacts on large rectangular blocks (semi-infinite targets) are summarized in table 1.

The basalt spheres were prepared by the Optical Laboratory at Ames Research Center. The 2-inch spheres were attached to a string with rubber cement and suspended in a lucite box $8\frac{1}{4}$ x $8\frac{1}{4}$ x $12\frac{1}{4}$ inches. The lucite box was closed except for a lucite tube 2 inches in diameter, which allowed projectile entry. After entry of the projectile, the tube was sealed by a spring-loaded trap door actuated by explosives to prevent loss of debris.

Basalt from Putnam Peak near Vacaville, California, was used for the large spheres and projectiles. The density of the basalt was near 2.8 g/cm^3 and, by volume, was 53 percent plagioclase, 31 percent augite, 9 percent magnetite and ilmenite, 5 percent celadonite(?), and 2 percent apatite. The modal grain size was near 0.08 mm, but the size ranged between 0.3 and 0.003 mm, with very few grains between 0.3-0.2 mm and 0.02-0.003 mm. The acoustic velocity of the basalt was near 5.5 km/sec, and measured strengths were near 2.56 x 10^9 dynes/cm^2 for unconfined compressive strength and near 1.42 x 10^8 dynes/cm^2 for tensile strength. One 24.0836-g sphere of basalt was broken by slowly compressing it between a plate and mortar; it was broken in water to reduce the loss of fines. During the size-distribution analysis, 24.0810 g of fragments was recovered.

128

Table 1. Experimental conditions

Target		Projectile				Debris	
Material*	Density (g/cm³)	Material and mass (g)	Shape and diameter	Velocity (km/sec)	Kinetic energy (10⁹ ergs)	Mass finer than 1.0 mm (g)	Size passing 3.0 g (mm)
1. 2-in. basalt sphere, 191.16 g (P466)	2.78	basalt, 0.1600	sphere, 3/16 in.	1.39	1.55	1.3	3.0
2. 2-in. basalt sphere, 193.42 g (P467)	2.82	basalt, 0.1620	sphere, 3/16 in.	≥1.37	≥1.52	1.2	3.1
3. 2-in. basalt sphere, 189.58 g (P468)	2.76	basalt, 0.1602	sphere, 3/16 in.	≥1.37	≥1.51	--	--
4. 2-in. basalt sphere, 190.69 g (P469)	2.79	basalt, 0.1615	sphere, 3/16 in.	1.38	1.54	1.4	2.6
5. 2-in. basalt sphere, 186.42 g (P470)	2.72	basalt, 0.1608	sphere, 3/16 in.	1.97	3.35	4.6	0.51

*All basalt from Vacaville, California.

Table 1--Continued. Experimental conditions

Target		Projectile				Debris	
Material*	Density (g/cm^3)	Material and mass (g)	Shape diameter	Velocity (km/sec)	Kinetic energy (10^9 ergs)	Mass finer than 1.0 mm (g)	Size passing 3.0 g (mm)
6. 2-in. basalt sphere, 194.70 g (P471)	2.83	basalt, 0.1618	sphere, 3/16 in.	2.48	4.95	6.2	0.17
7. Semi-infinite block of basalt (SP 445)	2.85	aluminum, 0.0460	sphere, 1/8 in.	6.2	≈8.8	4.7	0.17
8. Semi-infinite block of basalt (MS 503)	2.85	poly-ethylene, 4.25	cylinder, 20 mm	5.73	6.97	2.80	0.005
9. Semi-infinite block of pyrex glass (J-14)	2.23	pyrex, 0.0375	sphere, 1/8 in.	6.58	8.13	2.2	n.a.

*All basalt from Vacaville, California.

Standard sieving screens and techniques were used in conjunction with settling and centrifuging to obtain the size distributions of the debris. Indicated recoveries obtained by comparing the target mass loss with mass recovered were 99.1 to 93.9 percent for the impact experiments.

Description

The impact of the basalt projectiles with the lower energies produced small craters on the surfaces of the larger spheres (fig. 1) and projectiles with the higher energies completely disrupted the spheres (fig. 2).

The small craters in the basalt spheres are similar to craters in semi-infinite targets. Radial fractures are found around the craters, and the crater walls are spall surfaces. In contrast with craters in semi-infinite targets, crushed and sheared basalt from near the crater floors has been ejected, and fractures concentric to the crater and normal to the surface are well developed. The ejecta from the craters, which are similar to those from semi-infinite targets, are of two types: (1) fine debris ejected during the early stages of the event and derived from the target and projectile, and (2) spall fragments ejected during late stages of the event and derived from the periphery of the craters.

The spheres that were totally disrupted by the impact gave rise to four types of debris: (1) fine debris ejected during the early stages of the event and derived from the target and projectile, (2) small spall fragments from around a transient crater, (3) large shell-like fragments peeled from the sphere during the late stages of the event and (4) a spherical core (fig. 2).

In contrast with the spheres totally disrupted by the projectile

131

O   I CM

Fig. 1.--Sphere with impact crater produced by 3/16-inch basalt projectile at 1.55 km/sec.
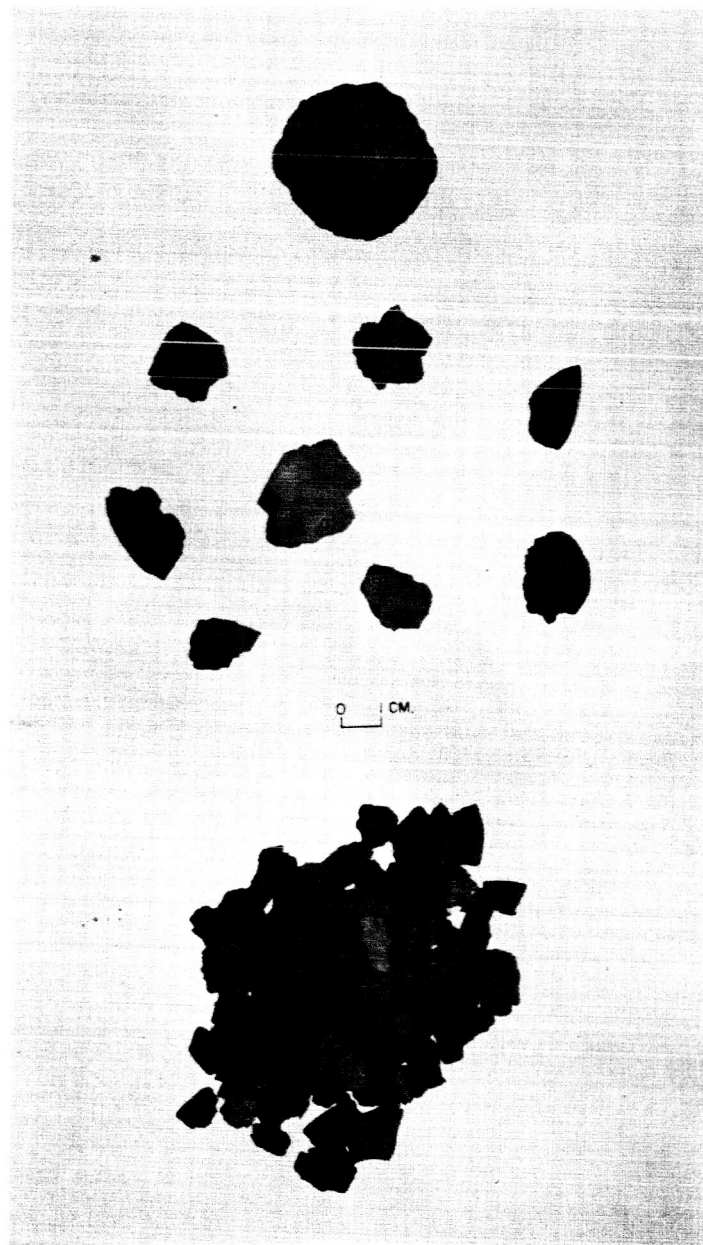
Fig. 2.--Core and fragments peeled from surface of a 2-inch basalt
sphere impacted by a 3/16-inch basalt sphere at 2.48 km/sec.

impact, debris from the basalt sphere broken by compression was composed of: (1) fine debris, (2) medium debris with varishaped fragments, including rods, and (3)"orange section"-shaped fragments similar to the lunes produced by fragmentation by compression of glass spheres (Bergstrom and Sollenberger,1961). Part of the debris is shown in figure 3.

Craters and ejecta from craters in semi-infinite targets of basalt have been described previously (Moore and others, 1962). In summary, the craters are shallow cones with depth-to-diameter ratios near 1 to 5. Radial fractures are found around the crater. The crater walls are gently sloping hummocky spall surfaces and the floors are underlain by crushed and sheared basalt. The ejecta are composed of: (1) fine debris derived from the projectile and basalt and ejected during the early stages, (2) fragments of intermediate size, and (3) large "piece of pie"-shaped spall fragments from the peripheral parts of the craters.

Size distributions

Comparison of the size distributions (figs. 4-7) shows that: (1) For fragments larger than 0.3 mm, the increase in amount of material with increasing fragment size is larger for the fragmented spheres than for the craters in semi-infinite targets and the increase is about equal to that of the sphere broken in compression. (2) The slopes of the cumulative size distribution curves are about the same for material finer than 0.01 mm for debris from the spheres and from craters in semi-infinite targets, but this slope is less for the sphere broken by compression.

Inspection of the size distributions of debris produced by impact of the spheres (figs. 4-6) reveals that the cumulative curves are not

linear. Although the curves have a slope near 1 below 0.01 mm, they flatten between 0.01 mm and 0.34 mm and then steepen again above 0.34 mm. The reason for this is illustrated by the histograms between 0.34 and 0.043 mm sizes, where the difference in weight percent retained between two size intervals tends to decrease. This effect is present to a greater or lesser degree in all size distributions for basalt, including the basalt sphere broken by compression (fig. 6). However, the change in slope in the cumulative curve for the basalt sphere broken by compression is not as marked as that for debris from the impacted spheres because the slope of the cumulative curve below 0.01 mm is smaller for the compressed sphere debris.

The increase of the weight fraction of coarse debris between two sizes with increasing fragment size is larger for the basalt sphere fragmented by compression than for the ejecta from the craters in basalt (compare figs. 6 and 7). Similar results are obtained when the size distribution of a glass sphere broken by compression (Bergstrom and Sollenberger, 1961) is compared with that of the ejecta from a crater in pyrex (fig. 8). For the fragmented sphere the cumulative curve has a slope near 1.0 in contrast with a slope near 0.6 for the coarser sizes of the debris from the crater in pyrex, thus illustrating the differences in the increase of weight fractions of the coarse debris. The increase in the weight fraction of debris between two sizes with increasing fragment size is about the same for the basalt spheres fragmented by impact and the basalt sphere fragmented by compression (fig. 6).

Comparison with meteorite distributions

There is no direct correlation of the size distribution of the debris

from the experiments using spheres with the size distribution of meteorites and meteoroids. For these experiments there is an increase in the amount of material in each logarithmic mass-size interval as the fragment size increases, except for a limited size range. For meteoroids and meteorites, most workers find a constant value or a decrease in the amount of material in each logarithmic mass-size interval (see, for example, McCracken and others, 1963, p. 10 and 11). This result does not imply that meteoroids and meteorites are not the result of fragmentation by impact since an integrated size distribution may be composed of a number of smaller size distributions with different forms. In addition, we know little about scaling relationships for very large events.

Frequency distributions of meteoroids and meteorites are generally expressed in the form:

$$n = k_1 M^\beta \tag{1}$$

where

> n is the cumulative frequency of meteorites with masses
>
> larger than M,
>
> β is a constant,
>
> k_1 is a constant.

The incremental frequency, Δn, for equal logarithmic intervals of M may be obtained as follows:

$$\Delta n = n_i - n_j; \tag{2a}$$

and

$$\Delta n = k_1 M_i^\beta - k_1 M_j^\beta; \tag{2b}$$

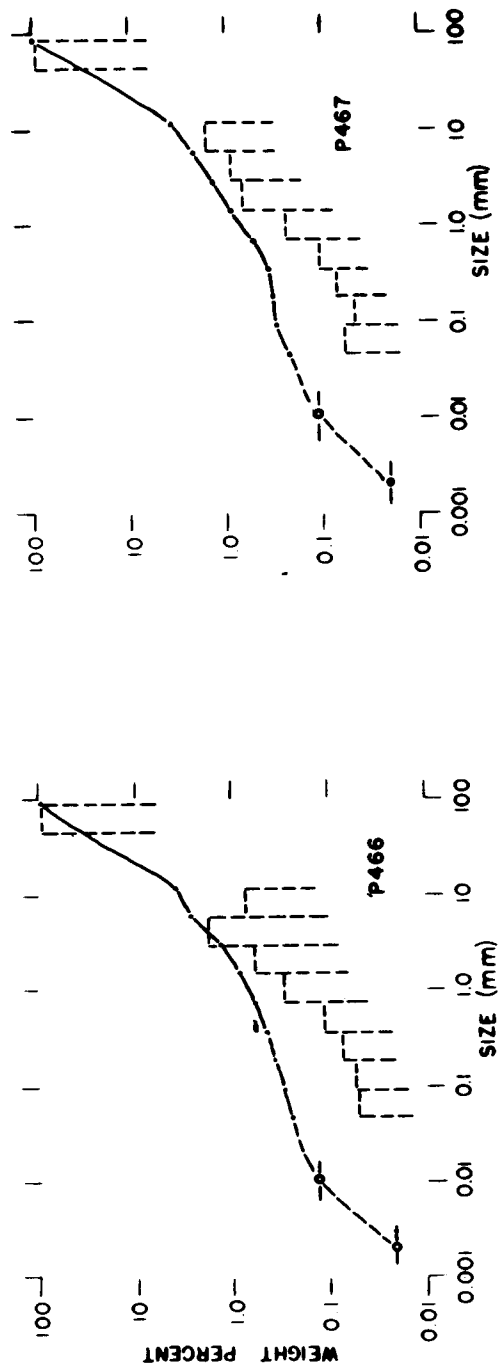Fig. 3.--Debris produced by compression of 24-g sphere of basalt.

Fig. 4.—Size distributions of debris produced by impact of 3/16-inch basalt spheres. Projectile velocities were 1.39 km/sec for P466 and about 1.37 km/sec for P467.
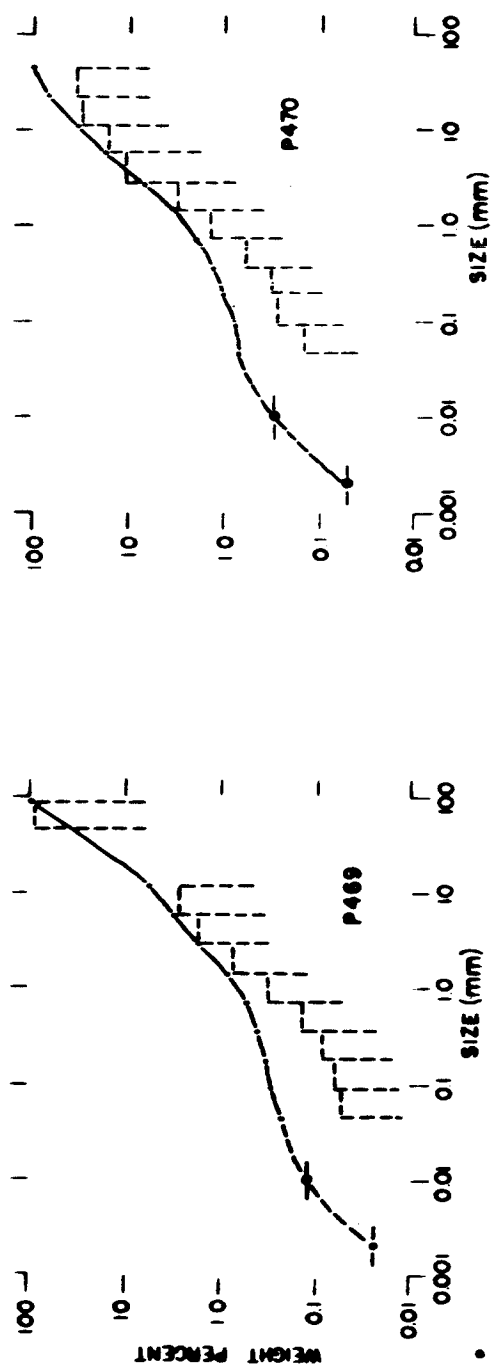
Fig. 5.—Size distributions of debris produced by impact of 3/16-inch basalt spheres with 2-inch basalt spheres. Projectile velocities were 1.38 km/sec for P469 and 1.97 for P470.
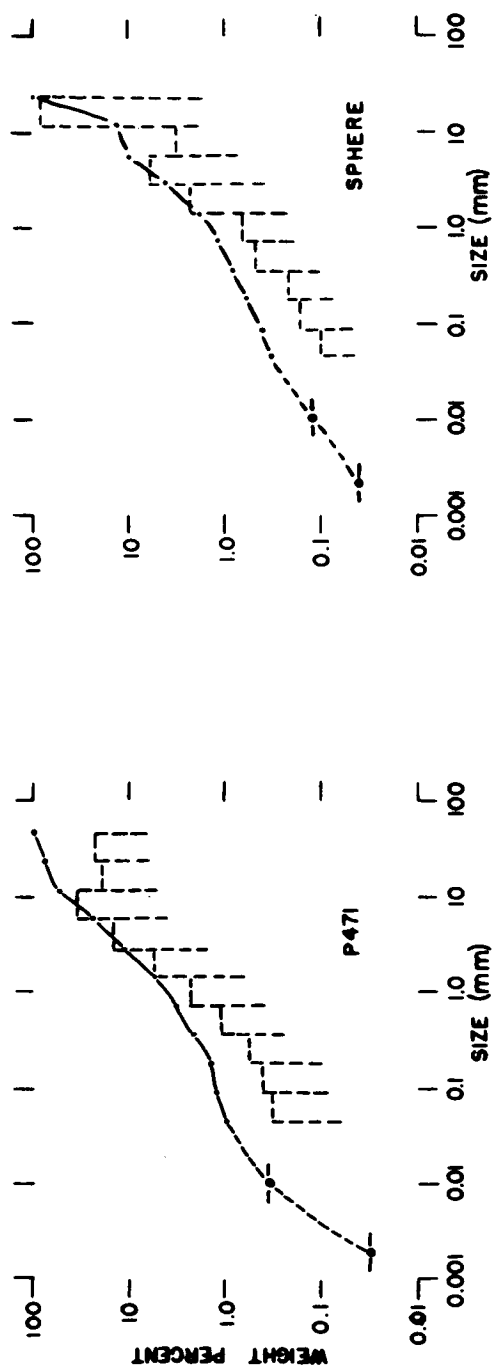
Fig. 6.—Size distributions of debris produced by impact of 3/16-inch basalt sphere at 2.48 km/sec with 2-inch basalt sphere (left) and of debris produced by compression of 24-g sphere (right).
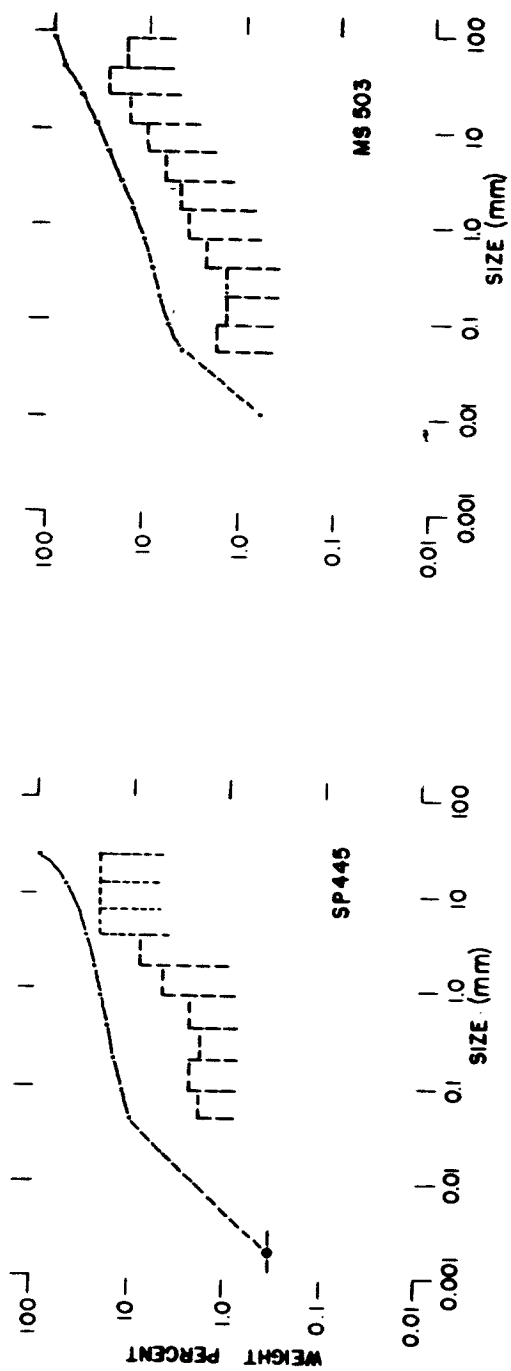
Fig. 7.—Size distributions of ejecta from craters produced by hypervelocity impacts with basalt.

Fig. 8.--Size distributions of ejecta from crater produced by hypervelocity impacts with basalt (left) and of debris produced by compression of glass sphere (right). (After Bergstrom and Sollenberger, 1961.)

142

where

Δn is the incremental frequency between masses

M_i and M_j, or cumulative frequencies n_i and n_j.

When

$$k_2 M_i^{\beta} = M_j^{\beta};$$ (2c)

then

$$\Delta n = k_1 M_i^{\beta} \left(1 - k_2 \right),$$ (2d)

where

$k_2^{\frac{1}{3}}$ is the size of the logarithmic interval M_i to M_j.

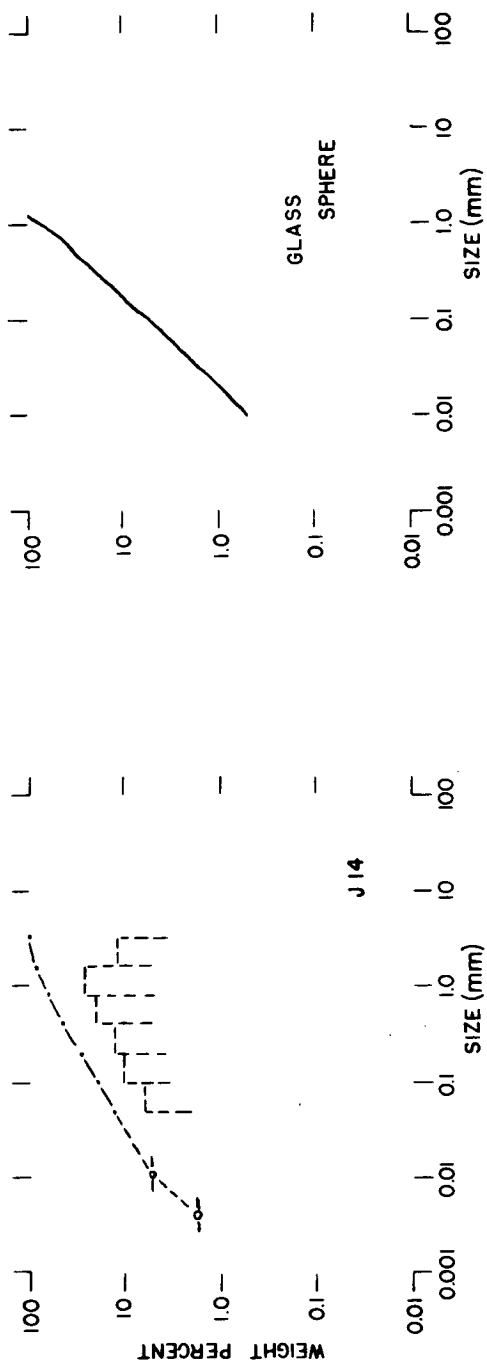The cumulative frequency of fragments in the size distributions of debris from the spheres may be determined when the cumulative curve of the size distribution has a constant slope and the fragments are assumed to be geometrically similar. The size distribution may then be represented by

$$M_e = \left(\frac{e}{b} \right)^{\alpha}$$ (3a)

where

M_e is the cumulative mass finer than diameter e,

b is the diameter of the largest fragment,

α is the slope of the size distribution curve,

or, in terms of mass

$$M_e = \left(\frac{m_e}{m_b} \right)^{\frac{\alpha}{3}}$$ (3b)

where

m_e is the mass of a fragment with diameter e,

m_b is the mass of a fragment with diameter b,

143

the incremental frequency, dn, is

$$dn = \frac{dM_e}{m_e} \; ;$$

(4a)

$$\frac{dM_e}{m_e} = \frac{\frac{\alpha}{3}}{m_b^{\frac{\alpha}{3}}} m_e^{\frac{\alpha}{3} - 2} dm_e$$

(4b)

and the cumulative frequency, n, is

$$n = \frac{\frac{\alpha}{3}}{\left(\frac{\alpha}{3} - 1\right) m_b^{\frac{\alpha}{3}}} m_e^{\frac{\alpha}{3} - 1} + c$$

(5a)

when the constant, c, is small and unimportant,

$$n = k_3 m_e^{\frac{\alpha}{3} - 1}$$

(5b)

and equation 5b has the same form as equation 1. The incremental fre-quency, Δn, for equal logarithmic intervals of m_e is

$$\Delta n = k_3 m_e^{\frac{\alpha}{3} - 1} (1 - k_4)$$

(6)

and has the same form as equation 2d.

In comparing equations 1 and 2 with 5b and 6, β and $\frac{\alpha}{3} - 1$ are com-parable. Values for β for meteroids and meteorites with masses between about 10^{-6} g and 10 g range from -1.0 and -1.48 (see for examples, Whipple, 1963; Kaiser, 1961; Hawkins and Upton, 1958; Millman and Burland, 1957; Watson 1956) and for meteoroids and dust with masses below 10^{-6} g the values for β range from -1.7 to -0.51 (see for examples, Crozier, 1962; McCracken and others, 1961; Beard, 1959; Van de Hulst, 1947). Values for $\frac{\alpha}{3} - 1$ near -0.66 were obtained for the debris from the spheres

for fragments between about 10^{-5} and 4.0 g. For the debris from the spheres with fragments between 10^{-8} and 10^{-5} g the value for $\frac{\alpha}{3} - 1$ was near -1.0; for fragments smaller than 10^{-8} g $\frac{\alpha}{3} - 1$ was near -0.60. Thus, the frequency distributions of the debris from the spheres do not agree with those for meteoroids and meteorites, except for a small interval in the smaller sizes.

Although the slopes of the frequency distributions of the debris from spheres do not generally agree directly with those determined for the meteoroids and meteorites, the difference could be accounted for by the frequency of events of various sizes; and thus the integrated distribution might bear no resemblance to the distributions produced by single events composing it.

Energy-size relationships

Comparisons between the kinetic energies of the projectile at impact and the size distributions of the debris produced from the spheres reveal that: (1) more fine material is produced by the higher energy projectiles, and (2) the size of holes in a sieve that will pass 3 g of debris is an inverse function of the kinetic energy of the projectile. In figure 9, kinetic energies have been plotted against cumulative masses finer than given size (x). The plot shows that the slopes of these curves decrease with increasing fragment size, illustrating that the amount of material broken is not a simple function of the kinetic energy of the projectile.

The plot of kinetic energy of the projectile and the size of holes in a sieve that will pass 3 g of debris suggests an energy relationship similar to that obtained in crushing experiments (Charles, 1957, and
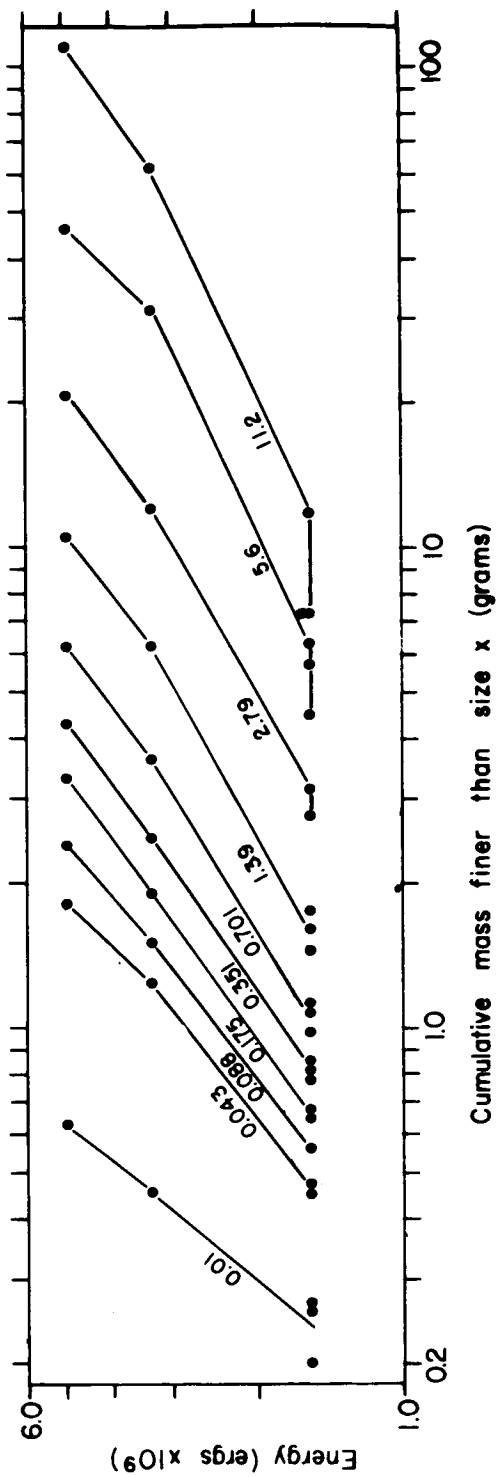
Fig. 9.--Comparison of kinetic energy of projectile and cumulative mass of debris finer than size x for impacts with spheres. Numbers on graph represent sieve openings in millimeters.
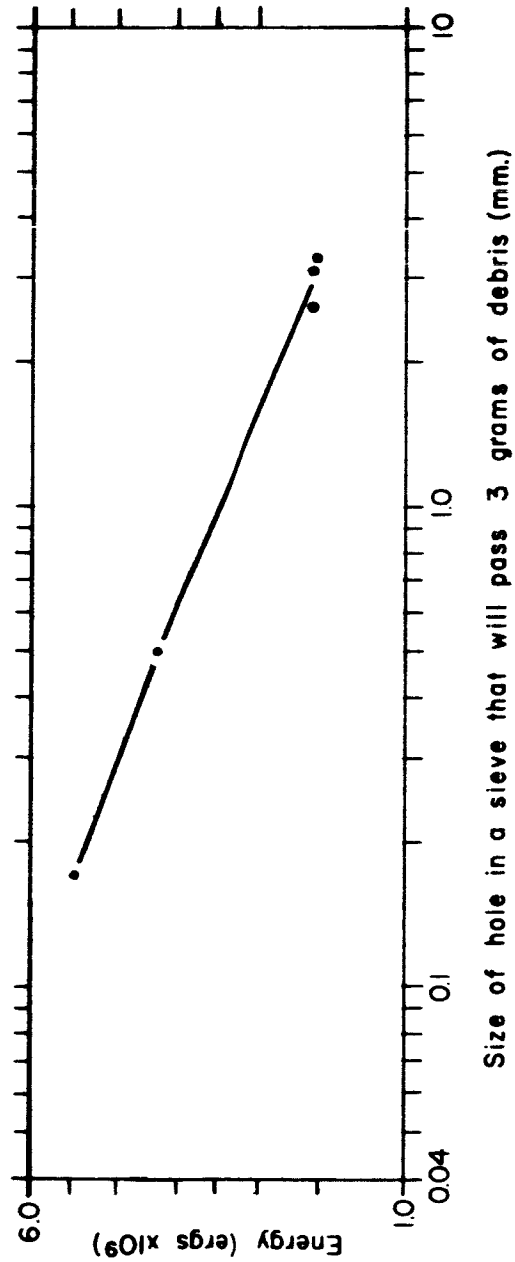
146

Fig. 10.--Comparison of kinetic energy of projectile and size of holes in sieve passing 3 g of debris from spheres.

Holmes, 1957). Charles and Holmes found that the size moduli of crushed products is an inverse function of the energy input of a comminution device. Figure 10 represents similar results.

Summary

The results of experimental impacts with spheres and semi-infinite targets show differences in fragmentation. The increase in the amount of debris with increasing fragment size is larger for the high-velocity impacts with spheres than for cratering experiments using semi-infinite targets. This increase is about equal for larger size fragments and for spheres broken by impact and by compression.

There is no direct correlation between the size distributions of the debris from the spheres and those of meteoroids and meteorites. For the spheres, the absolute values of the slopes of the cumulative frequency curves are generally less than those for meteoroids and meteorites.

There are parallels between fragmentation produced by high-velocity impacts on spheres and spheres broken by compression. The size distributions of the debris produced is similar in form, especially for the coarse debris.

The amount of material broken by impacts on spheres is partly related to the kinetic energy of the projectile. More fine debris is produced by projectiles with higher kinetic energies than by those with lower kinetic energies.

References

Beard, D. B., 1959, Interplanetary dust distribution: Astrophys. Jour., v. 129, p. 496-506.

References--Continued

Bergstrom, B. H., and Sollenberger, C. L., 1961, Kinetic energy effect in single particle crushing: Am. Inst. Mining Metall. Petroleum Engineers Trans., v. 220, p. 373-379.

Charles, R. J., 1957, Energy-size reduction relationships in comminution: Am. Inst. Mining Metall. Petroleum Engineers Trans., v. 208, p. 80-88.

Crozier, W. D., 1962, Five years of continuous collection of black, magnetic spherules from the atmosphere: Jour. Geophys. Res., v. 67, p. 2543-2548.

Hawkins, G. S., and Upton, E. K. L., 1958, The influx rate of meteors in the Earth's atmosphere: Astrophys. Jour., v. 128, p. 727-735.

Holmes, J. A., 1957, A contribution to the study of comminution--a modified form of Kick's law: Inst. Chem. Engineers Trans., v. 35, p. 125-141.

Kaiser, T. R., 1961, The determination of the incident flux of radio-meteors, II--Sporadic meteors: Monthly Notices Royal Astronomical Society, v. 123, no. 3, p. 265-271.

McCracken, C. W., Alexander, W. M., and Dubin, M., 1961, Direct measurement of interplanetary dust particles in the vicinity of the Earth: NASA Tech. Note D-1174.

Millman, P. M., and Burland, M. S., 1957, in Highlights of some papers presented at the 96th meeting of the American Astronomical Society: Sky and Telescope, v. 16, no. 5, p. 222.

Moore, H. J., Gault, D. E., and Heitowit, E. D., 1963, Change in effective target strength with increasing size of hypervelocity impact craters, in Astrogeologic Studies Ann. Prog. Rept., Aug. 25, 1962-July 1, 1963, pt. D: U.S. Geol. Survey open-file report, p. 52-63.

References--Continued

Moore, H. J., Lugn, R. V., and Gault, D. E., 1962, Experimental hyper-
velocity impact craters in rock, _in_ Symposium on hypervelocity
impact, 5th, Denver 1961, Proc., v. 1, pt. 2: San Diego, U.S. Naval
Research Laboratory, p. 625-643.

Van de Hulst, H. C., 1947, Zodiacal light in the solar corona: Astrophys.
Jour., v. 105, p. 471-488.

Watson, F. G., 1956, Between the planets: Cambridge, Harvard Univ.
Press, 188 p.

Whipple, F. J., 1963, On meteoroids and penetration: Jour. Geophys. Re-
search, v. 68, p. 4929-4939.

MERCURY DISTRIBUTION AT THE
ODESSA METEORITE CRATERS, TEXAS

by C. H. Roach, S. P. Lassiter, and T. S. Sterrett

Introduction

Five closely spaced meteorite craters have been recognized and
studied near Odessa, Texas (Evans, 1961). These craters are being studied
to determine if any physical or chemical properties of the exposed rocks
can be uniquely related to the physical environment that must have been
created by the impact of the meteoritic shower that formed the craters.
The results of preliminary thermoluminescence investigations at the cra-
ters have been previously reported (Roach and others, 1963).

Chemical investigations of the changes of chemical characteristics
of the rocks in the vicinity of the craters have been started. Both tran-
sient and postimpact alteration of chemical properties of the affected
rocks might be expected. One would expect that the high shock pressures,
elevated temperatures, and extensive rock brecciation created during the
impact event might have depleted or redistributed the more volatile con-
stituents of the rocks. One important permanent feature produced by
the impact event was the lens of brecciated rocks beneath the main Odessa
crater, a physical feature that may have prepared the rock strata for much
later chemical modification by the process of weathering because vadose
water could penetrate much deeper into the brecciated rocks than elsewhere.
Chemical investigations of rocks at the sites of known terrestrial impact
structures should contribute to a better understanding of impact structures
and should be useful in distinguishing craters and structures produced by
impacts from those produced by volcanism and hydrothermal processes.

This report compares the mercury content of subsurface rocks at the
main Odessa meteorite crater with that of stratigraphically equivalent
subsurface rocks about 1 mile from the Odessa craters.

Semiquantitative spectrographic and atomic absorption analyses for
other elements are being obtained on each of the subsurface samples, but
these chemical data are not yet complete enough for analysis and will be
described in future reports.

Geologic setting of the Odessa craters

The geologic setting of the Odessa meteorite craters has been described by Evans (1961, p. D-3) as follows: "In the crater vicinity, rock strata immediately underlying the plains surface consist of compact, calcareous sands and clays having an average thickness of 20 to 25 feet. A zone of hard, platy caliche, irregular in thickness, is typically present in the upper part of this unit. Underlying these near-surface deposits is a section about 50 feet thick consisting of flat-lying marine limestones and shales of Cretaceous age. These strata are in turn underlain by the Cretaceous basement sands which have an average thickness of 125 feet. The basement sands rest upon continental red beds of Triassic age. The main crater penetrates the upper formations and about 30 feet into the Cretaceous basement sands. Crater no. 2 and the smaller craters are developed entirely in the near-surface sands and clays." The Cretaceous basement sands have calcareous cement.

The main crater has an average rim diameter of 550 feet and a maximum depth of about 100 feet. Crater no. 2 is about 70 feet in diameter and 17 feet in depth. Three small, poorly preserved craters have depths from 6 to 10 feet. "The rim of the main crater is formed by strongly folded, distorted and thrust-faulted strata. The oldest strata involved in the overthrust rim folds have been uplifted as much as 50 feet from their original position, which is equivalent to one-half the depth of the crater. In crater no. 2, however, the rim exhibits only simple and comparatively slight upfolding which involved only the near-surface soil and caliche units. . . .In the preserved parts of the smaller crater rims no displacement of bedrock could be detected." (Evans, 1961, p. D-8.)

Sampling

During the period July - September, 1964, two vertical holes were core-drilled near the Odessa meteorite craters to obtain subsurface samples of the rock strata most likely to have been affected by the impacting meteorites that formed the craters. These core samples are being used to study the physical and chemical properties of rocks that occur at depth below the preimpact land surface. One core hole drilled about 5 feet
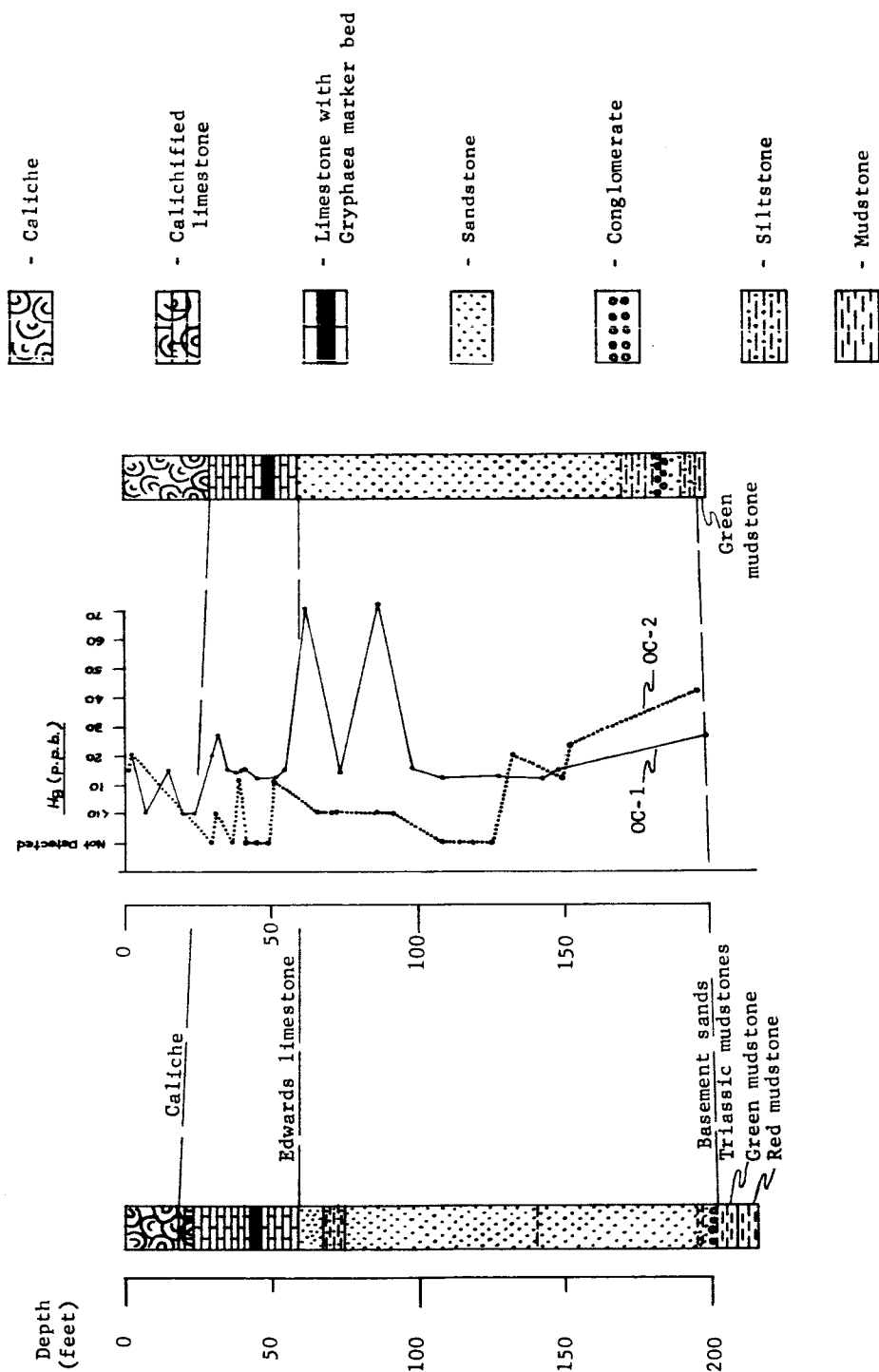
Fig. 1.--Condensed lithologic logs and mercury content of drill holes OC-1 and OC-2.

from the northeast crater lip of the main Odessa crater represents the upturned and deformed rocks that were affected greatly by the physical environment created by the impacting meteorites. The second core hole was drilled about 1.1 miles west of the site of the main Odessa crater and is herein used as a control hole to represent the same rock strata in their preimpact or unaffected condition (fig. 1). The depths at which samples were selected for mercury measurements are shown in tables 1 and 2.

Mercury measurements

All measurements of mercury concentration were made with a portable type S-1 mercury detector manufactured by the Lemaire Instruments Company, Reno, Nevada. With this detector, the amount of mercury volatilized from a heated rock sample is measured by atomic absorption. One gram of finely disaggregated rock sample (less than 200 mesh) is placed in a small metal sample bulb. The sample bulb is then attached with an airtight connection to a piston-type intake hand pump. The bottom part of the sample bulb is then placed directly in the flame from a small butane torch and is heated for 1 minute. During heating, the piston is slowly moved outward so that volatile materials liberated during heating of the sample will be continuously drawn into the chamber of the intake pump. After heating and collection of the volatilized materials has been completed, the hand pump and sample bulb are separated, and the outlet to the hand pump is then inserted into the airtight connection to the atomic absorption chamber. Then the voltmeter on the absorption unit is zeroed and the collected vapor phase is injected into the absorption chamber by a forward movement of the plunger of the hand pump. The absorption chamber has a photomultiplier mounted on one side and, on the other side, a mercury lamp to produce the ultraviolet radiation required for the absorption measurement of mercury. As the volatilized materials traverse the part of the chamber between the photomultiplier and the light source, any substances that absorb ultraviolet radiation will cause a deflection of the voltage output of the photomultiplier tube. This voltage deviation is then amplified electronically, giving a voltage reading which is proportional to the concentration of absorbing material present in the absorption chamber.

154

Since the Lemaire mercury detector does not contain a monochromator, mercury is not selectively determined within the absorption chamber. However, only two substances commonly present in rocks of the type herein studied will absorb in the ultraviolet spectral region of the source lamp, and therefore might be falsely interpreted as mercury present in the sample. Smoke (and other particulate matter) generated from heating organic matter and sulfur dioxide from heated sulfide minerals can both absorb in parts of the spectrum of mercury and might therefore be interpreted as representing mercury in the sample being measured. Smoke and other particulate matter generated from heated organic matter was eliminated from the system by means of a special filter (provided by the Lemaire Instruments Company) that was placed in the intake part of the hand pump and did not therefore occur in the gaseous sample that is injected into the absorption chamber. Sulfur dioxide was eliminated from the system by placing a thin layer of finely ground metallic iron on top of each disaggregated rock sample before it was heated. The finely ground metallic iron reacts with the sulfur dioxide generated from the rock sample during heating and prevents the sulfur dioxide from entering the chamber in the intake pump. These precautions were taken to raise the probability that none of the samples would produce atomic absorption in the chamber unless mercury vapor was present.

A set of mercury standards was prepared by adding known quantities of pure cinnabar to Ottawa sand that contains no detectable mercury. These standards were then used to develop a curve expressing the relation between voltage produced by the atomic absorption chamber and the known mercury content of the standard samples. These standards were also checked with a more elaborate and more precise mercury detection apparatus designed by the Geological Survey (Vaughn and McCarthy, 1964). Voltage readings produced by the absorption of ultraviolet radiation by the mercury vapor from each sample were recorded, and the amount of mercury in the original sample was obtained from the calibration graph. Mercury was measured on 3 splits of each sample analyzed, and the 3 measurements were averaged for the comparative studies.

The reproducibility of measurements with the Lemaire mercury detector

is good and the limit of detection for this field instrument has been determined to be about 10 parts per billion if careful precedures are conducted by only one operator.

Mercury content of subsurface rocks at Odessa craters

The mercury analyses show that many of the subsurface rock samples to a depth of about 130 feet below the main Odessa meteorite crater have significantly lower concentrations of mercury than do stratigraphically equivalent samples collected 1.1 miles west of the main Odessa crater (tables 1 and 2 and fig. 1). Beneath the northeast lip of the main Odessa crater, only four samples above a depth of about 128 feet contained greater than the detection limit of 10 parts per billion mercury (table 2). Two of these four samples were taken from the near-surface caliche, within 3 feet of the ground surface, and may have contained mercury added during recent time either by rainfall or by man during periods when various fluids and constructional materials were disposed of along this portion of the crater lip, as reported by Glen L. Evans (personal communication, 1962). For these reasons, the upper 5 feet of the caliche at the main crater is not considered to be reliable material to analyze for mercury content. The chemical analyses show that above a depth of about 130 feet each stratigraphic unit sampled contains significantly greater concentrations of mercury at 1.1 miles west of the crater than equivalent units sampled at the edge of the main Odessa crater. Below a depth of about 130 feet, samples of Cretaceous basement sands and the underlying Triassic mudstone at both locations consistently contain detectable concentrations of mercury in about the same order of magnitude, although the rocks at this depth have a slightly higher average mercury content beneath the main crater. More data are needed to determine if these deeper horizons actually have significantly more mercury beneath the main crater than at the more distant location. It is interesting to note that the depth of 133 feet, above which almost all samples at the main crater have either undetectable concentrations of mercury or less than 10 parts per billion, is only about 30 to 40 feet stratigraphically below the point in the Cretaceous basement sands that corresponds to the maximum depth reported for

156

Table 1. Mercury content of samples in OC-1 drill hole (1.1 miles west of main Odessa crater)

Sample depth (feet)	Rock unit sampled	Voltage reading (volts)				Average mercury content (parts per billion)
		1st	2d	3d	Avg.	
1.95 - 2.05	Caliche	0.25	0.25	0.25	0.25	20
7.10 - 7.20	"	0.00	0.12	0.12	0.08	< 10
15.40 - 15.50	"	0.25	0.25	0.20	0.23	15
20.61 - 20.71	Calichified Edwards limestone	0.00	0.12	0.12	0.08	< 10
24.30 - 24.40	Edwards limestone	0.12	0.15	0.00	0.08	< 10
30.03 - 30.13	"	0.25	0.25	0.25	0.25	20
32.40 - 32.50	"	0.10	0.50	0.50	0.37	27
35.95 - 36.05	"	0.00	0.40	0.30	0.23	15
38.05 - 38.15	"	0.20	0.20	0.20	0.20	14
40.33 - 40.43	"	0.25	0.25	0.20	0.23	15
42.55 - 42.65	"	0.25	0.20	0.20	0.22	15
44.95 - 45.05	Edwards limestone (Gryphaea marker bed)	0.25	0.00	0.25	0.17	12
52.01 - 52.11	Edwards limestone	0.12	0.20	0.20	0.17	12
56.38 - 56.48	"	0.25	0.20	0.20	0.22	15
62.15 - 62.25	Basement sands	0.75	0.50	0.60	0.62	70
74.20 - 74.30	"	0.20	0.20	0.20	0.20	14
86.55 - 86.66	"	0.65	0.65	0.65	0.65	72
98.80 - 98.90	"	0.25	0.25	0.20	0.23	15
109.51 - 109.61	"	0.12	0.12	0.25	0.16	12

Table 1. Mercury content of samples in OC-1 drill hole (1.1 miles west of main Odessa crater) - Cont'd.

Sample depth (feet)	Rock unit sampled	Voltage reading (volts)				Average mercury content (parts per billion)
		1st	2d	3d	Avg.	
128.97 - 129.07	Basement sands	0.20	0.15	0.20	0.18	13
143.50 - 143.60	"	0.10	0.20	0.20	0.17	12
148.39 - 148.49	"	0.20	0.25	0.20	0.22	15
200.00 - 200.10	Triassic green mudstone	0.37	0.37	0.37	0.37	27

the center of the main crater (Evans, 1961, p. D-3). Also, it is worth noting that drill core from OC-2 drill hole was intensely to moderately fractured to a depth of about 60 feet, and moderately to slightly fractured to a depth of about 100 feet.

Preliminary interpretation of mercury data

Except for those samples collected from the surface to a depth of about 130 feet at the main crater, the mercury content of all subsurface rock samples is within the range of the values to be expected for sedimentary rock of the type occurring at the Odessa craters. The upper part of the section of rocks at the main crater appears to be unusually low in mercury content. Rocks deeper than 130 feet below the main crater might have slightly higher than average mercury content, but additional data are needed before this can be determined. If the assumption is made that the subsurface rock at the two sites studied had about the same content of mercury before the impact event, an explanation is needed for the apparent depletion of mercury content in the rocks from the surface to a depth of about 130 feet beneath the main Odessa crater and possible increased concentration below. At this time, two possible theories can be offered to explain the depletion of mercury in rocks beneath the main crater: (1) mercury indigenous to the rocks could have been depleted or mobilized as a direct result of the high shock pressures and elevated temperatures that must have accompanied the impact of the meteoritic shower and (2) the mercury content of the brecciated rock formed by the impact event might have been depleted, or redistributed, by postimpact leaching by vadose waters as they moved downward through the lens of brecciated rock.

The impact event at the Odessa craters probably was accompanied by pressure and temperature gradients that could have mobilized and transferred some of the indigenous mercury. The degree to which mercury might be transferred by an impact event would of course be dependent on projectile properties such as mass, velocity, and composition, as well as target properties such as water content, porosity, and composition. Previous work by the authors has shown that the mercury content of subsurface rocks adjacent to underground nuclear explosions may have been significantly

159

Table 2. Mercury content of samples in OC-2 drill hole (northeast lip of main Odessa crater)

Sample depth (feet)	Rock unit sampled	Voltage reading (volts)				Average mercury content (parts per billion)
		1st	2d	3d	Avg.	
0.54 - 0.64	Caliche	0.20	0.20	0.20	0.20	15
2.20 - 2.25	"	0.25	0.25	0.25	0.25	20
29.27 - 29.37	Edwards limestone	0.00	0.00	0.00	0.00	not detected
31.10 - 31.20	"	0.10	0.00	0.00	0.03	< 10
37.04 - 37.14	"	0.00	0.00	0.00	0.00	not detected
39.13 - 39.23	"	0.25	0.10	0.10	0.15	11
41.59 - 41.69	"	0.00	0.00	0.00	0.00	not detected
45.15 - 45.20	"	0.00	0.00	0.00	0.00	not detected
50.06 - 50.16	Edwards limestone (Gryphaea marker bed)	0.00	0.00	0.00	0.00	not detected
52.00 - 52.05	Edwards limestone	0.20	0.10	0.12	0.14	11
66.60 - 66.70	Basement sands	0.00	0.10	0.00	0.03	< 10
71.17 - 71.27	"	0.00	0.12	0.00	0.04	< 10
73.09 - 73.19	"	0.00	0.00	0.10	0.03	< 10
86.30 - 86.40	"	0.00	0.10	0.10	0.07	< 10
92.66 - 92.76	"	0.10	0.00	0.10	0.07	< 10
108.40 -108.50	"	0.00	0.00	0.00	0.00	not detected
115.05 -115.15	"	0.00	0.00	0.00	0.00	not detected
120.85 -120.95	"	0.00	0.00	0.00	0.00	not detected

Table 2--Continued. Mercury content of samples in OC-2 drill hole (northeast lip of main Odessa crater)

Sample depth (feet)	Rock unit sampled	Voltage reading (volts)				Average mercury content (parts per billion)
		1st	2d	3d	Avg.	
127.76 - 127.86	Basement sands	0.00	0.00	0.00	0.00	not detected
133.80 - 133.90	"	0.20	0.30	0.25	0.25	20
149.35 - 149.45	"	0.20	0.10	0.20	0.17	12
153.50 - 153.60	"	0.37	0.30	0.30	0.32	24
196.68 - 196.78	Triassic green mudstone	0.30	0.65	0.60	0.52	42

depleted above the detonation and for a short distance below it. The physical environment created by impacting meteorites has been previously stated to be responsible for greatly reducing the radiogenic argon content of granitic rocks at the Ries crater (Signer, 1964). Although none of these data are conclusive, they do suggest that strong shock and elevated temperatures accompanying strong shock events can volatilize mercury indigenous to the shocked rocks, and that the net result of the shock event is a depletion or redistribution of mercury content in the affected rocks.

Very little is known about the geochemical behavior of mercury, particularly in an oxidizing environment such as has existed at the site of the Odessa craters since their formation. Rain water is known to contain a small amount of mercury and may represent a possible source of mercury added to the near-surface (within 5 feet of the ground surface) rocks at the main Odessa crater since its formation. Present chemical data is insufficient to evaluate the possibility that mercury in the rocks at the main Odessa crater has been strongly leached to a depth of about 130 feet. Chemical analyses by spectrography and atomic absorption are being made for each sample listed in tables 1 and 2, and when these data are available it may be possible to determine whether mercury has been redistributed in the subsurface rocks at the main crater by leaching of downward-percolating meteoric water.

Conclusions

The depletion of mercury content of rocks beneath the main Odessa crater may have resulted from processes caused by the impact event that formed the craters. On the other hand, postimpact leaching by meteoric waters cannot be omitted as a possible cause of the depletion. Additional chemical studies now under way may help to resolve this problem and also to determine if only the mercury content of the samples is being measured by the Lemaire instrument. Regardless of the cause, the variations in mercury content of the rocks beneath the main Odessa crater may provide a useful technique for studying other terrestrial structures whose origin is now uncertain. Many complex structures of volcanic and hydrothermal origin should contain rocks that may be significantly enriched in mercury and

therefore contrast greatly with rocks found at impact structures.

Acknowledgments

References

Evans, G. L., 1961, Investigations at the Odessa meteor craters, *in* Proceedings of the Geophysical Laboratory/Lawrence Radiation Laboratory Cratering Symposium: California Univ., Livermore, Lawrence Radiation Lab. Rept., UCRL-6438, pt. 1, paper D, 11 p. (Paper prepared for U. S. Atomic Energy Commission.)

Roach, C. H., Johnson, G. R., McGrath, J. G., Merritt, V. M., and Sterrett, T. S., 1963, Thermoluminescence investigations at the Odessa meteorite craters, Texas, *in* Astrogeologic Studies Ann. Prog. Rept., Aug. 25, 1961 to Aug. 24, 1962, pt. B: U. S. Geol. Survey open-file report, p. 107-117.

Signer, Peter, 1964, Argon concentrations in two granite specimens from the Ries crater, *in* Astrogeologic Studies Ann. Prog. Rept., July 1, 1963 to July 1, 1964, pt. B: U. S. Geol. Survey open-file report, p. 35-38.

Vaughn, W. W., and McCarthy, J. H., Jr., 1964, An instrumental technique for the determination of submicrogram concentrations of mercury in soils, rocks, and gas: U. S. Geol. Survey Prof. Paper 501-D, p. D123-D127.

COLLECTION OF METEORITE SPECIMENS AT METEOR CRATER, ARIZONA

by D. J. Milton and A. J. Swartz

Considerable variation is known among specimens of the Canyon Diablo irons, fragments of the meteorite that formed Meteor Crater. Some of the differences seem to correlate with the find site of the fragments. For example, it has been stated that diamonds occur only in irons on the rim of the crater and not in those farther out on the plains (Nininger, 1956; Anders, 1965). Systematic studies, however, have been hindered by uncertainty as to the find site of most of the specimens.

As part of the comprehensive study of Meteor Crater, irons were systematically searched for with U. S. Army AN/PRS-3 mine detectors during the summer of 1965. Search grids were laid out along radial lines from the crater in each of the cardinal directions. About 90 specimens of meteoritic iron were recovered. Most weighed about 100 g, but some larger ones, up to 15 kg, were found. In addition to the irons, oxidized meteoritic material was collected from the ground surface. All specimens were accurately located with respect to surveyed points.

Preparation of the specimens for study has begun with extraction of the carbon minerals from oxidized material by digestion in acid and with the sawing of iron specimens for polished sections.

We are grateful to Meteor Crater Enterprises, Inc., for allowing us to make the collection. We also thank George Morrison of the Department of Chemistry, Arizona State College, for providing laboratory space and Carleton Moore, curator of the Nininger Meteorite Collection, Arizona State University, for providing facilities for sawing irons.

References

Anders, Edward, 1965, Diamonds in meteorites: Sci. American, v. 213, p. 26-36.

Nininger, H. H., 1956, Arizona's meteorite crater: Sedona, Arizona, American Meteorite Museum, 232 p.